

UC Santa Barbara

UC Santa Barbara Electronic Theses and Dissertations

Title

Exotic Quantum Phases and Phase Transitions of Strongly Interacting Electrons in Low-Dimensional Systems

Permalink

<https://escholarship.org/uc/item/73r0v1c7>

Author

Mishmash, Ryan Victor

Publication Date

2014

Peer reviewed|Thesis/dissertation

UNIVERSITY of CALIFORNIA
Santa Barbara

**Exotic Quantum Phases and Phase Transitions of Strongly Interacting Electrons
in Low-Dimensional Systems**

A dissertation submitted in partial satisfaction of the
requirements for the degree

Doctor of Philosophy

in

Physics

by

Ryan V. Mishmash

Committee in charge:

Professor Matthew P. A. Fisher, Chair

Professor S. James Allen

Professor Andreas W. W. Ludwig

June 2014

The dissertation of Ryan V. Mishmash is approved:

Professor S. James Allen

Professor Andreas W. W. Ludwig

Professor Matthew P. A. Fisher, Chair

June 2014

**Exotic Quantum Phases and Phase Transitions of Strongly Interacting Electrons
in Low-Dimensional Systems**

© Copyright 2014

by

Ryan V. Mishmash

To Vic and Alice, my loving parents.

Acknowledgments

My time at Santa Barbara has been an incredibly stimulating and enjoyable six years. The person most responsible for this is certainly my advisor, Matthew Fisher, probably the most creative, deep-thinking, open-minded individual I have ever met. His excitement and attitude towards physics is something we should all strive for. I thank him for providing such a comfortable and open, yet intense and state-of-the-art, research environment—a setting which is ideal for the growth of young researchers such as myself. His incredibly deep *and* broad knowledge of condensed matter physics never fails to amaze and amuse, nor does his blunt honesty and humility¹ given his stature! Overall, I feel extremely fortunate to have Matthew as my advisor, as well as my friend.

I am also very thankful to Lesik Motrunich for his support and guidance on several of the projects contained in this dissertation. He has taught me how to be a careful, diligent, and thorough researcher. Indeed, convincing Lesik that a result is correct is no easy task, almost like having the world’s toughest referee on your own team. His skills on technical matters such as bosonization and variational Monte Carlo have rubbed off on me in a way which I will surely use for years to come.

I am equally grateful to Iván González and Donna Sheng for their heroic programming efforts and generously allowing me to use their core DMRG codes in attacking some of these very difficult problems. Without their work, as well as that of Hongchen Jiang, many of the achievements in this dissertation, notably those of Chapters 2 and 4, would not have been possible.

¹Some example MPAF quotes which come to mind: “Group theory is over my head.” and “I always get confused when we have spin.”

I would very much like to thank Cenke Xu for proposing the project which culminated in Chapter 3, and which turned out to be a very fruitful and enjoyable collaboration with Cenke, Jim Garrison, and Samuel Bieri. I would particularly like to thank Jim for his close collaboration and always patiently sharing his paramount expertise on all matters programming and computing related.

My early, formative graduate school years benefitted enormously from close collaborations that I will never forget with Matt Block and Ribhu Kaul. Many thanks go to Roger Melko for his support, collaboration, and friendship over the years; he and Lori sure know how to have a good time!

I would also like to thank the many amazing resident postdocs for their help and advice, especially Max Metlitski, Tarun Grover, Eun-Gook Moon, Mike Mulligan, Adrian Feiguin, Bryan Clark, and Bela Bauer. And I am of course very fond of interactions with my fellow students in the condensed matter theory group at UCSB, especially Miles Stoudenmire, Hyejin Ju, Sungbin Lee, Ru Chen, and Lucile Savary; as well as the professors, Leon Balents, Andreas Ludwig, Chetan Nayak, and Cenke Xu.

I am very appreciative of Jim Allen and Andreas Ludwig for setting aside time from their busy schedules to serve on my advancement and defense committees. I would like to thank Microsoft Station Q for funding support during my first two years at UCSB, and also Sean Fraer at Station Q and Jennifer Farrar for being so helpful regarding all administrative matters. I am also indebted to Paul Weakliem for all his great work as our computer admin at CNSI.

My physics journey began at Colorado School of Mines under the direction of Lincoln Carr, my undergraduate and Master's advisor, and Chris Kelso and David Flammer, my very

first physics instructors, and I am grateful to them all and for providing me the foundation to pursue a Ph.D. More generally, I would like to thank *all* of my teachers throughout my academic career, and especially my high school teachers Pat Mara and Richard Ransome who taught me mathematics (Pat) and writing (Rich) *so amazingly well*.

I would like to acknowledge my close friendships throughout my grad school years with the likes of David (Cotton) Toyli, Dustin McIntosh, Bob Buckley, Ramsey Majzoub, Hyejin Ju, Bela Bauer, and Michael Wall. My girlfriend, Alex Miller, has made these last six months while I have finished my degree so very enjoyable and memorable; it is hard to express how much I appreciate her care and companionship.

Finally, I must thank my parents for their unwavering support and love throughout my entire life. They are the best parents imaginable. All I am I owe to them.

Curriculum Vitae

Ryan V. Mishmash

Education

- 2014 Ph.D. in Physics, University of California, Santa Barbara
- 2011 M.A. in Physics, University of California, Santa Barbara
- 2008 M.S. in Applied Physics, Colorado School of Mines
- 2007 B.S. in Engineering Physics, Colorado School of Mines

Publications

“A continuous Mott transition between a metal and a quantum spin liquid,” Ryan V. Mishmash, Iván González, Roger G. Melko, Olexei I. Motrunich, and Matthew P. A. Fisher, under review (2014) [[arXiv:1403.4258](#)].

“Theory of a Competitive Spin Liquid State for Weak Mott Insulators on the Triangular Lattice,” Ryan V. Mishmash, James R. Garrison, Samuel Bieri, and Cenke Xu, *Physical Review Letters* **111**, 157203 (2013) [[arXiv:1307.0829](#)].

“Non-Fermi-liquid *d*-wave metal phase of strongly interacting electrons,” Hong-Chen Jiang, Matthew S. Block, Ryan V. Mishmash, James R. Garrison, D. N. Sheng, Olexei I. Motrunich, and Matthew P. A. Fisher, *Nature* **493**, 39 (2013) [[arXiv:1207.6608](#)].

“Bose metals and insulators on multileg ladders with ring exchange,” Ryan V. Mishmash, Matthew S. Block, Ribhu K. Kaul, D. N. Sheng, Olexei I. Motrunich, and Matthew P. A. Fisher, *Physical Review B* **84**, 245127 (2011) [Editors’ Suggestion] [[arXiv:1110.4607](#)].

“Exotic Gapless Mott Insulators of Bosons on Multileg Ladders,” Matthew S. Block, Ryan V. Mishmash, Ribhu K. Kaul, D. N. Sheng, Olexei I. Motrunich, and Matthew P. A. Fisher, *Physical Review Letters* **106**, 046402 (2011) [[arXiv:1008.4105](#)].

“Quantum Many-Body Dynamics of Dark Solitons in Optical Lattices,” R. V. Mishmash, I. Danshita, Charles W. Clark, and L. D. Carr, *Physical Review A* **80**, 053612 (2009) [[arXiv:0906.4949](#)].

“Ultracold Atoms in 1D Optical Lattices: Mean Field, Quantum Field, Computation, and Soliton Formation,” R. V. Mishmash and L. D. Carr, [Mathematics and Computers in Simulation](#) **80**, 732 (2009) [[arXiv:0810.2593](#)].

“Quantum Entangled Dark Solitons Formed by Ultracold Atoms in Optical Lattices,” R. V. Mishmash and L. D. Carr, [Physical Review Letters](#) **103**, 140403 (2009) [[arXiv:0710.0045](#)].

Abstract

Exotic Quantum Phases and Phase Transitions of Strongly Interacting Electrons in Low-Dimensional Systems

by

Ryan V. Mishmash

Experiments on strongly correlated quasi-two-dimensional electronic materials—for example, the high-temperature cuprate superconductors and the putative quantum spin liquids κ -(BEDT-TTF)₂Cu₂(CN)₃ and EtMe₃Sb[Pd(dmit)₂]₂—routinely reveal highly mysterious quantum behavior which cannot be explained in terms of weakly interacting degrees of freedom. Theoretical progress thus requires the introduction of completely new concepts and machinery beyond the traditional framework of the band theory of solids and its interacting counterpart, Landau’s Fermi liquid theory. In full two dimensions, controlled and reliable analytical approaches to such problems are severely lacking, as are numerical simulations of even the simplest of model Hamiltonians due to the infamous fermionic sign problem.

In this dissertation, we attempt to circumvent some of these difficulties by studying analogous problems in quasi-one dimension. In this lower dimensional setting, theoretical and numerical tractability are on much stronger footing due to the methods of bosonization and the density matrix renormalization group, respectively. Using these techniques, we attack two problems: (1) the Mott transition between a Fermi liquid metal and a quantum spin liquid as potentially directly relevant to the organic compounds κ -(BEDT-TTF)₂Cu₂(CN)₃ and

EtMe3Sb[Pd(dmit)2]2 and (2) non-Fermi liquid metals as strongly motivated by the strange metal phase observed in the cuprates. In both cases, we are able to realize highly exotic quantum phases as ground states of reasonable microscopic models. This lends strong credence to respective underlying slave-particle descriptions of the low-energy physics, which are inherently strongly interacting and also unconventional in comparison to weakly interacting alternatives.

Finally, working in two dimensions directly, we propose a new slave-particle theory which explains in a universal way many of the intriguing experimental results of the triangular lattice organic spin liquid candidates κ -(BEDT-TTF)₂Cu₂(CN)₃ and EtMe3Sb[Pd(dmit)2]2. With use of large-scale variational Monte Carlo calculations, we show that this new state has very competitive trial energy in an effective spin model thought to describe the essential features of the real materials.

Contents

List of Figures	xiv
1 Introduction: Many-Body Systems of Interacting Electrons	1
1.1 Overview: From Weakly Interacting Electrons to Quantum Spin Liquids and Non-Fermi Liquids	1
1.1.1 Organic Spin Liquid Candidates and the Mott Transition	7
1.1.2 High-Temperature Superconductors and Non-Fermi Liquid Metals	10
1.2 Parton Constructions and Gauge Theories	13
1.3 Multileg Ladders: Bosonization and the Density Matrix Renormalization Group	16
1.4 Variational Monte Carlo: Modeling Exotic Many-Body States with Projected Wave Functions	23
1.5 Outline and Remarks	24
2 A Continuous Mott Transition Between a Metal and a Quantum Spin Liquid	26
2.1 Background and Introduction	26
2.2 Extended Hubbard Model on the Two-Leg Triangular Strip	29
2.3 Mott Metal-Insulator Transition and Realization of the Electronic Spin Bose Metal	32
2.4 Discussion and Outlook	41
3 Theory of a Competitive Spin Liquid State for Weak Mott Insulators on the Triangular Lattice	44
3.1 Background and Introduction	44
3.2 New Z_2 Spin Liquid: $d + id$ Ansatz with Quadratic Band Touching	47
3.3 Variational Monte Carlo Results	51
3.3.1 Nearest-Neighbor Heisenberg Model with Ring Exchange: $J_2 = 0$	52
3.3.2 Full Variational Phase Diagram with Finite J_2	57
3.4 Discussion and Outlook	59
4 Non-Fermi Liquid d-wave Metal Phase of Strongly Interacting Electrons	61
4.1 Background and Introduction	61
4.2 Gauge Theory and Variational Wave Functions for the d -wave Metal	64
4.3 Microscopic Ring-Exchange Model	67

4.4	Two-Leg Study: DMRG and VMC	69
4.5	Eliminating Conventional Luttinger Liquid Scenarios in Favor of the <i>d</i> -wave Metal	79
4.6	Discussion and Outlook	82
5	Concluding Remarks	84
5.1	Speculations on Future Directions	86
A	Details of the Numerical Calculations	89
A.1	DMRG on the Extended <i>t-t'</i> Hubbard Model (Chapter 2)	89
A.2	VMC on the Heisenberg Model Plus Ring Exchange (Chapter 3)	92
A.3	DMRG on the Two-Leg <i>t-J-K</i> Electron Ring-Exchange Model (Chapter 4) . .	95
B	Interacting Electrons on the Two-Leg Triangular Strip: Luttinger Liquid Description and Solution by Bosonization	97
B.1	Long-Wavelength Description of C2S2 Metal and C1S2 Spin Bose Metal	98
B.2	Renormalization Group Analysis of the C2S2→C1S2 Mott Transition	104
B.3	Observables and Stiffness Parameters	108
B.3.1	Establishing the Result $\Delta[\mathcal{H}_8] = 4g_{\rho+}$	108
B.3.2	Bosonized Representation of Operators at Finite Wavevectors	110
B.3.3	Assessing Gaplessness of the Spin Sector Through $g_{\sigma+}$	118
B.4	Further Analysis of $g_{\sigma+}$ DMRG Data	121
C	Determinantal Representation of BCS-type Wave Functions	126
C.1	Calculating the Pair Wave Function in Real Space: Bogoliubov-de Gennes Approach	127
C.2	Avoiding Bogoliubov-de Gennes with a Particle-Hole Transformation on $f_{r\downarrow}$	132
D	Bosonization Analysis of a $c = 5$ Mode <i>d</i>-wave Metal Phase on the Two-Leg Ladder	137
D.1	Long-Wavelength Bosonized Description	140
D.2	Stability Analysis in the Presence of all Allowed Short-Range Interactions	144
D.3	Conclusion	148
Bibliography		150

List of Figures

2.1	Schematic of the half-filled extended Hubbard model on the two-leg triangular strip and its phase diagram.	28
2.2	Electron/spinon bands on the two-leg triangular strip.	31
2.3	Density structure factor: Locating the Mott transition and power-law Friedel oscillations in a Mott insulator.	34
2.4	Spin structure factor: Watching electrons evolve into spinons.	36
2.5	Dimer structure factor: Period-2 valence bond solid order in the strong Mott insulator.	39
2.6	Electronic momentum distribution function: Disappearance of the Fermi surface.	41
3.1	Summary of our variational phase diagram along the line $J_2 = 0$	54
3.2	Heisenberg and ring exchange expectation values for $d + id$ and nodal d -wave trial wave functions.	55
3.3	Energy versus K for $d + id$ and nodal d -wave trial wave functions.	56
3.4	Full variational phase diagram of the spin Hamiltonian, Eq. (3.1).	58
4.1	Schematic of the t - J - K model Hamiltonian.	67
4.2	Picture of the parton bands for the d -wave metal phase.	69
4.3	Phase diagram of the t - J - K electron ring-exchange model at electron density $\rho = 1/3$ on the two-leg ladder.	71
4.4	DMRG measurements in the conventional Luttinger liquid phase at $J/t = 2$ and $K/t = 0.5$	73
4.5	DMRG measurements in the unconventional d -wave metal phase at $J/t = 2$ and $K/t = 1.8$	74
4.6	Evolution of singular wavevectors in the d -wave metal phase.	76
4.7	Central charge c as a function of interaction K/t	78
B.1	Finite-size estimates of $g_{\sigma+}$ [see Eq. (B.86)] versus U/t : Extended Hubbard model for the same parameters used in Chapter 2.	122
B.2	Finite-size estimates of $g_{\sigma+}$ [see Eq. (B.86)] versus U/t : On-site t - t' - U Hubbard model at $t'/t = 0.8$	124

D.1	Picture of the parton bands for the putative $c = 5$ mode d -wave metal phase on the two-leg ladder.	139
D.2	Scaling dimensions of the interactions $\mathcal{H}_{RL,w}^{d1}$ [Eq. (D.33)] and $\mathcal{H}_{RL,w}^{f\sigma}$ [Eq. (D.37)] versus $k_{Fd1}^{(\pi)}$	147

Chapter 1

Introduction: Many-Body Systems of Interacting Electrons

1.1 Overview: From Weakly Interacting Electrons to Quantum Spin Liquids and Non-Fermi Liquids

Understanding the effects of *interactions* between constituents of a given physical system is ubiquitous in all fields of physics, from the classical mechanics of everyday life to the collisions between subatomic particles in high-energy accelerators to the evolution and structure of stars and galaxies. The effects of interactions between a system's many degrees of freedom can be profound and often times determine the *qualitative* behavior of the system as a whole. These points are perhaps most dramatically exemplified in modern-day condensed matter physics, where we are interested in understanding the collective behavior of $\sim 10^{23}$ interacting quantum mechanical degrees of freedom! The degrees of freedom are generally the (nonrelativistic)

valence electrons in a crystalline solid; the problem requires a quantum mechanical description because even a laboratory at room temperature is to a good approximation near absolute zero¹; and the interactions are the repulsive electrostatic Coulomb forces between electrons.

Remarkably, however, one can often make enormous theoretical progress describing real materials by ignoring electron-electron interactions completely. This is the famous band theory of solids [1] wherein we mathematically account only for the quantum mechanical behavior of the electrons and their interaction with a periodic lattice of atoms. In fact, this more traditional realm of solid state theory is responsible for our understanding of the semiconductor [1], and it thus directly underlies the function of basically every modern-day electronic device.

However, in terms of bare numbers, the strength of the Coulomb interaction in ordinary solids is not small and is typically comparable to the kinetic energy, yet the free-electron approximation in spatial dimensions $d > 1$ usually remains valid. This remarkable fact was explained in 1957 by the seminal work of Landau [2]—a theoretical framework known today as (Landau-)Fermi liquid theory [3]. At its simplest level [4], Landau’s Fermi liquid theory argues that the excited states of an interacting electronic system are in one-to-one correspondence with the corresponding noninteracting electron gas; that is, the excitations are described by nearly free, long-lived fermionic quasiparticles with the same internal quantum numbers as the electron only with a renormalized effective mass². With respect to most physical properties, Fermi liquids thus behave as if they were noninteracting. One of the most notable physical consequences is a jump discontinuity $Z < 1$ in the electron momentum distribution function at the Fermi surface, whose enclosed volume is determined entirely by the electron density; the

¹For example, the Fermi energy of copper is around 7 eV, or about 80,000 K \gg 300 K.

²This is pushed to the extreme in certain “heavy fermion” materials [5, 6] where Fermi liquid theory may apply, albeit with effective charge carriers hundreds of times more massive than the bare electron.

latter remarkably robust phenomenon is known as Luttinger's volume theorem [7] to which we will return later in Chapter 4.

While band theory and its interacting cousin, Fermi liquid theory, stand as pillars of condensed matter physics, some systems exhibit electron-electron correlations so strong that a noninteracting starting point is simply inapplicable. One of the most dramatic failures of the noninteracting picture occurs when strong interactions produce an insulating state in systems with an odd number of electrons per unit cell—band theory tells us such a situation is impossible and that these materials need be metallic [1]. These systems are today known as *Mott insulators* after Sir Nevill Mott, who speculated as early as 1937 [8] that strong Coulomb repulsion could explain the mysterious insulating behavior observed in various transition metal oxides with partially filled d shells [9]. Still some 80 years later, Mott insulators stand as the paradigmatic example of strongly correlated electron physics [10, 11].

The physical intuition underlying Mott insulation is quite simple. In systems with partially filled d or f shells, the hopping overlap integral between neighboring lattice sites, t , is substantially reduced due to the presence of filled outer shells with larger principal quantum numbers (which essentially increase the lattice spacing). With an odd number of electrons per unit cell, band theory would predict that these materials should still be metallic, albeit with a very small bandwidth $\sim t$. However, for two electrons to occupy a given site, they must pay an energy cost, U , due to Coulomb repulsion, which may in fact dominate over the kinetic energy, t . This physics can be encapsulated in the famous Hubbard model:

$$H = -t \sum_{\langle i,j \rangle} \sum_{\alpha=\uparrow,\downarrow} (c_{i\alpha}^\dagger c_{j\alpha} + \text{H.c.}) + U \sum_i n_{i\uparrow} n_{i\downarrow}, \quad (1.1)$$

where the operator $c_{i\alpha}$ destroys an electron at site i with spin $\alpha = \uparrow, \downarrow$, $n_{i\alpha} = c_{i\alpha}^\dagger c_{i\alpha}$ is the

associated electron number operator, and $\langle i, j \rangle$ denotes a sum over all nearest-neighbor sites on the lattice. At say one electron per lattice site (a “half-filled band”), for large repulsive interactions $U \gg t$, we clearly expect the electrons to localize on their respective lattice sites. There is then a large gap to charge-carrying excitations and the system is said to be a Mott insulator. However, electrons carry spin-1/2, so there are residual spin degrees of freedom which are still active. A strong-coupling expansion of Eq. (1.1) (see, e.g., Ref. [12]) leads to an effective spin model, the leading order term of which is known as the Heisenberg spin Hamiltonian:

$$H = J \sum_{\langle i,j \rangle} \mathbf{S}_i \cdot \mathbf{S}_j + \dots, \quad (1.2)$$

where $J = 4t^2/U$.

Almost invariably in spatial dimensions $d > 1$, real Mott insulating materials and numerical simulations of the Heisenberg model, Eq. (1.2), give rise to spontaneous symmetry breaking and long-range order as the temperature goes to zero; this order is usually of the antiferromagnetic (Néel) type, but the symmetry breaking could also be discrete such as in a valence bond solid. Then, the unit cell is generally enlarged to include an even number of electrons. Even though this enlargement of the unit cell occurs dynamically and solely due to the presence of strong interactions, quantum ground states such as those exhibiting long-range Néel or valence bond solid order are generally continuously connected to simple band insulators³. Therefore, as a matter of principle, Mott insulators with long-range order and an enlarged unit cell are not actually distinct quantum phases from the conventional insulators obtainable via band theory [1, 14].

Even though strong interactions are inarguably present in these Mott insulators, it might

³In the case of Néel order, the connected band insulator must of course also be antiferromagnetic [13].

thus seem that the resulting physics is still of the weakly interacting variety. In a sense, this is true. However, if we can avoid spontaneously broken symmetries and corresponding enlargement of the unit cell, exotic and interesting physics is *guaranteed*. Specifically, due to a theorem by Hastings [15]—a two-dimensional generalization of the Lieb-Schultz-Mattis theorem in one-dimension [16]—it is known that for spin systems on a torus with spin-1/2 per unit cell and no unit cell doubling, a unique quantum ground state with a finite energy gap to all excitations in the thermodynamic limit is forbidden. This fact has truly dramatic consequences and underlies the entire field of *quantum spin liquids* [17], to which Chapters 2 and 3 of this dissertation are largely devoted.

Traditionally [18], quantum spin liquids have been defined as a zero-temperature quantum ground states which spontaneously break no symmetries, most notably the SU(2) spin symmetry. However, Hastings’ theorem implies that such ground states [19, 20] must either have *topological order* or have low-lying *gapless* excitations which are inherently strongly interacting, both exceedingly interesting scenarios⁴. There is thus a pervading modern viewpoint which defines quantum spin liquids with the more positive signature as quantum ground states which have *long-range entanglement* [21, 22], i.e., they cannot be continuously deformed into a trivial direct product state. This notion has led to significant advances in our understanding of and appreciation for the beautiful, yet challenging, complex quantum many-body physics governing the behavior of quantum spin liquids.

Led by Philip W. Anderson, theorists have been thinking about quantum spin liquid ground states since the 1970s [18] and most vigorously since the discovery of the cuprate supercon-

⁴In the case of topological spin liquids, gapless excitations may also exist but they are generally weakly interacting (for examples, see Chapter 3).

ductors (see below) in 1986 [23]. However, it is only within the last decade that experimental evidence has been mounting which has finally brought the notion of quantum spin liquids to reality. At present, tantalizing evidence for spin liquid behavior has been observed, for example, in the following spin-1/2 experimental systems: the quasi-two-dimensional triangular lattice organic materials κ -(BEDT-TTF)₂Cu₂(CN)₃ [24, 25] and EtMe₃Sb[Pd(dmit)₂]₂ [26, 27, 28], the quasi-two-dimensional kagome lattice mineral ZnCu₃(OH)₆Cl₂ (herbertsmithite) [29, 30, 31], and the three-dimensional hyperkagome lattice oxide Na₄Ir₃O₈ [32].

This is very exciting for at least two reasons. Firstly, quantum spin liquids by themselves are very interesting phases of matter which demonstrate highly unusual quantum behavior, and thus may very well eventually be useful technologically. For example, exploiting the topological order in a putative gapped spin liquid for universal topological quantum computation [33] is one long-term dream.

Secondly, if hole-doped away from half-filling, many theoretically envisioned quantum spin liquid ground states become superconductors, and in particular, *high-temperature superconductors*. This was the original groundbreaking insight of Anderson, who proposed that a *resonating valence bond* ground state of a half-filled Mott insulating spin system—basically the topological spin liquids discussed above—may explain high-temperature superconductivity in the newly discovered (at the time) copper-oxide (cuprate) superconductors [23]. While it is still highly controversial whether or not this is the correct approach in describing the cuprates themselves (see Ref. [34] for a review arguing in its favor), these theoretical ideas are to this day still extremely inspiring and influential. The basic idea is that a topological spin liquid contains low-energy degrees of freedom that closely resemble the Cooper pairs known to condense in

a superconductor. In fact, at the mean-field level, topological spin liquids are often just superconductors⁵ described by ordinary Bardeen-Cooper-Schrieffer (BCS) theory [35, 36, 37, 38]. The “preformed” Cooper pairs remain both in the presence of gauge fluctuations (see Sec. 1.2) in the Mott insulating quantum spin liquid itself and also upon doping the system with a finite density of holes. The important point is that the pairing (gap) scale, which determines T_c [37], is then set by the scale of the electronic exchange energy in the Mott insulator, and this scale can potentially (but not necessarily) be very large, perhaps on the order of hundreds of kelvin. Therefore, at least in theory, doping of quantum spin liquids offers a clear and direct route to realizing real materials that superconduct with high critical temperatures. In the future, it will thus be very interesting to see if experimentalists can successfully dope the present-day spin liquid candidates in search of high-temperature superconductivity.

We conclude this section by briefly reviewing the main established experimental and theoretical results, as relevant to the work presented in this dissertation, pertaining to (1) the organic spin liquids κ -(BEDT-TTF)₂Cu₂(CN)₃ and EtMe₃Sb[Pd(dmit)₂]₂ and (2) the cuprates. These two classes of experiments form the main underlying motivation for the theoretical studies presented in the chapters that follow.

1.1.1 Organic Spin Liquid Candidates and the Mott Transition

The two materials κ -(BEDT-TTF)₂Cu₂(CN)₃ and EtMe₃Sb[Pd(dmit)₂]₂ (abbreviated as κ -BEDT and DMIT, respectively) are quasi-two-dimensional, nearly isotropic, layered organic charge-transfer salts. Rather remarkably, both compounds are believed to be described to a

⁵This is the picture within a fermionic slave-particle approach with a Z_2 gauge redundancy (see Chapter 3 and Appendix C).

good approximation by half-filled (one electron per site) Hubbard-type models. For recent reviews on these and related materials, including the detailed microscopic (including chemical) considerations at play, we refer the reader to Refs. [39, 40].

Both κ -BEDT and DMIT are insulating at ambient pressure and show no signs of magnetic ordering down to very low temperatures ~ 30 mK, much lower than the Heisenberg exchange energy $J \sim 250$ K (as estimated by high-temperature series expansion) [24, 27]. Just these facts alone place these materials as strong quantum spin liquid candidates. It has historically been believed that the triangular lattice does not contain sufficient geometrical frustration to suppress long-range Néel order, and this is known to be the case for the nearest-neighbor Heisenberg model [41, 42, 43], i.e., the leading term in Eq. (1.2). However, when compared with other spin liquid candidates like $\text{ZnCu}_3(\text{OH})_6\text{Cl}_2$, perhaps the most distinguishing feature of κ -BEDT and DMIT is the large degree to which *charge fluctuations* are important, i.e., physics represented by the subleading terms in Eq. (1.2) (see Chapter 3). In fact, under moderate hydrostatic pressure of ~ 0.4 GPa, both materials undergo a Mott transition to metallic phases; that is, κ -BEDT and DMIT are *weak* Mott insulators. Furthermore, even though they are electrical insulators, both materials show low-temperature specific heat [44, 45] and spin susceptibility [24, 27, 46] behavior reminiscent of a metal [1], i.e., respectively, C_v/T and χ go to finite constants as $T \rightarrow 0$. Also, thermal transport measurements indicate gapless metallic-like behavior in DMIT ($\kappa/T \rightarrow \text{const.}$) [47] and a very small gap ~ 0.4 K in κ -BEDT [48, 47]. All in all, these are very striking experimental facts which suggest highly interesting quantum many-body behavior, and thus likely require “exotic” theoretical description.

Based on the metallic-like thermodynamics and proximity to a pressure-induced Mott metal-

insulator transition, a very natural and beautiful theoretical starting point to describe these putative spin liquids is to couple a Fermi sea of spinons to a U(1) gauge field [49, 50], a theoretical framework which has been around since the 1990s in the context of the cuprates and the half-filled Landau level [51, 52, 53, 54, 55, 56, 57]. At its simplest level in the context of a Mott insulator at half-filling as appropriate to the organics [49, 50, 58, 59], the spinon Fermi sea state can be modeled by a wave function in which one simply projects out all doubly-occupied sites from an unpolarized spin-1/2 free Fermi gas Slater determinant [49]. One then has a spin-1/2 wave function with power-law “ $2k_F$ ” spin-spin correlations which behave in the same qualitative manner as one has in a simple spinful metal [1]! That is, we have an insulator with metallic-like spins, and since the spin operator is a bosonic object, we often refer to this remarkable quantum phase as the “spin Bose metal” [58, 59].

In Chapter 2, inspired by transport measurements on the organics [25], we study the zero-temperature Mott transition between an ordinary Fermi liquid metal and the above spin Bose metal. Expanding on previous mean-field analysis by Florens and Georges [60], Senthil has recently argued in groundbreaking work [61] that such a Mott transition may be continuous and in the same universality class as the corresponding superfluid-Mott transition for bosons, i.e., the $(d+1)$ D XY universality class [62]. If this scenario were to come to fruition—either experimentally in the organic compounds⁶ or in numerical simulations of relevant lattice models—it would be vindication for Mott who long believed [10, 11] that a continuous interaction-driven metal-insulator transition should be possible in the absence of magnetism. In this disserta-

⁶For κ -BEDT, below ~ 5 K on the metallic side of the Mott transition, the Fermi liquid is unstable to a superconductor; therefore, when applied to that material the ideas of Ref. [61] are valid only on temperature scales above this low-temperature pairing instability. DMIT, on the other hand, apparently has no such instability, although its Mott transition has been studied in less detail compared to κ -BEDT.

tion, using large-scale numerical simulations complemented with analytical bosonization (see Sec. 1.3), we present in Chapter 2 a fully controlled quasi-one-dimensional realization of such a continuous Mott transition into an exotic spin Bose metal insulator on the two-leg triangular strip.

In Chapter 3, on the other hand, we propose a new theory for the low-energy behavior of κ -BEDT and DMIT as a particular gapless topological spin liquid with quadratic band touching (QBT) [63] at the center of the Brillouin zone. We argue that this state is largely consistent with many of the experimental facts summarized above. While the theoretical starting point of our QBT state uses the same variables as the U(1) spinon Fermi sea (spin Bose metal), its underlying physical character is completely different. However, with the presently available experimental data, both the U(1) spinon Fermi sea and QBT states stand as viable theoretical candidates. Only with future experiments will we be able to favor one state over the other, or perhaps another theory entirely—for example, see Refs. [64, 65, 66, 67, 68, 69]—will emerge as the best description.

1.1.2 High-Temperature Superconductors and Non-Fermi Liquid Metals

The field of high-temperature superconductivity began in 1986 with the stunning discovery by Bednorz and Müller that a quasi-two-dimensional ceramic copper-oxide system, LaBaCuO, undergoes a transition to a superconducting state at an anomalously high critical temperature of $T_c \simeq 35\text{ K}$ [70]. Previously, the highest observed T_c had been around 20 K. Since the initial work of Bednorz and Müller, experimentalists have found high-temperature superconductivity in a whole host of copper-oxide materials similar to LaBaCuO. Known collectively

as the “cuprates”, these include $\text{La}_{2-x}\text{Sr}_x\text{CuO}_4$ ($T_c \simeq 40$ K [71]), $\text{YBa}_2\text{Cu}_3\text{O}_{6+x}$ ($T_c \simeq 92$ K; the first superconductor found with T_c above the boiling point of liquid nitrogen [72]), and $\text{HgBa}_2\text{Ca}_2\text{Cu}_3\text{O}_8$ ($T_c \simeq 135$ K; the record T_c at ambient pressure [73, 74]). Such high transition temperatures cannot be accommodated using ordinary phonon-mediated BCS theory [35, 36], and the cuprates are thus often referred to as *unconventional* superconductors⁷.

The precise underlying physical mechanism responsible for high- T_c superconductivity in the cuprates remains to this day a very hotly debated topic. Even a summary of all the proposed theoretical scenarios and how they relate to the vast volume of available experimental data is well beyond the scope of this dissertation. Since at half filling ($x = 0$ doping) all cuprates are (antiferromagnetically ordered) Mott insulators, it is generally agreed upon in most [34] (but not all [14]) theories that strong electron-electron interactions play an absolutely essential role. The majority of theoretical efforts focus on the region of the phase diagram at temperatures just above the superconducting dome and below optimal doping (generally $x \lesssim 0.15$): the so-called “pseudogap” regime. (Recent X-ray scattering data and numerical simulations [76, 77] suggest that the pseudogap may actually be a result of several competing classical orders.) Instead, we here focus on the enigmatic “strange metal” behavior which occurs above T_c and near optimal doping.

The strange metal is the prototypical example of a *non-Fermi liquid* metal, i.e., a conducting state which violates Fermi liquid theory in some way. Specifically, the strange metal in the cuprates displays a robust, but extremely mysterious, resistivity that is linear in temperature [78]: $\rho \sim T$. Remarkably, this anomalous behavior persists from T_c all the way up to

⁷While for many years the cuprates were synonymous with high- T_c , they have recently been joined by a new class of iron-based materials known as the “pnictides” which also exhibit unconventional superconductivity [75].

temperatures on the order of several hundreds of kelvin. Furthermore, angle-resolved photoemission spectroscopy (ARPES) measurements [79] indicate a complete lack of coherent Landau quasiparticles: $Z \rightarrow 0$. Based on these facts alone, the strange metal cannot possibly be described as a traditional Landau Fermi liquid [3].

It is important to note that the superconductor itself develops out of the normal state, i.e., the strange metal (or the pseudogap) in the case of the cuprates⁸. Therefore, in analogy with understanding a conventional BCS superconductor as a (marginal) low-temperature instability of the Landau Fermi liquid [81], it is reasonable to believe that we may be able to understand high-temperature superconductivity, say in the cuprates, as a natural instability of some more exotic *non-Fermi liquid* quantum state. While finite-temperature non-Fermi liquid behavior is often associated with a quantum critical point, as in the case of the heavy fermion materials [5, 6], recent evidence suggests that this may not be the correct approach for the cuprates; instead the strange metal may actually be an *extended* quantum phase [78, 80]. One is then faced with the task of constructing a theory for a zero-temperature non-Fermi liquid metal that is likely inherently strongly interacting and not continuously connected to any weakly interacting state. Historically, this has been a nearly impossible task [51, 52, 81].

In Chapter 4 and Ref. [82], we succeed in constructing a concrete theory for a particular example of a two-dimensional non-Fermi liquid quantum phase—the “*d*-wave metal”—and present numerical evidence for its stability in a reasonable microscopic model in quasi-one dimension. However, we do not at the moment claim any particular relevance to *the* strange metal of the cuprates. Still, being basically the first of its kind, we believe that this study

⁸These states are called “normal” because they are not superconducting, yet they are highly abnormal in character [80].

represents a significant advance in our conceptual understanding of such strongly interacting non-Fermi liquids. Only through time and future work will we be able to determine its true applicability to real materials.

1.2 Parton Constructions and Gauge Theories

A common theme present in all results contained in this dissertation is the use of “slave particles” or “partons” for describing the low-energy physics of a given quantum phase. Within such constructions, we take the physical operator of interest, e.g., the electron operator or spin operator, and write it in terms of a new set of (slave) operators. The hope is that such a change of variables will be useful in describing the low-energy behavior of a given physical system, say of a model Hamiltonian or of an actual experiment. Such descriptions lead to a local redundancy in the definition of the physical operators and this necessitates the introduction of an appropriate gauge field in the action. It is this gauge field which is responsible for “gluing” the partons back together to recover the physical Hilbert space of the problem.

What often happens is that this gauge theory is in its *confined* phase, i.e., the partons are at all energies bound together in analogy with quark confinement in QCD [83]. However, if we are lucky, we may find the system in its *deconfined* phase, a truly strongly interacting many-body state. The partons at low energies then obtain a life of their own and affect the physical system in interesting and perplexing (gauge-invariant) ways; our change of variables has thus proven useful, and we typically anoint the phase as “exotic”. We note that it has in the past been rather difficult to use such an approach to have meaningful say about a given, specific microscopic Hamiltonian, say the Hubbard model or Heisenberg model on some lattice. However,

in recent years, we have been successful in reverse engineering reasonable candidate microscopic models which indeed happen to subsequently show strong numerical evidence for such exotic behavior (see Chapter 4 and Refs. [84, 85, 86, 82]). Such numerical verification is an extremely important step in establishing the validity of the parton approach; it is only then that the partons seem “real”.

We now briefly illustrate the above considerations in an example directly relevant to the two-dimensional versions of the exotic states at the focus of Chapters 2 and 4: the electronic spin Bose metal and electronic d -wave metal, respectively. This type of construction, which goes by the name “slave-boson”, dates back to the earliest days of theories on the cuprates [51, 52]. We begin by writing the electron operator at lattice site i as product of a spinless bosonic operator carrying the physical charge of the electron (“chargon”) and a neutral fermionic operator carrying its spin $\alpha = \uparrow, \downarrow$ (“spinon”):

$$c_{i\alpha} = b_i f_{i\alpha}, \quad (1.3)$$

This decomposition is invariant under *local* U(1) phase rotations, $b_i \rightarrow e^{i\phi_i} b_i$ and $f_{i\alpha} \rightarrow e^{-i\phi_i} f_{i\alpha}$, and thus we must couple the chargons and spinons to an emergent U(1) gauge field; under this gauge field a_μ , the b and f partons carry opposite gauge charge ± 1 . Depending on context, b_i may be taken to be, for example, a rotor $b_i = e^{i\varphi_i}$ when treating the electronic Mott transition [60, 50, 61] or a hard-core boson $(b_i^\dagger)^2 = 0$ for doped strongly interacting models relevant to the cuprates [34].

For concreteness, we now focus on the former and write down an appropriate (2+1)D action [50] for the Mott transition in the organic spin liquids using this framework (similar considerations apply to doped models [34]; see Chapter 4). In this case, following Senthil [61] and

passing to the continuum limit, we have

$$S = S_b + S_f + S_{bf} + S_a , \quad (1.4)$$

where

$$S_b = \int d^2r d\tau [|(\partial_\mu - ia_\mu)b|^2 + V(|b|^2)] , \quad (1.5)$$

$$S_f = \int_{\mathbf{r},\tau} \bar{f}(\partial_\tau - \mu_f + ia_0)f + \int_{\mathbf{k},\omega} \bar{f}_{\mathbf{k},\omega} \epsilon_{\mathbf{k}+\mathbf{a}}^f f_{\mathbf{k},\omega} , \quad (1.6)$$

are the respective actions for the chargons and spinons; S_{bf} represents residual short-range density-density interactions between the chargons and spinons; and $S_a \sim \int_{\mathbf{r},\tau} (\epsilon_{\mu\nu\lambda} \partial_\nu a_\lambda)^2$ is the Maxwell term for the U(1) gauge field, which in this situation it is reasonable to take as noncompact [87, 88]. For $V(|b|^2)$, we can take the standard ‘‘Mexican hat’’ form: $V(|b|^2) = r|b|^2 + u|b|^4$.

We then have two drastically different situations depending on if the bosons condense into a superfluid, $\langle b \rangle \neq 0$, or if they localize into a unit filled bosonic Mott insulator, $\langle b \rangle = 0$. Since the boson is charged under a_μ , spontaneously breaking the U(1) symmetry associated with chargon number conservation, i.e., $\langle b \rangle \neq 0$, leads to a mass term for the gauge field via the usual Higgs mechanism [89]. In this case, as the f ’s fill a Fermi sea, our action S describes an ordinary electronic Fermi liquid. This is the confined phase of the theory [90] in which the chargons and spinons are tightly bound together; thus, with respect to the realized quantum phase itself, our change of variables in Eq. (1.3) was not particularly useful⁹. If, on the other hand, the chargons are in a gapped Mott insulator so that $\langle b \rangle = 0$, the situation is completely different. We can then integrate out the b ’s from the action, and the resulting theory is precisely

⁹It is, however, very useful for describing the Mott *transition* out of the Fermi liquid [61].

that of a half-filled Fermi sea of spinons coupled to a U(1) gauge field, the exotic “spin Bose metal” insulator introduced in Sec. 1.1.1 above. While the system is a charge insulator, it still “knows about” the Fermi statistics of the electron through the remaining gapless fermionic spinons. And although it has a finite charge correlation length, this insulator qualitatively resembles the Fermi liquid metal in basically all other physical properties, even in the response of the electron density at finite wavevectors [91]!

Within this general framework, we can also naturally describe exotic *conducting* non-Fermi liquid states if we could somehow put the b ’s into an uncondensed, yet conducting, Bose fluid with $\langle b \rangle = 0$, i.e., a “Bose metal”¹⁰. We take this approach in Chapter 4 and Ref. [82], where following Refs. [92, 84, 86], we further decompose the (hard-core) bosonic chargon into two more slave fermions, $b = d_1 d_2$, giving a novel *three-fermion* decomposition of the electron: $c_\alpha = d_1 d_2 f_\alpha$. The resulting theory now includes two U(1) gauge fields and two extra emergent Fermi surfaces (from d_1 and d_2). As detailed in Chapter 4, this is a truly remarkable phase of quantum matter, the non-Fermi liquid “ d -wave metal”.

1.3 Multileg Ladders: Bosonization and the Density Matrix Renormalization Group

Full two-dimensional (2D) gauge theories of the typed sketched above have traditionally been approached analytically within certain random phases approximation (RPA) [93, 94, 95, 52, 53] and large- N approaches [55, 54, 96]. However, recent groundbreaking work [97, 98] has called into question the general reliability of these early results, requiring the invention of

¹⁰Not to be confused with the Mott insulating “spin Bose metal”.

novel techniques to be able to make controlled expansions in some instances [99, 56, 57].

In Chapters 2 and 4, we take a completely different and complementary approach by exploring analogs of the electronic spin Bose metal and *d*-wave metal phases in quasi-one-dimensional (quasi-1D) *ladder* systems (see also Refs. [100, 84, 58, 85, 59, 86, 82]). In this lower-dimensional setting, we have access to extremely powerful and fully controlled analytical and numerical machinery, namely bosonization and the density matrix renormalization group, respectively. While both of these methods can be rather involved on a technical level, we here only briefly summarize the main points as pertinent to the results of Chapters 2 and 4.

Bosonization [101, 102, 103, 104, 105, 4] exploits the *bosonic* nature of particle-hole excitations in one dimension to provide a controlled field theoretic description of the universal low-energy physics of one-dimensional (1D) interacting fermions purely in terms of bosonic degrees of freedom¹¹. Remarkably, the technique allows us to represent both the kinetic energy and, nonperturbatively, the forward scattering interactions of a single one-dimensional band of spinless fermions as a single massless, collective (1+1)D boson represented by a pair of dual bosonic fields (θ, φ) . More specifically, the Hamiltonian for the massless boson reads

$$\mathcal{H} = \frac{v}{2\pi} \left[\frac{1}{g} (\partial_x \theta)^2 + g (\partial_x \varphi)^2 \right], \quad (1.7)$$

where v is the velocity of the collective excitation and g is the corresponding *Luttinger parameter* which encodes the forward scattering interactions. For noninteracting fermions, the Luttinger parameter is trivial, $g = 1$, and the velocity is simply the Fermi velocity, $v = v_F$. Forward scattering interactions will renormalize the velocity v as well as the Luttinger parameter such that $g < 1$ ($g > 1$) corresponds to repulsive (attractive) interactions; however, these

¹¹Since the excitation spectrum of such interacting one-dimensional systems is qualitatively similar to that of an exactly soluble model first considered by Luttinger [106], Haldane [107, 101, 102] called such states *Luttinger liquids* in analogy with Fermi liquids which are the interacting generalization of the soluble free Fermi gas.

four-fermion interactions are still quadratic in terms of the bosons¹². Hence, we remarkably have complete access to the *interacting* fermionic system in terms of a simple (1+1)D *Gaussian* bosonic field theory.

In terms of θ and φ , the slowly varying (relative to the interparticle spacing $\sim 1/k_F$) part of the (spinless) electron operator near the Fermi points $\pm k_F$ reads

$$c_P \sim e^{i(\varphi + P\theta)}, \quad (1.8)$$

where $P = R/L = \pm$ corresponds to electrons near $+k_F$ (“right movers”) and $-k_F$ (“left movers”), respectively. Starting on a lattice, Eq. (1.8) can be motivated in a physically transparent way [102, 103, 105] by performing a Jordan-Wigner transformation on a system of 1D spinless electrons: $c_i \rightarrow \exp \left[i\pi \sum_{j < i} n_j \right] b_i$, where b_i is a hard-core boson operator and $n_i = b_i^\dagger b_i = c_i^\dagger c_i$. We can then proceed by representing the boson in terms of its density and phase: $b_i \rightarrow \sqrt{n_i} \exp(i\varphi_i)$. Passing to the continuum limit, i.e., focusing on scales much longer than the lattice spacing, we can represent the slowly varying part of the electron density as $n(x) = n_0 + \delta n(x) = k_F/\pi + \partial_x \theta/\pi$, where $n_0 = k_F/\pi$ is the mean electron density and $\theta(x)$ is a phonon displacement field such that its derivative measures density fluctuations: $\delta n(x) = \partial_x \theta/\pi$. Furthermore, we simply identify $\varphi(x)$ as the appropriate phase field. In conjunction with the Jordan-Wigner representation, these considerations give precisely the result (1.8) (see also Ref. [105]).

Furthermore, the density-phase uncertainty relation, $[\delta n(x), \varphi(x')] = i\delta(x - x')$, suggests that θ and φ must satisfy

$$[\varphi(x), \theta(x')] = i\pi\Theta(x - x'), \quad (1.9)$$

¹²This is actually rather obvious; a less trivial result [4] concerns our ability to represent the *kinetic energy* of 1D Dirac fermions in the form (1.7).

i.e., $\partial_x \theta$ is canonically conjugate to φ , while $\partial_x \varphi$ is canonically conjugate to θ . This provides full meaning to our Hamiltonian Eq. (1.7) above and allows us to obtain a Lagrangian emphasizing either θ or φ , by integrating out the conjugate field from $\mathcal{L} = \mathcal{H} + \frac{i}{\pi}(\partial_x \theta)(\partial_\tau \varphi)$. For θ , we have

$$\mathcal{L} = \frac{1}{2\pi g} \left[\frac{1}{v} (\partial_\tau \theta)^2 + v (\partial_x \theta)^2 \right], \quad (1.10)$$

while the corresponding Lagrangian for φ is simply (1.10) with $\theta \rightarrow \varphi$ and $g \rightarrow 1/g$.

Generalization of the above Abelian bosonization to systems with spin and multiple bands is straightforward (see Appendix B). However, in contrast to simple forward scattering, various interaction terms in the fermion language—namely backscattering and umklapp ones—produce cosines of the bosonized fields and thus interact beyond quadratic order. When relevant in the renormalization group (RG) sense, these terms open gaps in the system and qualitatively change the nature of the quantum phase, although in a way which is often made physically transparent by the bosonization [108, 104]. All in all, formulating the low-energy physics of interacting 1D or quasi-1D fermionic systems in terms of collective bosonic modes is an extremely powerful and ultimately very intuitive technique. It is one that we employ extensively in Chapters 2 and 4 (and the corresponding Appendices B and D) as applied to quasi-1D studies of the exotic spin Bose metal spin liquid and d -wave metal non-Fermi liquid.

On the numerical front, the density matrix renormalization group (DMRG) [109, 110, 111, 112] stands alone as by far the most successful approach for 1D lattice systems with or without a sign problem [113]. In fact, it has recently been applied to ladders so wide ($\sim 10\text{-}20$ legs) [114] that they are believed to capture the full 2D physics of several long-standing problems in quantum magnetism, including the kagome lattice Heisenberg model [115, 116, 21]

and the square lattice J_1 - J_2 model [117, 118]. The essence of DMRG lies in its ability to efficiently truncate the exponentially large many-body Hilbert space¹³ in a specific way which is optimal for representing the ground state and low-lying excited states of local Hamiltonians in one dimension. We now briefly describe the specifics of how this is done.

Traditional implementation follows the original formulation of White [109, 110, 111], in which one partitions the lattice into two halves, say A and B , and then traces out one half of the system thereby obtaining a reduced density matrix for the other half, say $\rho = \text{Tr}_B |\Psi\rangle\langle\Psi|$. Here, $|\Psi\rangle$ is an approximate representation of the ground state of our Hamiltonian H which in practice is obtained previously through an iterative sweeping procedure. We then fully diagonalize ρ and retain only its m largest-weight eigenvectors, which we subsequently use to represent all operators associated with region A . This step gives DMRG its name in that it renormalizes the Hilbert space (since generally the rank of ρ will be larger than m) based on the eigenspectrum of the reduced density matrix. We then use this new truncated basis to perform large-sparse matrix diagonalization of H , e.g., using the Lanczos algorithm [119], to find a new and better approximation for $|\Psi\rangle$. In practice, at each step we must keep two sites free, i.e., in their original bases, which allows a significant Hilbert space truncation to occur, and through “sweeping” these two free sites back and forth through the lattice we are able to get better and better representations of the “environment” basis representing states in region B . It can be shown that truncating the Hilbert space based on the largest-weight eigenstates of ρ is *optimal* in representing expectation values, the ground state wave function, and entanglement in the full L site system [111]. The method is often termed *quasi-exact* because for a large enough number of basis states m we can obtain results, e.g., ground state energy, expectation

¹³For a spin-1/2 system of L sites and ignoring conservation laws, the Hilbert space dimension is 2^L .

values, etc., arbitrarily close to the exact values.

For all DMRG results presented in this dissertation, we use the “classic” formulation of the algorithm as summarized in the previous paragraph. However, in the past ten years, input from the quantum information community has led an explosion in understanding of the underlying structure of the wave functions produced by DMRG [120, 121, 122]. In particular, it is now widely appreciated that DMRG is actually a variational method for a specific class of wave functions known as *matrix product states* (MPS) [112], a concept which has been reinvented many times over in the last two decades [123, 124, 125, 120, 121, 122, 126]. In an MPS representation of a many-body state $|\Psi\rangle = \sum_{i_1, \dots, i_L} c_{i_1, \dots, i_L} |i_1, \dots, i_L\rangle$, we write the coefficients c_{i_1, \dots, i_L} as a product of L matrices A^{i_j} each of dimension $m \times m$ (m is usually called the “bond dimension”)¹⁴:

$$c_{i_1, \dots, i_L} = A^{i_1} A^{i_2} \cdots A^{i_{L-1}} A^{i_L}. \quad (1.11)$$

The DMRG algorithm is ultimately a way of efficiently optimizing over the elements of the matrices A^{i_j} [122]. In fact, most modern-day implementations of the algorithm explicitly work with the matrices A^{i_j} , which makes the codes more flexible and versatile [112, 127]. On the other hand, the MPS structure is only an implicit feature in the more classic implementations as summarized above [111].

Perhaps the most important conceptual development spawned by the MPS perspective of DMRG lies in its ability to classify when the algorithm works and when it does not. These days, DMRG is best thought of as a *low-entanglement* approximation of the ground state. Specifically, the number of basis states (or bond dimension) m required to obtain a given

¹⁴To obtain a scalar c_{i_1, \dots, i_L} , for periodic boundary conditions, we take a trace of the full matrix product, while for open boundary conditions, A^{i_1} and A^{i_L} are taken to be m -dimensional vectors.

accuracy grows exponentially with the amount of entanglement, $S = -\text{Tr}(\rho \log \rho)$, between regions A and B : $m \sim e^S$. For gapped 1D systems with an “area law” for the entanglement entropy, $S \sim \text{const.}$, so that m is independent of system size L . On the other hand, for gapless 1D or quasi-1D systems with an entanglement entropy scaling¹⁵ $S \sim \frac{c}{3} \log L$ [128], we have $m \sim L^{c/3}$. The number c is known as the *central charge*, and it directly counts the number of 1D gapless modes of the realized Luttinger liquid [see Eq. (1.10)]. Therefore, scaling of m is at worst a power law in the system length L ; this permits the study of rather large system sizes, often on the order of hundreds or thousands of sites.

However, exotic 2D phases such as the spin Bose metal and d -wave metal at the focus of Chapters 2 and 4 are actually highly entangled quantum states and are thus very challenging for the DMRG algorithm. Due to the underlying Fermi surfaces [129, 130] in the low-energy description of these phases [49, 92], we expect that when placed on an N -leg ladder the number of gapless modes grows linearly with N , i.e., $c \sim N$. Hence, the required number of basis states grows exponentially with the number of legs and with a base proportional to the longitudinal length: $m \sim L^N$. This is clearly computationally prohibitive for a large number of legs, and for these states we are typically only able to reliably study ladder systems of width $N \sim 2, 3, 4$. In fact, the electronic problems presented in Chapters 2 and 4 are already extremely computationally challenging on $N = 2$ -leg ladders. Remarkably, however, even on such narrow systems we are able to clearly see descendants of the exotic 2D physics at play.

¹⁵This is for periodic boundary conditions; for open boundary conditions, we have $S \sim \frac{c}{6} \log L$.

1.4 Variational Monte Carlo: Modeling Exotic Many-Body States with Projected Wave Functions

Although DMRG and its two-dimensional generalizations [131, 132] are variational in nature¹⁶, when compared to famous variational wave functions such as those of BCS [35, 36] or Laughlin [137], they are hardly intuitive from a physical point of view. Therefore, it is very desirable to be able to compare unbiased, quasi-exact methods such as DMRG with results from a set of more tangible trial wave functions. Such a class of methods goes by the name *variational Monte Carlo* (VMC), so-called since due to the many-body nature of the problem we must use Monte Carlo importance sampling when actually calculating properties of our trial wave functions [138, 139, 140]. Furthermore, although they are by construction very biased, VMC methods are really the only available choice when attacking sign-problem plagued Hamiltonians in full 2D. With judiciously chosen trial wave functions, however, VMC can be exceedingly useful in understanding the low-energy behavior of a given model Hamiltonian or even a real experiment.

Luckily, the low-energy physics of exotic gauge theories such as those discussed in Sec. 1.2 can often times be faithfully represented by starting with a weakly interacting (or noninteracting) state determined from the postulated emergent degrees of freedom, and simply projecting out those parts of the wave function not in the physical Hilbert space¹⁷. For example, as in Chapter 3, the weakly interacting wave function may be a single BCS determinant (see Ap-

¹⁶The latter of which are still not equipped to address the most entangled quantum states [133, 134, 135, 136].

¹⁷This goes by the name ‘‘Gutzwiller projection’’, and although it generally captures the essential physics of the corresponding gauge theory, it has been known to fail in reproducing correct long-distance physics in some cases [141].

pendix C) after which we project out all doubly-occupied sites to model various spin liquid states. Similarly, in Chapter 4, we construct conducting non-Fermi liquid electronic wave functions by taking an appropriately projected product of three Slater determinants which correspond to the underlying fermionic partons in the $c_\alpha = d_1 d_2 f_\alpha$ construction (see Sec. 1.2). In the former case, we use VMC to argue in favor of a particular new ground state for the organic spin liquid materials described above, while in the latter case, we use it to help us understand in detail the non-Fermi liquid ground state of a particular model Hamiltonian of strongly interacting electrons. All in all, VMC serves as a bridge connecting low-energy effective field theories with numerics and/or experiment and is thus an invaluable method for the types of problems addressed in the remainder of this dissertation.

1.5 Outline and Remarks

The remainder of this dissertation is organized as follows. In Chapter 2, we present a DMRG and bosonization study of the continuous Mott metal-insulator transition between a two-band metal and a two-band descendant of the spin Bose metal as discussed above; this work is currently under review, and the preprint is available at Ref. [142]. In Chapter 3, we propose a new state to describe the low-energy behavior of κ -(BEDT-TTF)₂Cu₂(CN)₃ and EtMe₃Sb[Pd(dmit)₂]₂ and show that our state has very competitive variational energy in an appropriate spin model; this work has been published previously in Ref. [143]. In Chapter 4, we construct a theory for a concrete realization of a conducting non-Fermi liquid fluid, the *d*-wave metal, and present extensive evidence for its stability as the ground state of a reasonably simple microscopic model on the two-leg square ladder; this work has been published previously in

Ref. [82]. Finally, in Chapter 5, we conclude and speculate on where the field of strongly correlated electrons may be headed in the years to come.

This dissertation contains four appendices. Appendix A contains some general details regarding the numerical calculations pertinent to Chapters 2, 3, and 4; much of this discussion was taken from the appendices of Refs. [142], [143], and [82], respectively. Appendix B contains details of the bosonization and Luttinger liquid physics as relevant to Chapter 2; this material was taken from the Supplementary Information of Ref. [142]. In Appendix C, we spell out details of the determinantal representation of the BCS wave functions used in Chapter 3. Finally, in Appendix D, using bosonization we present a stability analysis of a new *d*-wave metal phase on the two-leg ladder which is qualitatively distinct from that at the focus of Chapter 4 (central charge $c = 5$ versus $c = 3$).

Chapter 2

A Continuous Mott Transition Between a Metal and a Quantum Spin Liquid

2.1 Background and Introduction

Strongly correlated electronic systems may have insulating phases that originate entirely from electron-electron interactions¹. These insulators, and their phase transitions to metallic phases have a long history reaching back into the pioneering work of Mott [10, 11]. However, despite decades of study, metal-insulator transitions driven by strong correlations—Mott’s namesake—remain rather poorly understood. Central to this difficulty is the fact that Mott transitions exhibit strong quantum fluctuations, which can inherit correlations from both the adjacent metallic and insulating phases. Thus, the nature of the Mott transition may depend crucially on the properties of each of these phases.

¹Excerpts and figures appearing in this chapter are reprinted from R. V. Mishmash, I. González, R. G. Melko, O. I. Motrunich, and M. P. A. Fisher, arXiv:1403.4258 [cond-mat.str-el].

Conventional insulating phases, such as those with magnetic long-range order, appear to predominantly give rise to first-order Mott transitions, as has been observed in a number of experimental systems in the past [144, 145, 146, 147, 148]. The reason for first-order behavior is simple: The properties of *both* the spin and charge sectors change qualitatively at the transition, the former developing magnetic long-range order and the latter localizing to form an insulating state. In contrast, systems that harbor unconventional, exotic insulating phases showing no symmetry breaking down to zero temperature—so-called quantum spin liquids [18, 23, 34, 17]—offer a promising playground for finding the long-sought-after continuous Mott transition. For example, one beautiful possibility is that the spin sector on the insulating side may be described by a spinon Fermi surface coupled to a U(1) gauge field [50] (the so-called “spin Bose metal” [58]). In this case, the behavior of the spin correlations would be qualitatively unchanged [49] upon crossing the transition, making the nature of the transition determined entirely by the charge sector. Thus, as proposed in Refs. [60, 61, 149], perhaps the electronic Mott transition in d spatial dimensions can be in the $(d + 1)$ D XY universality class, the same as obtained for bosons [62]!

Fortunately, this sort of physics is more than just a theorist’s dream, as recently several experimental groups have found strong evidence for spin-liquid behavior proximate to a Mott transition in two separate quasi-two-dimensional triangular lattice organic materials. In 2003, a putative spin-liquid phase in κ -(BEDT-TTF)₂Cu₂(CN)₃ was discovered [24], which is insulating at ambient pressure with no apparent long-range order but can indeed be driven metallic by application of moderate pressure [25]. More recently, Itou *et al.* found a spin-liquid candidate in EtMe₃Sb[Pd(dmit)₂]₂ [27]. Further experiments indicated the existence of highly mobile

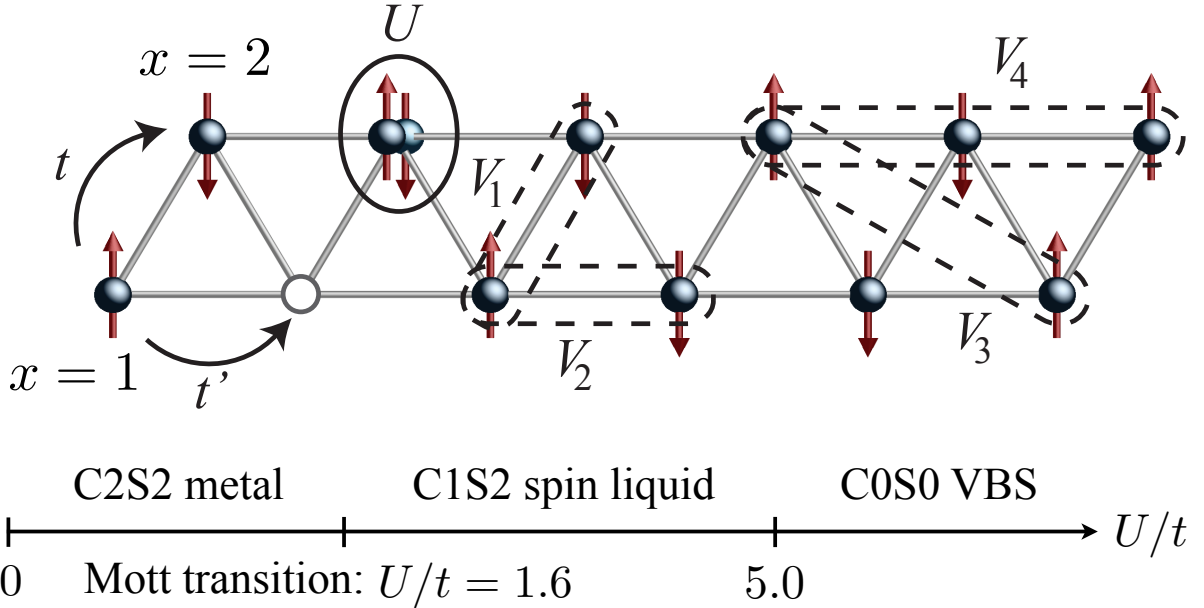


Figure 2.1: *Schematic of the half-filled extended Hubbard model on the two-leg triangular strip and its phase diagram.* Top: Our electronic model contains electron hoppings t and t' in addition to repulsive Hubbard interactions up to fourth neighbor [see Eqs. (2.1)-(2.2)]. As shown, we view the two-leg triangular strip as a 1D chain and attack the problem with DMRG and bosonization. Bottom: The phase diagram of our model as a function U/t for the chosen characteristic parameters (see text).

gapless spin excitations in both compounds [44, 47], although the precise nature of the spin excitations in κ -(BEDT-TTF)₂Cu₂(CN)₃ at the lowest temperatures is still highly controversial [48]. These findings suggest that the spin Bose metal is likely a good starting point for understanding the spin-liquid behavior observed in these two materials [50, 49]. In addition, the pressure-induced Mott transition from the metal to the spin liquid is observed to be either only very weakly first order [25], or perhaps even continuous [150].

Motivated by these experiments, we consider a model of interacting electrons on a half-filled triangular lattice “strip” geometry (see Fig. 2.1), which we solve using large-scale density matrix renormalization group (DMRG) calculations. By increasing the strength of the repulsive electron-electron interactions, we drive the ground state of the system from a metallic Fermi

liquid-like phase to an insulating phase identified as the electronic spin Bose metal [50, 151] via an intervening continuous Kosterlitz-Thouless-like quantum phase transition. Further increasing the electron interactions eventually drives the system into a spin-gapped valence bond solid (VBS) insulator—the phase realized by the effective Heisenberg spin model that our half-filled electronic model approaches at strong repulsion. Our calculations thus represent a direct quasi-one-dimensional (quasi-1D) analog of tuning a two-dimensional (2D) half-filled Hubbard-type model from a metal to a quantum spin liquid to a conventional ordered phase via increasing overall electron repulsion [152, 153, 154, 155], a result with clear potential relevance to the Mott physics observed in the organic spin liquid materials [25].

2.2 Extended Hubbard Model on the Two-Leg Triangular Strip

The most appropriate microscopic model for the triangular-lattice organic materials is a Hamiltonian consisting of electron hopping plus moderately strong, possibly extended [156], Coulomb repulsion. As is well-known from some 30 years of research on the high-temperature cuprate superconductors [34], such a model does not succumb easily to either exact analytical field theory nor direct numerical simulations in two dimensions due to the fermionic “sign problem”.

Recently, some of us have proposed a novel approach to the 2D limit of such models through a sequence of studies on quasi-1D ladder geometries, which have the significant advantage that they can be solved exactly with DMRG [109]. Sheng *et al.* used this line of attack

to extensively study an effective spin model appropriate for the “weak” Mott insulating regime of the organic materials [49, 153] and indeed found exceptionally strong evidence that quasi-1D descendants of the spin Bose metal exist as the ground state over a large region of the phase diagram [58, 59]. The low-energy degrees of freedom of this exotic spin liquid are modeled as mobile and charge-neutral spin-1/2 fermionic spinons coupled to a U(1) gauge field. In 2D, these gapless spinons give rise to a spin structure factor with power-law singularities residing on an entire “Bose surface” in momentum space. However, in quasi-1D the Bose surface is reduced to a set of points, so that quasi-1D descendants of the 2D spin liquid are dramatically recognizable on ladders, making the quasi-1D approach very fruitful [58, 59, 86, 82].

Inspired by these recent developments and restricting ourselves to the two-leg triangular strip for numerical tractability, we consider the following extended Hubbard model (see Fig. 2.1):

$$H = - \sum_{x,\alpha} [t c_\alpha^\dagger(x) c_\alpha(x+1) + t' c_\alpha^\dagger(x) c_\alpha(x+2) + \text{H.c.}] + \frac{1}{2} \sum_{x,x'} V(x-x') n(x) n(x'), \quad (2.1)$$

where $c_\alpha(x)$ destroys an electron at site x with spin $\alpha = \uparrow, \downarrow$, $n(x) \equiv \sum_\alpha c_\alpha^\dagger(x) c_\alpha(x)$ is the electron number operator, and we take the system to be half-filled with one electron per site.

In the usual on-site Hubbard model, we would have $V(x-x') = U\delta_{x,x'}$. However, inspired by the results of Ref. [151], we allow for longer-ranged repulsion in our Hamiltonian. For

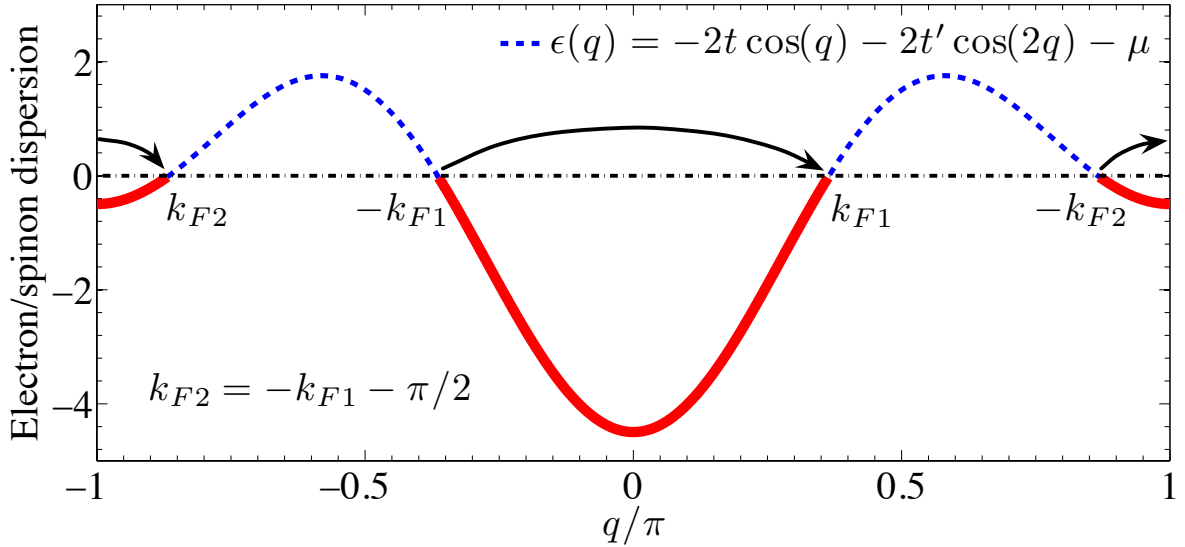


Figure 2.2: *Electron/spinon bands on the two-leg triangular strip.* In the noninteracting $U/t = 0$ limit, the ground state of our model for $t'/t > 0.5$ consists of two disconnected Fermi seas (bands) with Fermi points as labeled above. On the other hand, the insulating two-band spin Bose metal can be modeled, in a pure spin system, by Gutzwiller projecting the same band structure (see Ref. [58]). Here, we realize a continuous Mott transition between these two phases driven at strong interactions by an eight-fermion umklapp term which scatters both spin-up and spin-down electrons across each Fermi sea (black arrows).

concreteness, we take the following model potential:

$$V(x - x') = \begin{cases} U & , \quad |x - x'| = 0 \\ \kappa U e^{-\gamma|x-x'|} & , \quad 1 \leq |x - x'| \leq 4 \\ 0 & , \quad |x - x'| > 4. \end{cases} \quad (2.2)$$

The reasoning for considering such longer-ranged repulsion in the model Hamiltonian is twofold. First, such terms are well-motivated by recent ab initio calculations [156], which indicate a substantial long-ranged tail in the effective screened Coulomb repulsion appropriate for κ - $(\text{BEDT-TTF})_2\text{Cu}_2(\text{CN})_3$. Second, on the two-leg ladder, such terms fight the spin-gap tendencies present in the metallic phase of the t - t' - U Hubbard model (i.e., our model with $\kappa = 0$; see, for example, Refs. [108, 157, 158]), thus at least allowing for the possibility of a direct,

continuous transition between a spin gapless two-band metal and two-band spin Bose metal spin liquid [151]. Guided by the weak and intermediate coupling analysis of Ref. [151], in what follows we choose characteristic parameters $t'/t = 0.8$, $\kappa = 0.5$, and $\gamma = 0.2$, leaving the single dimensionless ratio U/t to control the overall strength of electron repulsion.

2.3 Mott Metal-Insulator Transition and Realization of the Electronic Spin Bose Metal

We first sketch the low-energy effective theory describing the putative metal to spin Bose metal transition and then present strong numerical evidence that this exotic scenario is indeed realized. In the absence of interactions ($U/t = 0$), our model for $t'/t > 0.5$ simply describes two bands of noninteracting spinful electrons (see Fig. 2.2). Importantly, the weak-coupling analysis of Ref. [151] indicates that this spin gapless two-band metallic state—so-called C2S2 in the literature, where $\text{CaS}\beta$ denotes a Luttinger liquid with α gapless charge modes and β gapless spin modes [108]—is stable in our extended Hubbard model, Eqs. (2.1)-(2.2), in the presence of infinitesimal U/t . At half-filling, there is an allowed *eight-fermion* umklapp term in our two-band system (see Fig. 2.2). Bosonizing (see, e.g., Refs. [102, 104, 105, 4]) this interaction gives

$$\mathcal{H}_8 = 2u \cos(4\theta_{\rho+}), \quad (2.3)$$

where $\theta_{\rho+}$ is the density field for the overall charge mode, i.e., $\delta n(x) = 2\partial_x\theta_{\rho+}/\pi$ is the coarse-grained electron density. Assuming the C2S2 metal is stable against opening of a spin gap [151], then the fixed-point Lagrangian $\mathcal{L}_{\text{C2S2}}$ involves four gapless bosonic modes, one

being $\theta_{\rho+}$ (see Appendix B and Ref. [151] for details). For free electrons, the scaling dimension of the eight-fermion umklapp term is $\Delta[\mathcal{H}_8] = 4 > 2$, so that \mathcal{H}_8 is strongly irrelevant at weak coupling. However, increasing U/t in our microscopic model will feed into “stiffening” $\theta_{\rho+}$ in $\mathcal{L}_{\text{C2S2}}$, thus decreasing $\Delta[\mathcal{H}_8]$. Eventually $\Delta[\mathcal{H}_8] = 2$, beyond which the umklapp is relevant so that u grows at long scales pinning $\theta_{\rho+}$ into one of the minima of the cosine potential in \mathcal{H}_8 . The resulting phase is a remarkable C1S2 Luttinger liquid, which is precisely the electronic spin Bose metal [58], where the remaining “charge mode” does not transport charge along the ladder but rather represents local current loop fluctuations.

The critical theory describing the C2S2 \rightarrow C1S2 metal-insulator transition is a sine-Gordon-like theory [159], with a technical complication arising because $\theta_{\rho+}$ is coupled to the “relative charge” field $\theta_{\rho-}$ in $\mathcal{L}_{\text{C2S2}}$ (see Appendix B.2). Nonetheless, the transition is still Kosterlitz-Thouless-like [160] [(1 + 1)D XY] and represents a direct, nontrivial two-leg analog of the (2 + 1)D scenario recently proposed by Senthil [61, 149].

We now present our numerical results, giving strong evidence that the above scenario is actually realized. To numerically characterize the system, we focus on four main quantities: the density structure factor $\langle \delta n_q \delta n_{-q} \rangle$, the spin structure factor $\langle \mathbf{S}_q \cdot \mathbf{S}_{-q} \rangle$, the dimer structure factor $\langle \mathcal{B}_q \mathcal{B}_{-q} \rangle$, and the electron momentum distribution function $\langle c_{q\alpha}^\dagger c_{q\alpha} \rangle$, where δn_q , \mathbf{S}_q , \mathcal{B}_q , and $c_{q\alpha}$ are the Fourier transforms of the local operators $\delta n(x) \equiv n(x) - \langle n(x) \rangle$, $\mathbf{S}(x) \equiv \frac{1}{2} \sum_{\alpha,\beta} c_\alpha^\dagger(x) \boldsymbol{\sigma}_{\alpha\beta} c_\beta(x)$, $\mathcal{B}(x) \equiv \mathbf{S}(x) \cdot \mathbf{S}(x + 1)$, and $c_\alpha(x)$, respectively. In the data presented here, we consider systems up to $L = 96$ sites with periodic boundary conditions. (See Appendix A.1 for all details, including discussion of boundary conditions and convergence, as well as Appendix B.4 for further complementary data.)

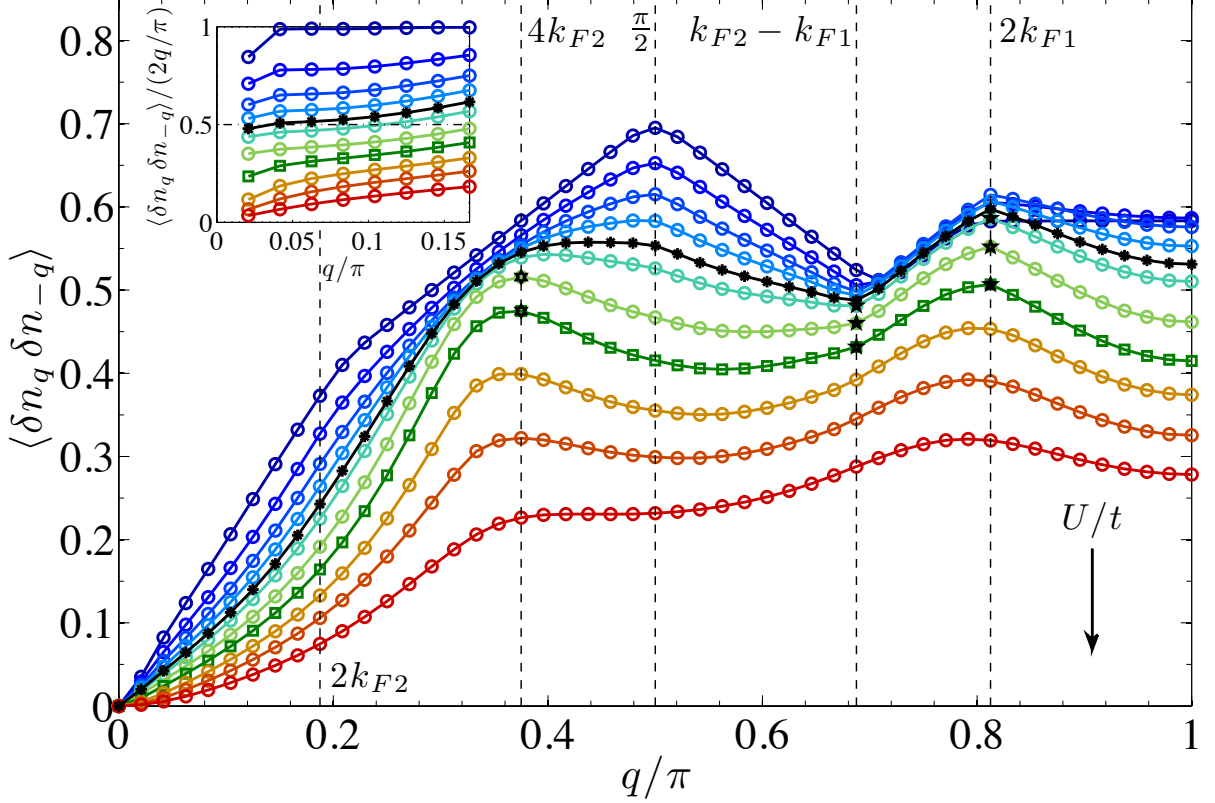


Figure 2.3: *Density structure factor: Locating the Mott transition and power-law Friedel oscillations in a Mott insulator.* Measurements of the density structure factor, $\langle \delta n_q \delta n_{-q} \rangle$, allow us to locate the Mott transition near $U/t = 1.6$ (black curve with * symbols). The onset of the Mott transition occurs when the overall charge Luttinger parameter $g_{\rho+}$ drops below 1/2. We measure $g_{\rho+}$ via the slope of $\langle \delta n_q \delta n_{-q} \rangle$ at $q = 0$, as shown in the inset [see Eq. (2.4)]. For $U/t > 1.6$, the system is insulating, yet displays power-law singularities in $\langle \delta n_q \delta n_{-q} \rangle$ at finite wavevectors [91] (see black * and hexagram symbols). Data correspond to a system of length $L = 96$ with $U/t = 0, 0.4, 0.8, 1.2, 1.6, 2.0, 3.0, 4.0, 5.0, 6.0, 7.0$ (from top to bottom, blue to red).

We focus first on the density (charge) structure factor $\langle \delta n_q \delta n_{-q} \rangle$. A crucial aspect of $\langle \delta n_q \delta n_{-q} \rangle$ lies in its ability to distinguish metallic from insulating behavior at small wavevectors q . For a metallic state, we expect $\langle \delta n_q \delta n_{-q} \rangle \sim |q|$ for $q \sim 0$. Specifically, for the two-band C2S2 metal, the slope of $\langle \delta n_q \delta n_{-q} \rangle$ at $q = 0$ is related to the “Luttinger parameter” $g_{\rho+}$ for the overall charge mode $\theta_{\rho+}$:

$$\langle \delta n_q \delta n_{-q} \rangle = 2g_{\rho+}|q|/\pi \text{ as } q \rightarrow 0. \quad (2.4)$$

Importantly, the quantity $g_{\rho+}$ as determined from Eq. (2.4) gives a direct measure of the scaling dimension of \mathcal{H}_8 : $\Delta[\mathcal{H}_8] = 4g_{\rho+}$ (see Appendix B.3.1). Once $\Delta[\mathcal{H}_8] < 2$ [corresponding to measured $g_{\rho+} < 1/2$ in Eq. (2.4)], then the umklapp is relevant, and the system is necessarily insulating. We then expect $g_{\rho+} \rightarrow 0$ at long scales so that $\langle \delta n_q \delta n_{-q} \rangle$ becomes quadratic at small q : $\langle \delta n_q \delta n_{-q} \rangle \sim q^2$ in the Mott insulator.

In Fig. 2.3, we show a series of density structure factor measurements ranging from the noninteracting limit at $U/t = 0$ to deep in the Mott insulating phase at $U/t = 7.0$. In the inset, we show estimates of $g_{\rho+}$ by plotting $\langle \delta n_q \delta n_{-q} \rangle / (2|q|/\pi)$ [see Eq. (2.4)]. Based on the above arguments, we see that the Mott transition occurs near a critical value of $U/t = 1.6$ where $g_{\rho+}$ drops below 1/2. Note, however, that for these system sizes $\langle \delta n_q \delta n_{-q} \rangle$ still appears linear in q until much larger overall repulsion, i.e., $U/t \simeq 5.0$. Still, we argue that the system becomes insulating at $U/t = 1.6$, as this is where \mathcal{H}_8 is determined to be relevant based on the measurement of $g_{\rho+}$. That is, we, rather remarkably, have an insulating state with a charge correlation length comparable to our system size ($L = 96$) for $1.6 \lesssim U/t \lesssim 5.0$. Indeed, such large correlation lengths are expected in the weak Mott insulating spin Bose metal, which we now argue is precisely the phase realized immediately on the insulating side of our model.

To this end, we now turn to the spin structure factor $\langle \mathbf{S}_q \cdot \mathbf{S}_{-q} \rangle$ in Fig. 2.4. In the noninteracting limit $U/t = 0$, we have familiar singularities at wavevectors $q = 2k_{F1}, 2k_{F2}, \pi/2, k_{F2} - k_{F1}$ originating from various “ $2k_F$ ” processes in our two-band system (see Fig. 2.2). These singularities are simple slope discontinuities, i.e., the scaling dimension for the spin operator at each wavevector is unity as guaranteed by Wick’s theorem. As we enter the putative interacting C2S2 metal by turning on finite U/t , the scaling dimensions at wavevectors

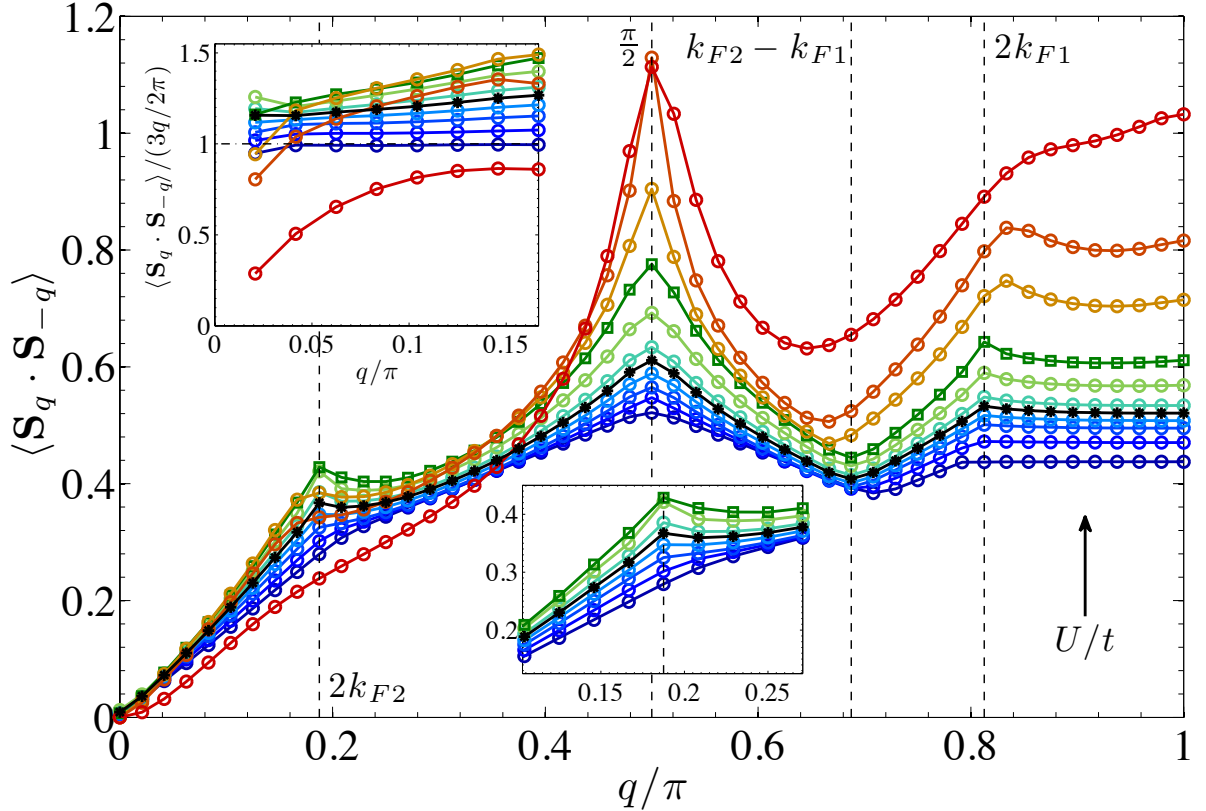


Figure 2.4: *Spin structure factor: Watching electrons evolve into spinons.* Measurements of the spin structure factor, $\langle \mathbf{S}_q \cdot \mathbf{S}_{-q} \rangle$, strongly point toward the presence of gapless spin excitations in both the metal and putative spin Bose metal immediately after the Mott transition at $U/t = 1.6$ (black curve with * symbols). Gapless spin excitations are characterized by $\langle \mathbf{S}_q \cdot \mathbf{S}_{-q} \rangle \sim |q|$ as $q \rightarrow 0$, and, as shown in the top inset, the opening of a spin gap occurs only for $U/t \gtrsim 5.0$, at which point the system dimerizes. The “ $2k_F$ ” features of the two electron bands in the metallic phase are inherited by the two spinon bands in the spin Bose metal, and, as highlighted in the bottom inset for $q = 2k_{F2}$, they are actually enhanced. Data correspond to the same U/t values and color scheme as in Fig. 2.3.

$2k_{F1}, 2k_{F2}, \pi/2, k_{F2} - k_{F1}$ are renormalized slightly but remain near unity.

Near the Mott transition value $U/t = 1.6$ as determined from $\langle \delta n_q \delta n_{-q} \rangle$ above, we observe the remarkable result that the singular features in $\langle \mathbf{S}_q \cdot \mathbf{S}_{-q} \rangle$ all survive, and those at $q = 2k_{F1}, 2k_{F2}, \pi/2$ are actually *enhanced* upon entering the insulating phase. Indeed, these are characteristic signatures of the spin Bose metal. (In Figs. 2.3-2.5, we display characteristic C1S2 spin Bose metal data at $U/t = 4.0$ with distinctive dark green square symbols.) First, the

singular features in $\langle \mathbf{S}_q \cdot \mathbf{S}_{-q} \rangle$ still correspond to the same “ $2k_F$ ” processes as in the metallic phase, but with the charge gapped they now correspond to *spinon* transfers across the Fermi sea. Second, in the spin Bose metal, we indeed expect the scaling dimensions of the spin operator at wavevectors $2k_{F1}, 2k_{F2}, \pi/2$ to be decreased (singularities enhanced) from their mean-field values [58]. This enhancement can be understood clearly within the bosonization framework. Specifically, when written in terms of bosonized fields, the slowly varying part of the spin operator at wavevectors $Q = 2k_{F1}, 2k_{F2}, \pi/2$ contains directly the field $\theta_{\rho+}$, i.e., $\mathbf{S}_Q \sim e^{\pm i\theta_{\rho+}}(\dots)$ —see Appendix B.3.2 and Ref. [58]. Thus, pinning of $\theta_{\rho+}$ at the Mott transition reduces the fluctuating content of the spin operator at these wavevectors, which in turn reduces the scaling dimensions and, ultimately, enhances the structure factor singularities. This enhancement is actually a (1+1)D realization of “Amperean” attraction between a spinon “particle” and “hole” moving in opposite directions [34, 58].

In the density structure factor measurements of Fig. 2.3, we also have singular features at the “ $2k_F$ ” wavevectors $q = 2k_{F1}, 2k_{F2}, \pi/2, k_{F2} - k_{F1}$ within the metallic phase, and in fact in the noninteracting $U/t = 0$ limit, the density and spin structure factors as defined are identical: $\langle \delta n_q \delta n_{-q} \rangle = \frac{4}{3} \langle \mathbf{S}_q \cdot \mathbf{S}_{-q} \rangle$. In the interacting C2S2 metal, the features at $q = 2k_{F1}, \pi/2, k_{F2} - k_{F1}$ are still clearly visible. In fact, some of these features survive even upon entering the putative spin Bose metal insulator and remain until $U/t \simeq 4.0$ (see black \star symbols in Fig. 2.3). That is, we have power-law density correlations at finite $2k_F$ wavevectors—a manifestation of which are the famous Friedel oscillations common in metals—even in a Mott insulator!

Indeed, this remarkable result is expected in the two-band spin Bose metal theory, where,

as with the spin operator, the slowly varying part of the density operator at wavevectors $Q = 2k_{F1}, 2k_{F2}, \pi/2$ again contains $\theta_{\rho+}$ (but not the wildly fluctuating conjugate field $\varphi_{\rho+}$), i.e., $\delta n_Q \sim e^{\pm i\theta_{\rho+}}(\dots)$. Thus, we should even expect the scaling dimension of the density operator at these wavevectors to be *reduced* due to the same Amperean attraction mechanism responsible for enhancement of spin correlations in Fig. 2.4. However, there are overriding nonuniversal amplitudes that are expected to be small in a Mott insulator thus preventing observation of this enhancement—this is likely the case in our data. Furthermore, we see development of a feature, though apparently weak or with very small amplitude, as anticipated, at a wavevector $q = 4k_{F2} = -4k_{F1}$ (see black hexagram symbols in Fig. 2.3). This feature is again expected from theory and is actually a *four-fermion* contribution to the density operator [58] (and thus is extremely weak at weak coupling). Interestingly, all these power-law density correlations in our electronic two-band spin Bose metal are a direct two-leg analog [161] of the charge Friedel oscillations expected on the insulating side of the continuous Mott transition in higher dimensions, as recently stressed by Mross and Senthil [91].

Returning to the spin sector, we can use the small q behavior of $\langle \mathbf{S}_q \cdot \mathbf{S}_{-q} \rangle$ to assess whether or not the spin sector is gapless in the realized phases. In analogy with Eq. (2.4), for a spin gapless state we have

$$\langle \mathbf{S}_q \cdot \mathbf{S}_{-q} \rangle = 3g_{\sigma+}|q|/2\pi \text{ as } q \rightarrow 0, \quad (2.5)$$

where $g_{\sigma+}$ is the “Luttinger parameter” associated with the overall spin mode $\theta_{\sigma+}$, which for a gapless SU(2) invariant fixed point is necessarily unity: $g_{\sigma+} = 1$ (see Appendix B.3.3 and also, e.g., Refs. [4, 162]). In the top inset of Fig. 2.4, we show $\langle \mathbf{S}_q \cdot \mathbf{S}_{-q} \rangle/(3|q|/2\pi)$, where we see that for free electrons $g_{\sigma+} = 1$, while increasing U/t pushes the $L = 96$ estimate

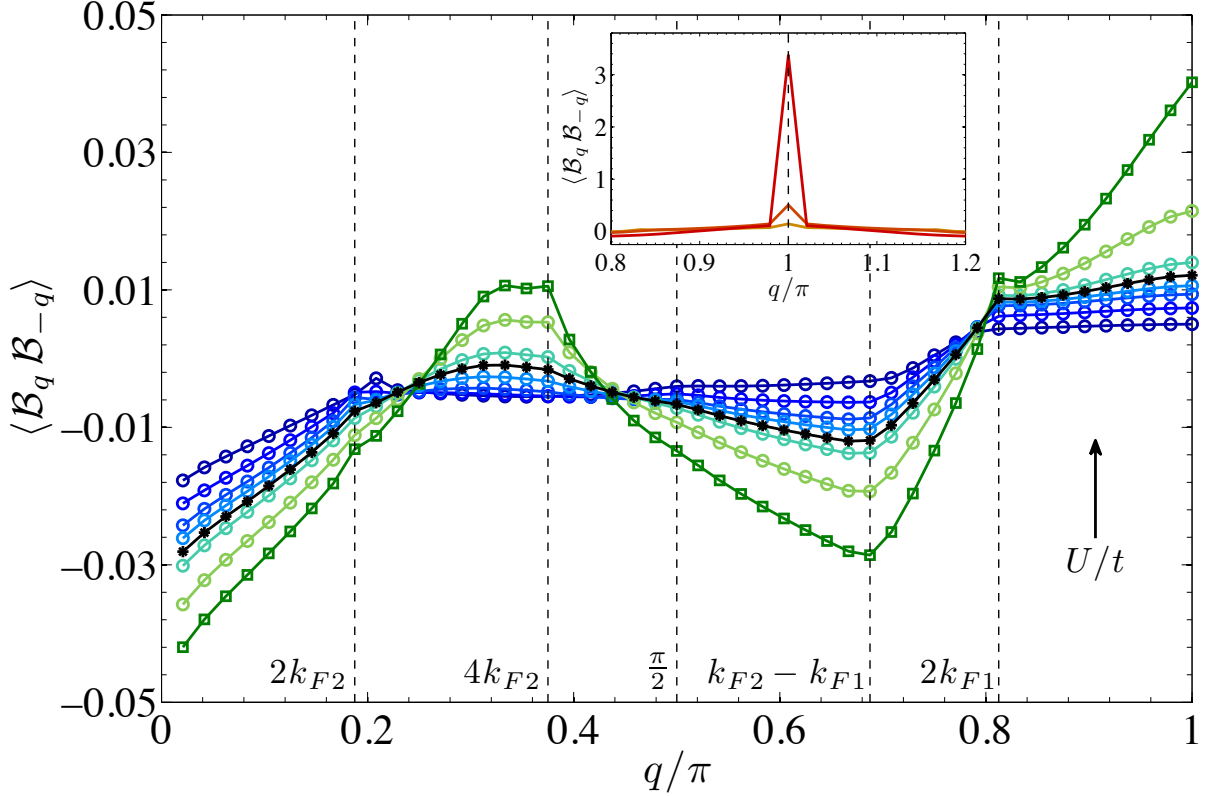


Figure 2.5: *Dimer structure factor: Period-2 valence bond solid order in the strong Mott insulator.* Measurements of the dimer structure factor, $\langle \mathcal{B}_q \mathcal{B}_{-q} \rangle$, show the emergence of a C0S0 period-2 valence bond solid for $U/t \gtrsim 5.0$. Its long-range order is very clearly demonstrated by the prominent Bragg peaks at $q = \pi$, as shown in the inset. Data correspond to the same U/t values and color scheme as in Figs. 2.3 and 2.4. In the main panel (inset), we show data only for the metal and spin Bose metal (valence bond solid) corresponding to values $U/t < 5.0$ ($U/t \geq 5.0$).

of $g_{\sigma+}$ above unity—this increasing trend continues until $U/t \simeq 4.0$, i.e., well beyond the Mott critical value of $U/t = 1.6$. This robust increasing measurement of $g_{\sigma+} > 1$ (we expect $g_{\sigma+} \rightarrow 1$ as $L \rightarrow \infty$) well into the insulator is a strong indicator that the spin is gapless on both the metallic and insulating sides of the Mott transition, lending strong credence that we are indeed observing the sought-after C2S2→C1S2 scenario described above. In Appendix B.4, we discuss these results in more depth and make comparisons to how $g_{\sigma+}$ behaves in the on-site t - t' - U Hubbard model at $\kappa = 0$.

Eventually, above $U/t \simeq 5.0$ we see that $g_{\sigma+}$ drops below unity and $\langle \mathbf{S}_q \cdot \mathbf{S}_{-q} \rangle \sim q^2$ for small q , indicating the opening of a spin gap. We identify this strong Mott insulating phase as a fully gapped (C0S0) period-2 valence bond solid, which is continuously connected to the dimerized phase realized by the J_1 - J_2 Heisenberg model [163] (and also the on-site t - t' - U Hubbard model at large U/t [164]). To this end, we turn to the dimer structure factor in Fig. 2.5. In the inset, we indeed see clear Bragg peaks developing in $\langle \mathcal{B}_q \mathcal{B}_{-q} \rangle$ at $q = \pi$ for $U/t \gtrsim 5.0$, hence strongly indicative of period-2 valence bond solid order. Furthermore, the operator content of the density, $\delta n(x)$, and bond energy, $\mathcal{B}(x)$, are identical at all wavevectors except π (see Ref. [58] and Appendix B.3.2). Thus, in the gapless phases (C2S2 and C1S2) we expect singularities in $\langle \mathcal{B}_q \mathcal{B}_{-q} \rangle$ at the same “ $2k_F$ ” wavevectors for which we find singularities in $\langle \delta n_q \delta n_{-q} \rangle$ (see Fig. 2.3). Indeed, in the main plot of Fig. 2.5 we clearly see features in $\langle \mathcal{B}_q \mathcal{B}_{-q} \rangle$ at $q = 2k_{F1}, 2k_{F2}, k_{F2} - k_{F1}$, and $4k_{F2}$. Once in the putative C1S2 insulator, these features are more apparent in $\langle \mathcal{B}_q \mathcal{B}_{-q} \rangle$ than in $\langle \delta n_q \delta n_{-q} \rangle$ since the latter are expected to have small amplitudes in a Mott insulator. In our data, this is especially true at wavevectors $2k_{F2}$ and $4k_{F2}$, the latter of which is the very nontrivial four-fermion contribution discussed above.

Finally, we discuss the behavior of the electron momentum distribution function $\langle c_{q\alpha}^\dagger c_{q\alpha} \rangle$ as shown for a dense scan of U/t values in Fig. 2.6. Beyond the Mott transition, when the field $\theta_{\rho+}$ gets pinned, we expect the electron Green’s function to decay exponentially so that the power-law singularities in $\langle c_{q\alpha}^\dagger c_{q\alpha} \rangle$ at the four Fermi points $q = \pm k_{F1}, \pm k_{F2}$ become gapped. While it is not exceedingly apparent that finite correlation lengths emerge at the Fermi points when we cross the Mott transition at $U/t = 1.6$ (as determined from $g_{\rho+}$ measurements—see Fig. 2.3), we believe this is another manifestation of the large charge correlation lengths present

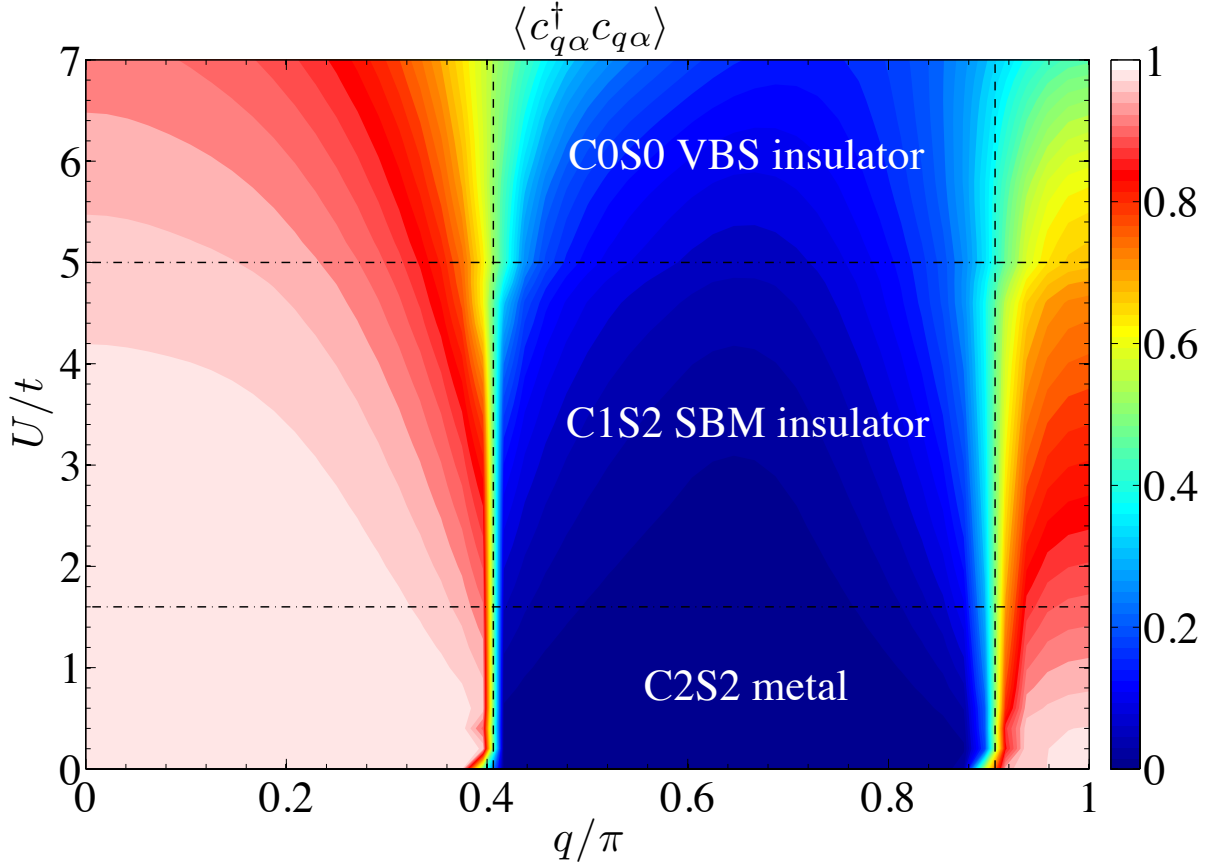


Figure 2.6: *Electronic momentum distribution function: Disappearance of the Fermi surface.* A dense scan of the electron momentum distribution function, $\langle c_{q\alpha}^\dagger c_{q\alpha} \rangle$, over U/t shows the gradual disappearance of the Fermi surface with increasing interactions, as we move from a two-band C2S2 metal ($U/t < 1.6$) across the insulating C1S2 spin Bose metal ($1.6 < U/t \lesssim 5.0$) to the C0S0 valence bond solid insulator ($U/t \gtrsim 5.0$). Vertical dashed lines mark the Fermi points (see Fig. 2.2), and the data is for the same $L = 96$ site system as shown in Figs. 2.3-2.5.

in the exotic C1S2 insulator. Deep into the putative C1S2 phase though, e.g., for $U/t \simeq 4.0$, finite correlation lengths are more apparent.

2.4 Discussion and Outlook

In this chapter, we have explored the Mott transition between a metal and a quantum spin liquid, presenting strong evidence through large-scale DMRG simulations in quasi-1D that such a continuous transition can be realized in reasonable electronic models. Our study is

strongly motivated by recent experiments on the quasi-two-dimensional organic materials κ -(BEDT-TTF)₂Cu₂(CN)₃ and EtMe₃Sb[Pd(dmit)₂]₂, each of which is a quantum spin liquid that can be driven through a Mott transition to a Fermi liquid under pressure. We believe our simulations of an extended Hubbard model—a model well-motivated by recent ab initio calculations [156] on κ -(BEDT-TTF)₂Cu₂(CN)₃—represent an important first step toward numerically characterizing this transition. While our study is restricted to the two-leg triangular strip, it does show the universal physics of a clear and direct quasi-1D analog of the continuous Mott metal-to-spin liquid transition in two dimensions [61].

Our calculations also elucidate the remarkable properties of the spin-liquid state stabilized on the insulating side. In many ways, this electronic “spin Bose metal” weak Mott insulator, as realized in our model, behaves very much like a metal on length scales shorter than the charge correlation length, and indeed exhibits long-distance density and spin correlations reminiscent of the nearby metallic phase (see Figs. 2.3 and 2.4). It is precisely this striking similarity between the metallic and insulating states—in basically all properties except the finite charge correlation length in the latter—which makes a continuous Mott metal-insulator transition plausible, perhaps even likely.

Going forward, it would clearly be desirable to move towards two dimensions and explore the Mott transition in models such as Eq. (2.1) on wider ladders and eventually in full 2D, with the goal to make real connections with the actual experiments [25, 150]. In the end, the transition may turn out to *not* be continuous but instead be weakly first order, as is perhaps realized in κ -(BEDT-TTF)₂Cu₂(CN)₃. Still, our numerical calculations presented here, as well as the recent field theoretic work of Senthil and Mross, suggest that a continuous Mott transition

in the $(d + 1)$ D XY universality class between a metal and quantum spin liquid is a very real, exciting possibility.

Chapter 3

Theory of a Competitive Spin Liquid State for Weak Mott Insulators on the Triangular Lattice

3.1 Background and Introduction

As introduced in Chapter 1, quantum spin liquids are exotic phases of quantum spin systems which break no global symmetries even when thermal fluctuations are completely suppressed at zero temperature [17, 165]¹. In the last decade, candidates of gapless spin liquid phases have been discovered in various experimental systems, including κ -(BEDT-TTF)₂Cu₂(CN)₃ [24, 25], EtMe₃Sb[Pd(dmit)₂]₂ [26, 27, 28], Ba₃CuSb₂O₉ [166], Ba₃NiSb₂O₉ [167], and ZnCu₃(OH)₆Cl₂ [29, 30, 31]. In all these materials, no evidence of magnetic order was found

¹Excerpts and figures appearing in this chapter are reprinted with permission from R. V. Mishmash, J. R. Garrison, S. Bieri, and C. Xu, Phys. Rev. Lett. **111**, 157203 (2013). Copyright 2013 by the American Physical Society.

at temperatures much lower than the spin interaction energy scale of the system. In the current chapter, we will focus on the organic spin liquid materials κ -(BEDT-TTF)₂Cu₂(CN)₃ (κ -BEDT) and EtMe₃Sb[Pd(dmit)₂]₂ (DMIT). These materials are quasi-two-dimensional Mott insulators which are close to a Mott metal-insulator transition [25], and thus exhibit substantial local charge fluctuations (see also Chapter 2). An effective spin model that may well describe the magnetic properties of these “weak” Mott insulators involves supplementing the usual (possibly extended) Heisenberg model with a four-site ring-exchange term [49]. Here, we consider the following Hamiltonian:

$$H = J_1 \sum_{\langle i,j \rangle} 2\vec{S}_i \cdot \vec{S}_j + J_2 \sum_{\langle\langle i,j \rangle\rangle} 2\vec{S}_i \cdot \vec{S}_j + K \sum_{\langle i,j,k,l \rangle} (P_{ijkl} + \text{H.c.}), \quad (3.1)$$

where the sums $\langle i,j \rangle$ and $\langle\langle i,j \rangle\rangle$ go over all first- and second-neighbor links of the triangular lattice, respectively, while $\langle i,j,k,l \rangle$ goes over all elementary four-site rhombi; P_{ijkl} rotates the spin configurations around a given rhombus. In what follows, we set $J_1 = 1$ as the unit of energy.

The two different organic spin liquids κ -BEDT and DMIT share two universal properties:

1. At low temperatures, despite the fact that the system is still a Mott insulator for charge transport, the specific heat scales linearly with temperature: $C_v = \gamma T$ [44]. This phenomenon demonstrates that the system has a large density of charge-neutral excitations. Furthermore, γ is very weakly dependent on a moderate external magnetic field.
2. The spin susceptibility shows no magnetic phase transition at any finite temperature, and it saturates to a finite constant χ at zero temperature [24].

These two phenomena are completely inconsistent with any semiclassical magnetic state and are strongly suggestive of the existence of a highly nontrivial quantum disordered phase.

To date, four main theoretical scenarios have been proposed to describe these experimental facts:

1. In the U(1) spinon Fermi surface state [49, 50], a fermionic spinon $f_{r\alpha}$ is introduced by decomposing the physical spin operator at site r as $\vec{S}_r = \frac{1}{2} \sum_{\alpha,\beta=\uparrow,\downarrow} f_{r\alpha}^\dagger \vec{\sigma}_{\alpha\beta} f_{r\beta}$ and taking the spinons to fill an ordinary Fermi sea at the mean-field level (see also Chapter 2). This gives rise to a finite density of states, consistent with the experimental results mentioned above. Furthermore, it has been demonstrated that for strong enough ring exchange K , the spinon Fermi sea state has very competitive variational energy in the microscopic spin model (3.1) [49]. However, once we go beyond the mean-field level, the U(1) gauge fluctuation will acquire singular overdamped dynamics $|\omega| \sim k^3$ due to its coupling with the Fermi surface [54]. This singular dynamics generates an even larger density of states at low temperature, which leads to a singular specific heat $C_v \sim T^{2/3}$. This specific heat behavior is not (unambiguously—see Ref. [168]) observed experimentally.

2. The most natural way to suppress the U(1) gauge fluctuation is to condense Cooper pairs of spinons and thus break the U(1) gauge fluctuation down to a fully gapped Z_2 gauge fluctuation. This possibility has been explored numerically in Ref. [64], where the authors concluded that the particular pairing pattern that is energetically favored by Eq. (3.1) has nodal $d_{x^2-y^2}$ -wave structure. However, this nodal d -wave pairing not only suppresses the gauge fluctuation, it also significantly suppresses the fermion density of states, and the system will no longer have finite γ and χ at low temperature, unless sufficient disorder is turned on.

However, under pressure the system is driven into a rather good metal, which suggests that disorder should not play an essential role. It is our view that the experimental facts of finite

γ and χ should be genuine properties of the spin liquid, independent of disorder. If the nodal d -wave pairing state is indeed the ground state of κ -BEDT and DMIT, it would imply that the experimental observations of finite γ and χ are a result of the disorder in the system and not properties of the spin liquid itself.

3. Another very different approach was taken in Ref. [67], where the authors proposed that κ -BEDT is a Z_2 spin liquid which is very close to the condensation quantum critical point of bosonic spinons. This quantum critical behavior is consistent with the NMR relaxation rate observed experimentally [169]. In particular, the small energy gap seen in thermal conductivity data [48] was identified with the gap of the topological defect of the Z_2 spin liquid [67]. However, no parent spin Hamiltonian has been found for this state so far. Thus, it is unknown whether this quantum critical spin liquid can be realized in any experimentally relevant lattice model.

4. A novel Majorana slave-fermion formalism was introduced in Ref. [68], where the authors proposed that the ground state of the organic spin liquids has a Majorana fermion Fermi surface. But, just like the previous theory, so far it is unclear in which lattice model this spin liquid can be realized.

3.2 New Z_2 Spin Liquid: $d + id$ Ansatz with Quadratic Band Touching

In this chapter, we propose an entirely new spin liquid. In Ref. [69], possible Z_2 spin liquids with an extended spinon Fermi surface were summarized. However, the spin liquid

state proposed in the present work is beyond the ones discussed in Ref. [69]. Our novel state has no spinon Fermi surface, but has a quadratic band touching (QBT) of fermionic spinons that is protected by the symmetry of the model: $\omega \sim \pm k^2$. In two dimensions, a quadratic band touching leads to a finite constant density of states, which automatically gives finite γ and χ at zero temperature. Besides being consistent with the major experimental facts of the organic spin liquid compounds, this state has the following advantages:

1. As we will show below, this state is a very competitive variational ground state for model (3.1) in the physically relevant regime $0.1 \lesssim K \lesssim 0.15$ and $J_2 \simeq 0$ (see Fig. 3.4).

2. The gauge fluctuation for this state is fully gapped, and hence plays no role at low energy.

Most field-theoretic calculations based on this state are thus well approximated at the mean-field level, and so, in contrast to the spinon Fermi surface state [97], they are well controlled.

3. Finite γ and χ are *generic* properties of our QBT spin liquid state which remain in the presence of gauge fluctuations. In contrast to the nodal d -wave state [64, 65, 66], these properties do not rely on disorder.

4. A very small energy gap, much smaller than the Heisenberg exchange J_1 , was observed by thermal conductivity measurements in κ -BEDT [48]. This small gap can be very elegantly explained by our QBT spin liquid without fine-tuning: an allowed short-range spinon interaction on top of our mean-field state may be marginally relevant, and thus naturally open up an exponentially small gap.

5. Since the gauge field fluctuation is fully gapped in our spin liquid, it does not respond to an external magnetic field. Thus our state has no obvious thermal Hall effect, which is consistent with experiments [47].

Let us first describe the QBT spin liquid state in detail. We take the standard slave-fermion (spinon) representation of spin-1/2 operators: $\vec{S}_r = \frac{1}{2} \sum_{\alpha, \beta=\uparrow, \downarrow} f_{r\alpha}^\dagger \vec{\sigma}_{\alpha\beta} f_{r\beta}$. The physical spin-1/2 Hilbert space is then recovered by imposing the on-site constraint $\sum_\alpha f_{r\alpha}^\dagger f_{r\alpha} = 1$, which introduces an SU(2) gauge symmetry to the low-energy dynamics of the spinons [19]. However, this SU(2) gauge symmetry will generally be broken by the mean-field dynamics, which can be described by a quadratic Hamiltonian of the form

$$H_{\text{MF}} = - \sum_{r, r'} \left[t_{rr'} f_{r\alpha}^\dagger f_{r'\alpha} + \left(\Delta_{rr'} f_{r\uparrow}^\dagger f_{r'\downarrow}^\dagger + \text{H.c.} \right) \right]. \quad (3.2)$$

The QBT spin liquid at the focus of this chapter corresponds to a mean-field ansatz for the spinons with $d + id$ pairing and vanishing hopping:

$$t_{rr'} = 0, \quad \Delta_{r, r+\hat{e}} = \Delta(e_x + ie_y)^2. \quad (3.3)$$

Here, \hat{e} is a first-neighbor unit vector of the triangular lattice. This mean-field ansatz breaks the SU(2) gauge symmetry down to Z_2 : $f_\alpha \mapsto -f_\alpha$. Thus, gauge fluctuations can be ignored in the low-energy dynamics of the system.

It is convenient to introduce a complex spinor ψ defined as $(\psi_1, \psi_2) = (f_\uparrow, f_\downarrow^\dagger)$. Expanded at the Γ -point $\vec{k} = 0$, the low-energy Hamiltonian for the mean-field ansatz mentioned above reads

$$H_0 = \psi^\dagger \{-\tau^x(\partial_x^2 - \partial_y^2) + 2\tau^y\partial_x\partial_y\} \psi. \quad (3.4)$$

This mean-field Hamiltonian has a quadratic band touching at $\vec{k} = 0$, which leads to a finite density of states in two dimensions. We propose that this finite density of states is responsible for finite γ and χ observed experimentally in κ -BEDT and DMIT. A similar QBT spin liquid state for the spin-1 material $\text{Ba}_3\text{NiSb}_2\text{O}_9$ [167] was proposed in Ref. [170], where an extra color index of the slave fermion has to be introduced for spin-1 [171].

In addition to the quadratic band touching at $\vec{k} = 0$, there are also Dirac fermions at the corners of the Brillouin zone: $\vec{Q}_{A,B} = \pm(4\pi/3, 0)$. Complex Dirac fermion fields $\psi_{A,B}$ at momenta $\vec{Q}_{A,B}$ can be defined as $\psi = \psi_A \exp(i\vec{Q}_A \cdot \vec{r}) + \psi_B \exp(i\vec{Q}_B \cdot \vec{r})$. The low-energy Hamiltonian for $\psi_{A,B}$ reads

$$H_{\pm(4\pi/3,0)} = \sum_{a=A,B} \psi_a^\dagger (-i\tau^x \partial_x - i\tau^y \partial_y) \psi_a. \quad (3.5)$$

At low temperature, the contribution of these Dirac fermions to γ and χ is much smaller than that resulting from the quadratic band touching at the Γ -point.

The spinon carries a projective representation of the physical symmetry group. In the Supplemental Material of Ref. [143], we demonstrate that the mean-field QBT discussed above preserves all the symmetries of the model (including the triangular lattice symmetry and time-reversal symmetry). As long as these symmetries are preserved, no relevant fermion bilinear terms can be added to Eqs. (3.4) and (3.5), and the low-energy dynamics is stable.

Let us now go beyond the mean field. As mentioned above, the mean-field ansatz breaks the gauge symmetry down to Z_2 , and the gauge fluctuations are thus quite harmless. But, besides the gauge fluctuation, local short-range four-fermion interactions exist at both the Dirac points $\vec{Q}_{A,B}$ and the QBT Γ -point. At the Γ -point, only the following four-fermion interaction needs to be considered:

$$H_4 = -g f_\uparrow^\dagger f_\uparrow f_\downarrow^\dagger f_\downarrow \sim g \psi_1^\dagger \psi_1 \psi_2^\dagger \psi_2. \quad (3.6)$$

The renormalization group flow of this term is very simple: depending on the sign of g , H_4 can be either marginally relevant or irrelevant [63]. When it is relevant ($g > 0$), the system spontaneously breaks time-reversal symmetry (it becomes a chiral spin liquid) and opens up an exponentially small gap at the Γ -point: $m f_\alpha^\dagger f_\alpha = m \psi^\dagger \tau^z \psi$. We identify this fluctuation

generated gap with the small gap observed by thermal conductivity in κ -BEDT [48].

In DMIT, on the other hand, thermal conductivity measurements indicate that the system is gapless at the lowest temperature [47]. Thus, we conjecture that DMIT corresponds to the case with a marginally irrelevant H_4 ($g < 0$), while κ -BEDT corresponds to $g > 0$. The thermal conductivity behavior with negative g will be studied in detail in the future [172], taking into account both interaction and disorder effects.

3.3 Variational Monte Carlo Results

Inspired by previous works [49, 64, 58, 59, 138, 139], we now revisit the variational phase diagram of model (3.1) using a wide range of correlated spin wave functions. The quadratic Hamiltonian, Eq. (3.2), allows straightforward construction of spin liquid wave functions by Gutzwiller projecting its ground state $|\Psi_0\rangle$. That is, we use as variational states

$$|\Psi(\{t_{rr'}\}, \{\Delta_{rr'}\})\rangle = \mathcal{P}_G \mathcal{P}_N |\Psi_0\rangle, \quad (3.7)$$

where \mathcal{P}_N is a projector to a state with N spinons, and N is the number of lattice sites ($N_\uparrow = N_\downarrow = N/2$). $\mathcal{P}_G = \prod_r [1 - n_{r\downarrow} n_{r\uparrow}]$ is the Gutzwiller projector which removes unphysical states containing doubly-occupied sites. We fix the spinon chemical potential $\mu = t_{rr}$ such that $|\Psi_0\rangle$ is half filled on average before projection, but other parameters in (3.2) are used as variational parameters. In Appendix C, we discuss in detail the determinantal representation of N -particle Bardeen-Cooper-Schrieffer (BCS) superconducting wave functions, $\mathcal{P}_N |\Psi_0\rangle$, as appropriate for our numerical calculations. The evaluation of expectation values in such fermionic wave functions can be done efficiently and with high accuracy using variational

Monte Carlo techniques [138, 139, 140, 171]. For competing long-range ordered states, we use Jastrow-type wave functions as pioneered by Huse and Elser [41] (see Appendix A.2 for more details on all states we studied).

3.3.1 Nearest-Neighbor Heisenberg Model with Ring Exchange: $J_2 = 0$

We first consider the case with $J_2 = 0$ in Eq. (3.1). Since the seminal work of Motrunich [49] it has been known that the U(1) projected Fermi sea state (or “spin Bose metal”—see Refs. [58, 59] and Chapter 2) with isotropic nearest-neighbor $t_{rr'} = t$ and $\Delta_{rr'} = 0$ has remarkably good variational energy and is clearly the best fermionic trial state for relatively large ring exchange $K \gtrsim 0.3$. This state is also consistent with recent large-scale DMRG calculations on the four-leg ladder [59]. On the other hand, exact diagonalization studies [173] indicate that the 120° antiferromagnetic (AFM) order, which is believed to characterize the ground state of the Heisenberg model at $K = 0$ [41, 42, 43], is destroyed at much smaller ring exchange $K \gtrsim 0.1$. Therefore, an intermediate spin liquid phase in the parameter regime $0.1 \lesssim K \lesssim 0.3$ may well be present in the model, and is likely to be relevant for the organic compounds.

The most natural candidate states are Z_2 spin liquids with finite spinon pairing $\Delta_{rr'} \neq 0$ in (3.2). Indeed, it has been known since the work of Motrunich that in the intermediate parameter regime of Eq. (3.1) such projected BCS states do have significantly lower energy than the 120° AFM and U(1) Fermi sea states. However, the nature of the spinon pairing pattern in this putative Z_2 spin liquid was still up for debate. In this chapter, we perform accurate large-scale simulations up to 30×30 lattice sites to check all singlet ($\Delta_{rr'} = \Delta_{r'r}$)

and triplet ($\Delta_{rr'} = -\Delta_{r'r}$) pairing instabilities (s , p , $p + ip$, d , $d + id$, and f -wave) of the U(1) Fermi sea state in model (3.1). We find the remarkable result that for $0.1 \lesssim K \lesssim 0.15$ our QBT $d + id$ state, as discussed above, is highly competitive, and perhaps has the lowest energy of *any* projected fermionic trial state, including the nodal d -wave state of Ref. [64].

The results of our variational study at $J_2 = 0$ are summarized in Fig. 3.1. Consistent with Refs. [49, 64], we find that the unpaired U(1) Fermi sea (FS) state and states with nodal d -wave and $d + id$ pairing symmetries are the most competitive spin liquid wave functions for this model. The gap functions for the $d + id$ and nodal d -wave states are given by $\Delta_{r,r+\hat{e}}^{(d+id)} = \Delta(e_x + ie_y)^2$ and $\Delta_{r,r+\hat{e}}^{(\text{nodal } d)} = \Delta(e_x^2 - e_y^2)$, respectively, where \hat{e} is a unit vector connecting nearest neighbors on the triangular lattice. Each of these ansätze thus has one variational parameter Δ/t which we parameterize by $\alpha = \tan^{-1}(\Delta/t)$. In the top panel of Fig. 3.1, we show the optimal energies per site, E_{minimum} , versus ring exchange K for the $d + id$, nodal d -wave, U(1) FS, and 120° AFM states. In the bottom panel, we show the corresponding optimal α for both the $d+id$ and nodal d -wave states. We see that the 120° AFM state wins for $K \lesssim 0.1$; however, immediately upon exiting the 120° phase for $0.1 \lesssim K \lesssim 0.15$, the $d + id$ and nodal d -wave states are extremely close in energy and are basically degenerate within statistical error. Remarkably, as seen in the bottom panel of Fig. 3.1, the optimal $d + id$ state in the entire range $0.1 \lesssim K \lesssim 0.17$ is in fact our exotic QBT state of interest: $\Delta/t \rightarrow \infty, \alpha = \pi/2$. For still larger K , $0.15 \lesssim K \lesssim 0.25$, the optimal ansatz is the nodal d -wave state, a result which is consistent with Ref. [64]. Finally, for $K \gtrsim 0.25$, the optimal pairing amplitude $\Delta \rightarrow 0$ for all spin liquid states, thus describing a crossover to the U(1) Fermi sea state of Refs. [49, 58, 59].

In the inset of the bottom panel of Fig. 3.1, we plot the variational energies per site versus

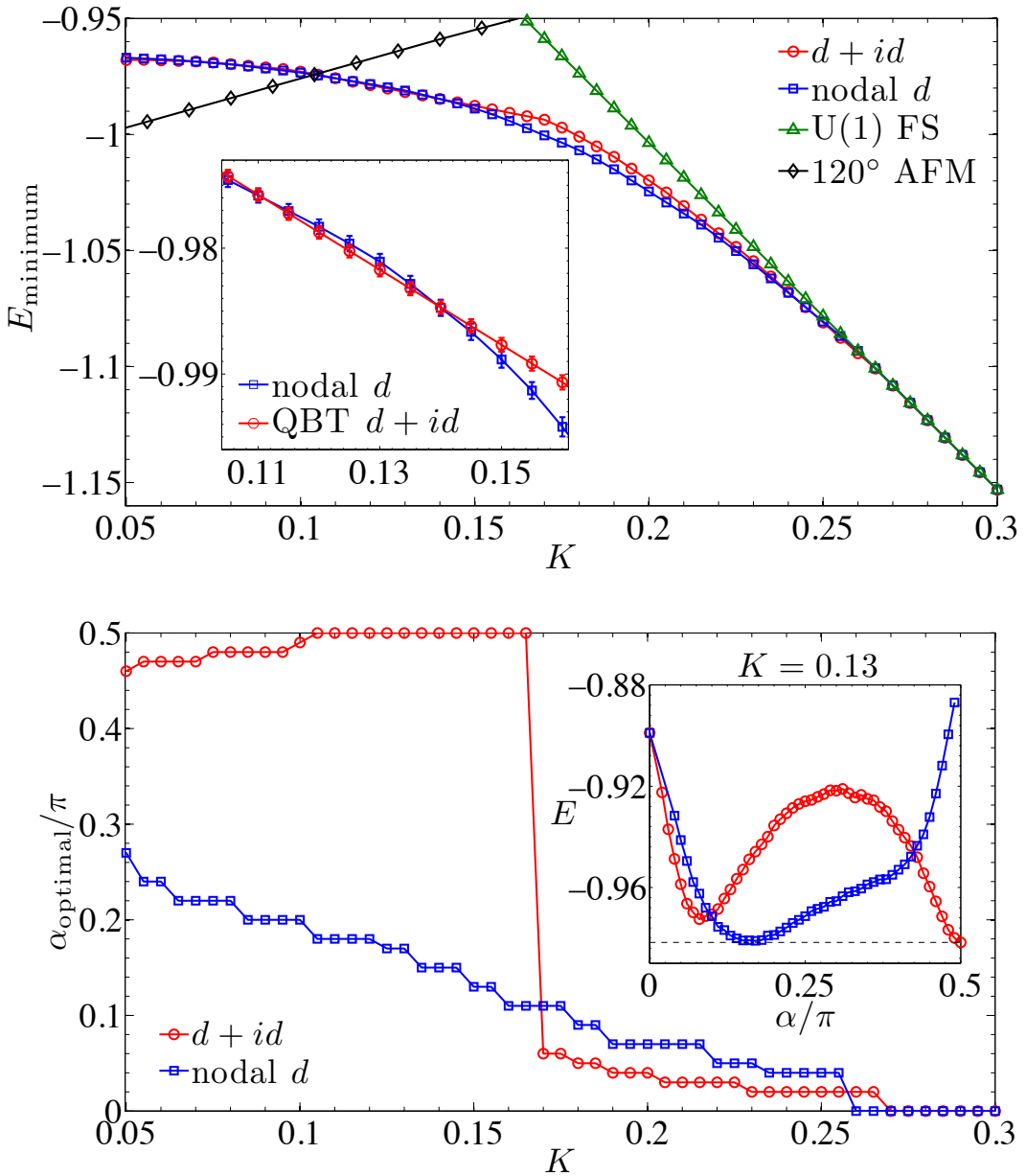


Figure 3.1: *Summary of our variational phase diagram along the line $J_2 = 0$.* Upper panel: Variational energies per site for the Hamiltonian, Eq. (3.1), at $J_2 = 0$ as a function of K for the most competitive trial states in our study; in the inset, we show a zoom of the region of the phase diagram where the QBT $d + id$ state is most competitive. Lower panel: The optimal variational parameter $\alpha = \tan^{-1}(\Delta/t)$ is plotted for the $d + id$ and nodal d -wave states; in the inset, we show the variational energies for all α at the point $K = 0.13$ where the dashed line indicates the energy of the QBT state.

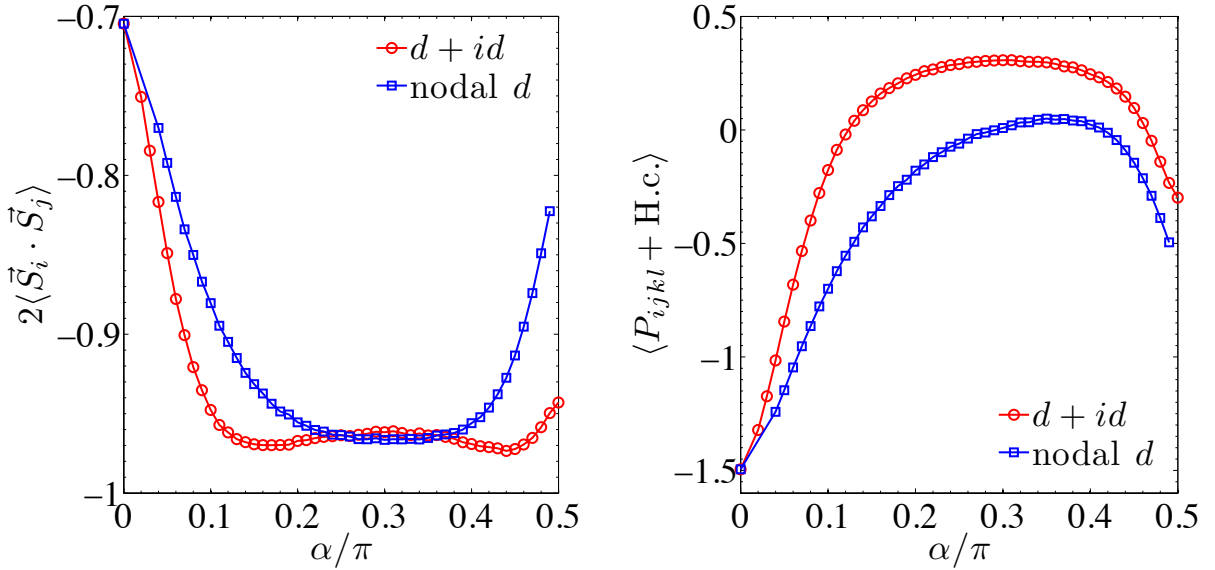


Figure 3.2: *Heisenberg and ring exchange expectation values for $d+id$ and nodal d -wave trial wave functions.* We plot first-neighbor Heisenberg exchange (left) and ring exchange (right) expectation values per site for the $d+id$ and nodal d -wave states as a function of $\alpha = \tan^{-1}(\Delta/t)$. In the case of $d+id$, the special QBT point lies at $\alpha/\pi = 0.5$.

α at the point $K = 0.13$ in the spin liquid phase. Interestingly, there are two local minima for the $d+id$ ansatz: the first minimum at small $\Delta \lesssim t$ is smoothly connected to the U(1) Fermi sea state at $\Delta = 0$, while the second minimum at $\Delta/t \rightarrow \infty$ is the qualitatively new QBT state at the focus of our work. For $0.1 \lesssim K \lesssim 0.17$, the latter is lower in energy than the former, but is almost degenerate with the optimal nodal d -wave state which always has small $\Delta \lesssim t$. Indeed, the two local minima in the $d+id$ ansatz are already present in the pure Heisenberg model ($K = J_2 = 0$), with a *large*- Δ state having minimum energy. Furthermore, the QBT state at $\alpha = \pi/2$ has surprisingly low ring-term expectation value, and this conspires with the good Heisenberg energy of the generic large- Δ $d+id$ state to make the QBT state the optimal fermionic spin liquid ansatz in the parameter window $0.1 \lesssim K \lesssim 0.15$.

To elaborate on these points further, we now consider the α -dependence of the expectation values $2\langle \vec{S}_i \cdot \vec{S}_j \rangle$ and $\langle P_{ijkl} + \text{H.c.} \rangle$ used to compute the variational energy per site, $E =$

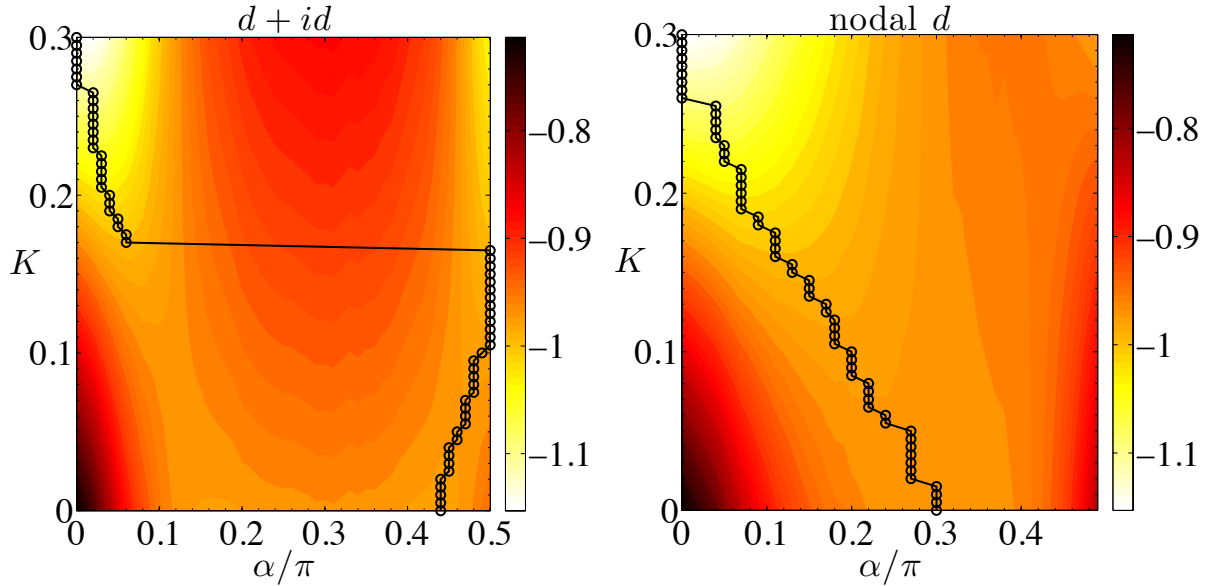


Figure 3.3: *Energy versus K for $d + id$ and nodal d -wave trial wave functions.* Here we show contour plots of the trial energy per site versus K and $\alpha = \tan^{-1}(\Delta/t)$ for the $d + id$ (left) and nodal d -wave (right) states ($J_2 = 0$). The black curves indicate the optimal α for each K (see also Fig. 3.1, bottom panel).

$$J_1 \left[2\langle \vec{S}_i \cdot \vec{S}_j \rangle \right] + K [\langle P_{ijkl} + \text{H.c.} \rangle], \text{ for both the first-neighbor } d + id \text{ and nodal } d\text{-wave states.}$$

These results are shown in Fig. 3.2. As mentioned above, we find the striking result that the two local minima in the $d + id$ ansatz apparent in Fig. 3.1 are actually present already in the pure Heisenberg model, with the *large- Δ* state ($\alpha/\pi \simeq 0.44$, $\Delta/t \simeq 5.2$) slightly lower in energy (see Fig. 3.2, left panel). Furthermore, we see in the right panel of Fig. 3.2 that beyond some large value of Δ ($\alpha/\pi \simeq 0.4$), we can gain substantial ring energy in both the $d + id$ and nodal d -wave states by actually further increasing Δ . In the case of $d + id$, going to the extreme limit $\Delta/t \rightarrow \infty$ loses only somewhat marginal Heisenberg energy while at the same time gains significant ring energy: It is ultimately a balance between these two effects which makes the QBT $d + id$ state highly competitive in the intermediate parameter regime of the ring model.

Finally, in Fig. 3.3 we show contour plots of the trial energy versus both K and α (for which

the inset of the bottom panel of Fig. 3.1 is a cross section). For the $d + id$ state (left panel), we can clearly see two basins of local minima: one of which connects to the QBT state at $\alpha = \pi/2$, the other of which connects to the U(1) state at $\alpha = 0$. Upon increasing K out of the pure Heisenberg model, the large- Δ $d + id$ state quickly tracks to the QBT state near $K \simeq 0.1$, at which it remains until $K \simeq 0.17$ where the optimal $d + id$ state dramatically changes to one with small Δ . These results clearly show that the QBT $d + id$ state is a qualitatively new phase, and that it is not continuously connected to the U(1) Fermi sea state at $\Delta = 0$. In sharp contrast, the optimal nodal d -wave state (right panel) is continuously connected to the U(1) state for all values of K .

The authors of Ref. [64] concluded that the nodal d -wave state is clearly the best variational ground state for intermediate $0.1 \lesssim K \lesssim 0.15$. We believe that there are two reasons for this discrepancy with our result. First, Ref. [64] considered only a restricted range of small Δ/t for the $d + id$ ansatz which excluded the QBT state altogether. Second, our extensive finite-size analysis shows that quite large lattices ($\gtrsim 18 \times 18$) are necessary to get well converged expectation values for the nodal d -wave state. Our calculations find poorly converged expectation values and strong dependencies on the spinon boundary conditions for a nodal d -wave state on the small 10×11 lattice that was used in [64].

3.3.2 Full Variational Phase Diagram with Finite J_2

Finally, we discuss the effect of a second-neighbor interaction J_2 . In Fig. 3.4, we present a variational phase diagram in the K - J_2 plane. A ferromagnetic interaction ($J_2 < 0$) quickly favors the 120° AFM state over the QBT $d + id$ state and destroys the spin liquid phase;

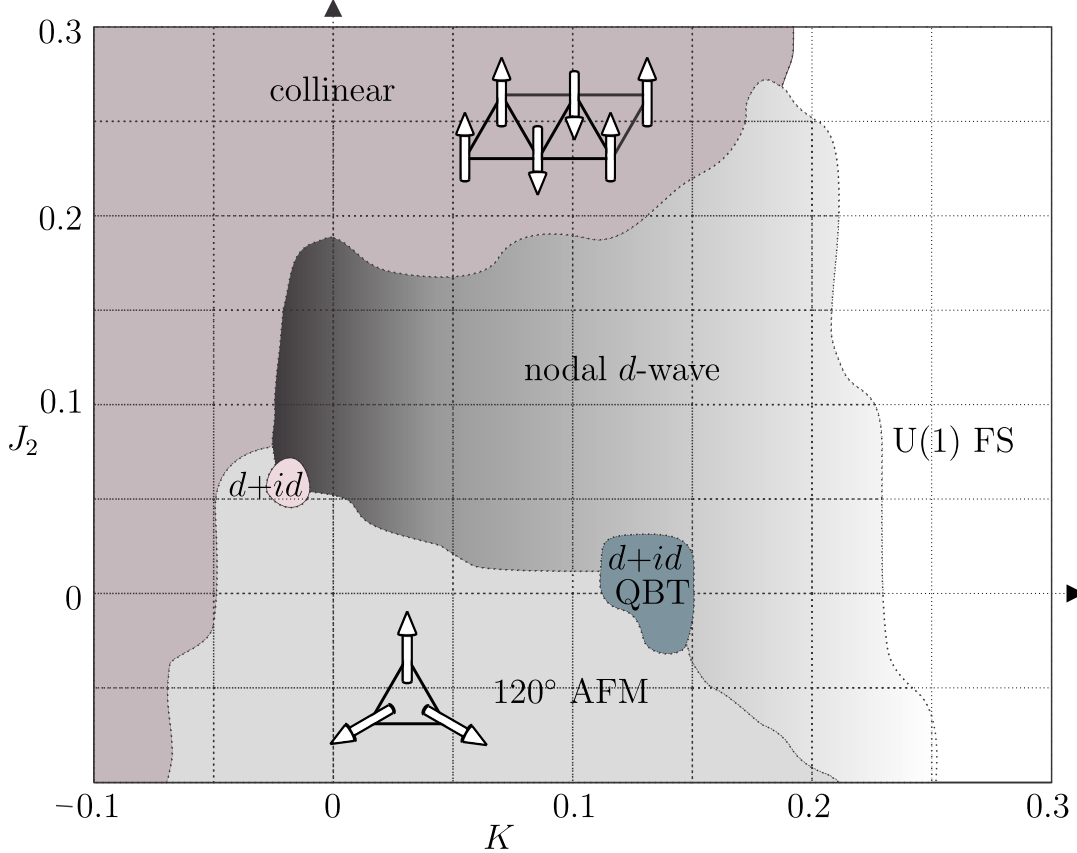


Figure 3.4: *Full variational phase diagram of the spin Hamiltonian, Eq. (3.1).* We propose that the $d+id$ QBT spin liquid phase is a very strong candidate for the ground state of κ -BEDT and DMIT in the parameter range $J_2 \simeq 0$ and $K \simeq 0.13$.

however, within the class of spin liquid wave functions, $J_2 \lesssim 0$ does clearly favor the QBT $d+id$ state over the nodal d -wave state for $K \simeq 0.15$. On the other hand, antiferromagnetic $J_2 > 0$ strongly frustrates the 120° AFM state and favors a nodal d -wave spin liquid. Negative ring exchange or larger values of $J_2 \gtrsim 0.17$ lead to a collinear phase. In Fig. 3.4, around $J_2 \simeq 0.05$ and $K \simeq -0.02$, a small fully gapped $d+id$ phase with finite Δ/t emerges. This is a chiral spin liquid with nontrivial topological order [174, 175]. Our preliminary results show that this phase will expand significantly once an antiferromagnetic third-neighbor Heisenberg coupling J_3 is added to Eq. (3.1). More details on this phase will be elaborated in future work.

The ability of the nodal d -wave state to beat the collinear state for $K \simeq 0$ may suggest

(see Refs. [176, 177]) that we are overestimating the extent of the nodal d -wave state in our phase diagram (see also Appendix A.2). Of course, a variational study can never claim to have the final say on the phase diagram of a given microscopic model, and quantitative locations of phase boundaries should not be taken too seriously. What is very robust, however, is the statement that our QBT $d + id$ state has both extremely competitive energetics in a realistic parameter regime and highly appealing phenomenology for the organic spin liquid compounds.

3.4 Discussion and Outlook

In this chapter, we have taken the experimental data on the organic spin liquid compounds κ -BEDT and DMIT at face value and have proposed a novel spin liquid state that is consistent with many of the experimental findings. The approach taken here is largely phenomenological in the sense that there is no particularly obvious (microscopic) physical reason why a $d + id$ ansatz for spinons with vanishing hopping should be an appropriate theoretical starting point to describe these materials. This should be contrasted with the U(1) spinon Fermi sea (spin Bose metal) state of Chapter 2, which is inarguably a very natural physical description given the proximity of the spin liquid phases observed in the organics to ordinary Fermi liquid metals. However, the QBT state does perhaps do a better job overall of describing the available experimental data on the insulating states observed in κ -BEDT and DMIT, at least qualitatively, and also does very well variationally close to the antiferromagnetically ordered state (see Fig. 3.1). Indeed, the QBT state is much closer in character to the 120° ordered state than it is to a metallic state. For example, it has power-law spin-spin correlations at wavevector $\vec{Q} = (4\pi/3, 0)$ which may be thought of as descendants of the AFM long-range order present in the 120° state.

In fact, this was one of the initial inspirations for constructing the QBT state [170]. In addition, the QBT $d + id$ state retains the fermionic parton description germane to the organic spin liquids, albeit by stretching the chosen ansatz all the way to a pairing only one.

In the future, we plan to carry out more detailed field-theoretic calculations based on the QBT state and hope to make more quantitative comparisons to the experimental data. Ultimately, it will be interesting to see if future experiments push the balance in favor of either the Z_2 QBT $d + id$ state presented here or the U(1) spinon Fermi sea state (or one of its natural instabilities), or perhaps a completely different theory altogether.

Chapter 4

Non-Fermi Liquid d -wave Metal Phase of Strongly Interacting Electrons

4.1 Background and Introduction

Over the past several decades, experiments on strongly correlated materials have routinely revealed, in certain parts of the phase diagram, conducting liquids with physical properties qualitatively inconsistent with Landau's Fermi liquid theory [3]¹. Examples of these so-called non-Fermi liquid metals [178] include the strange metal phase of the cuprate superconductors [34, 80] and heavy fermion materials near a quantum critical point [5, 6]. However, such non-Fermi liquid behavior has been notoriously challenging to characterize theoretically, largely owing to the failure of a weakly interacting quasiparticle description. It is even ambiguous to define a non-Fermi liquid, although possible deviations from Fermi liquid theory

¹Excerpts and figures appearing in this chapter are reprinted with permission from H. C. Jiang, M. S. Block, R. V. Mishmash, J. R. Garrison, D. N. Sheng, O. I. Motrunich, and M. P. A. Fisher, *Nature*, **493**, 39 (2013). Copyright 2013 by the Nature Publishing Group.

include, for example, violation of Luttinger’s [7] famed volume theorem, vanishing quasiparticle weight, and/or anomalous thermodynamics and transport [179, 180, 5, 181, 182, 183]. This theoretical quandary is rather unfortunate as it is likely prohibiting a full understanding of the mechanism behind high-temperature superconductivity, as well as stymying theoretically-guided searches for new exotic materials.

Pioneering early theoretical work on the cuprates relied on two main premises [23, 184, 51, 52, 185, 34], from which we will be guided but not constrained in our pursuit and understanding of a particular non-Fermi liquid metal: (1) that the microscopics can be described by the square lattice Hubbard model with on-site Coulomb repulsion, which at strong coupling reduces in its simplest form to the t - J model; and (2) that the physics of the system can be faithfully represented by the “slave-boson” technique, wherein the physical electron operator is written as a product of a slave boson (“chargon”), which carries the electronic charge, and a spin-1/2 fermionic “spinon” [186], which carries the spin, both strongly coupled to an emergent gauge field (see Sec. 1.2). However, within the slave-boson formulation, it has been difficult to access non-Fermi liquid physics at low temperatures because this requires the chargons to be in an uncondensed, yet conducting, quantum phase [187], i.e., some sort of the elusive “Bose metal”. Early attempts to describe the strange metal in this framework treated it as a strictly finite-temperature phenomenon in which the slave bosons form an uncondensed, but classical, Bose fluid [51, 52], a treatment which precludes the possibility that the strange metal is a true quantum phase at all.

In our view, the strange metal should be viewed as a genuine two-dimensional (2D) quantum phase, which can perhaps be unstable to superconducting or pseudogap behavior. Indeed,

recent experimental work on $\text{La}_{2-x}\text{Sr}_x\text{CuO}_4$ has shown that when superconductivity is stripped away by high magnetic fields, strange metal behavior persists over a wide doping range down to extremely low temperatures [78]. Thus, the strange metal in the cuprates is quite possibly a true, extended, zero-temperature quantum phase [80].

Inspired by these results and building on our previous work which proposed [92] and succeeded in realizing [84, 85, 86] a genuine, zero-temperature Bose metal, we employ a novel variant of the slave-boson approach to construct and analyze an exotic 2D non-Fermi liquid quantum phase, which we refer to as the “*d*-wave metal”. The *d*-wave metal is modeled by a variational wave function consisting of a product of a *d*-wave Bose metal wave function [92, 84, 85, 86] for the chargons and a usual Slater determinant for the spinon. Importantly, placing the chargons into the *d*-wave Bose metal state imparts the many-electron wave function with a sign structure qualitatively distinct from that of a simple Slater determinant, and in particular, imprints strong singlet *d*-wave two-particle correlations. This results in a gapless, conducting quantum fluid with an electron momentum distribution function which exhibits a critical, singular surface that violates Luttinger’s volume theorem [7], as well as prominent critical Cooper pairs with *d*-wave character. The *d*-wave nature of our phase is tantalizingly suggestive of incipient *d*-wave superconductivity and thus of possible relevance to the cuprates.

Furthermore, tying back into premise (1) above, we propose a reasonably simple model Hamiltonian to stabilize the *d*-wave metal by augmenting the traditional *t*-*J* model with a four-site ring-exchange term *K*. Then, owing to the afforded numerical and analytical tractability provided by the density matrix renormalization group (DMRG) [109, 110] and bosonization [4, 188, 104, 189], we place the problem on a quasi-one-dimensional (quasi-1D) two-leg

ladder geometry (see Fig. 4.1). In this system, we establish several lines of compelling evidence that the d -wave metal phase exists as the quantum ground state of our t - J - K model Hamiltonian, and we are able to characterize and understand the phase very thoroughly. Importantly, our realized two-leg d -wave metal state is *nonperturbative* in that it cannot be understood within conventional Luttinger liquid theory [4] starting from free electrons [108]. We believe this study to be one of the first unbiased numerical demonstrations of a non-Fermi liquid metal as the stable ground state of a local Hamiltonian. Finally, in Sec. 4.6, we will discuss straightforward extensions of these results to two dimensions, as well as comment on their potential relevance to the actual non-Fermi liquids observed in experiment.

4.2 Gauge Theory and Variational Wave Functions for the d -wave Metal

Our theoretical description of the non-Fermi liquid d -wave metal begins by writing the electron operator for site \mathbf{r} and spin state $s = \uparrow, \downarrow$ as the product of a bosonic chargon $b(\mathbf{r})$ and fermionic spinon $f_s(\mathbf{r})$; that is, $c_s(\mathbf{r}) = b(\mathbf{r})f_s(\mathbf{r})$. With $b(\mathbf{r})$ a hard-core boson operator, this construction prohibits doubly occupied sites, an assumption we make from here on. The physical electron Hilbert space is recovered by implementing at each site the constraint $b^\dagger(\mathbf{r})b(\mathbf{r}) = \sum_s f_s^\dagger(\mathbf{r})f_s(\mathbf{r}) = \sum_s c_s^\dagger(\mathbf{r})c_s(\mathbf{r}) = n_e(\mathbf{r})$, which physically means that a given site is either empty or contains a chargon and exactly one spinon to compose an electron. Theoretically, this is achieved by strongly coupling the b 's and f 's via an emergent gauge field [34].

Under the natural assumption that the spinons are in a Fermi sea state, the behavior of the

chargons determines the resulting electronic phase. Condensing the bosonic chargons so that $\langle b(\mathbf{r}) \rangle \neq 0$ implies $c_s(\mathbf{r}) \sim f_s(\mathbf{r})$; thus, in this case, the electronic phase is that of a Fermi liquid. It then follows that in order to describe a non-Fermi liquid conducting quantum fluid within this framework, we require that the chargons not condense, $\langle b(\mathbf{r}) \rangle = 0$, yet still conduct. However, accessing such a “Bose metal” phase has proven extremely difficult over the years. In recent work [92, 84, 85, 86], we have indeed succeeded in realizing a concrete, genuine Bose metal phase, which we named the “ d -wave Bose liquid” or, equivalently, “ d -wave Bose metal” (DBM). The DBM is central to our construction of the d -wave metal. Specifically, in the DBM, we decompose the hard-core boson as $b(\mathbf{r}) = d_1(\mathbf{r})d_2(\mathbf{r})$ with the constraint $d_1^\dagger(\mathbf{r})d_1(\mathbf{r}) = d_2^\dagger(\mathbf{r})d_2(\mathbf{r}) = b^\dagger(\mathbf{r})b(\mathbf{r})$, where d_1 (d_2) are fermionic slave particles (“partons”) with *anisotropic hopping patterns*: d_1 (d_2) is chosen to hop preferentially in the \hat{x} (\hat{y}) direction. The resulting bosonic phase is a conducting, yet uncondensed, quantum fluid, which is precisely the phase into which we place the charge sector of the d -wave metal. That is, for the d -wave metal we take a novel *all fermionic* decomposition of the electron,

$$c_s(\mathbf{r}) = d_1(\mathbf{r})d_2(\mathbf{r})f_s(\mathbf{r}), \quad (4.1)$$

subject to the constraint

$$d_1^\dagger(\mathbf{r})d_1(\mathbf{r}) = d_2^\dagger(\mathbf{r})d_2(\mathbf{r}) = \sum_s f_s^\dagger(\mathbf{r})f_s(\mathbf{r}) = n_e(\mathbf{r}). \quad (4.2)$$

The resulting theory now includes two gauge fields: one to glue together d_1 and d_2 to form the chargon and another to glue together b and f to form the electron. In the Supplementary Information of Ref. [82] and Appendix D of this dissertation, we give a detailed bosonization analysis of this novel gauge theory for the two-leg ladder system on which we focus below.

Guided by the slave-boson construction, one can naturally construct electronic variational wave functions by taking the product of a hard-core bosonic wave function ψ_b with a fermionic wave function ψ_f and evaluating them at the same coordinates (Gutzwiller projection):

$$\psi_c(\{\mathbf{r}_i^\uparrow\}, \{\mathbf{r}_i^\downarrow\}) = \mathcal{P}_G \left[\psi_b(\{\mathbf{R}_i\}) \times \psi_f(\{\mathbf{r}_i^\uparrow\}, \{\mathbf{r}_i^\downarrow\}) \right], \quad (4.3)$$

where \mathcal{P}_G performs the projection into the physical electronic Hilbert space: $\{\mathbf{R}_i\} = \{\mathbf{r}_i^\uparrow\} \cup \{\mathbf{r}_i^\downarrow\}$. If we put the f 's into a spin-singlet Fermi sea state with orbitals $\{\mathbf{k}_j\}$ (Slater determinant), i.e., $\psi_f(\{\mathbf{r}_i^\uparrow\}, \{\mathbf{r}_i^\downarrow\}) = \det[e^{i\mathbf{k}_j \cdot \mathbf{r}_i^\uparrow}] \det[e^{i\mathbf{k}_j \cdot \mathbf{r}_i^\downarrow}] = \psi_f^{\text{FS}}$, then we can model both the Fermi liquid metal and the non-Fermi liquid d -wave metal in a unified way. In both cases, the wave functions are straightforward to implement using variational Monte Carlo (VMC) methods [140, 139, 190].

For the Fermi liquid, we put the b 's into a superfluid wave function ψ_b^{SF} via a typical Jastrow form, so that, schematically, $\psi_c^{\text{FL}} = \mathcal{P}_G[\psi_b^{\text{SF}} \times \psi_f^{\text{FS}}]$. Note that since ψ_b^{SF} is a positive wave function, the sign structure [191] of ψ_c^{FL} is identical to that of the noninteracting Fermi sea state. In contrast, to model the d -wave metal, we put the b 's into a Bose metal wave function according to the DBM construction of Refs. [92, 84, 85, 86]:

$$\psi_b(\{\mathbf{R}_i\}) = \psi_{d_1}(\{\mathbf{R}_i\}) \times \psi_{d_2}(\{\mathbf{R}_i\}) = \psi_b^{\text{DBM}}, \quad (4.4)$$

where ψ_{d_1} (ψ_{d_2}) is a Slater determinant with a Fermi sea compressed in the \hat{x} (\hat{y}) direction [92].

Then, we have

$$\psi_c^{d\text{-metal}} = \mathcal{P}_G [\psi_b^{\text{DBM}} \times \psi_f^{\text{FS}}] = \mathcal{P}_G [\psi_{d_1} \times \psi_{d_2} \times \psi_f^{\text{FS}}]. \quad (4.5)$$

Interestingly, this construction, Eq. (4.5), is actually a time-reversal invariant analog of the composite Fermi liquid description of the half-filled Landau level [53], where the d -wave Bose

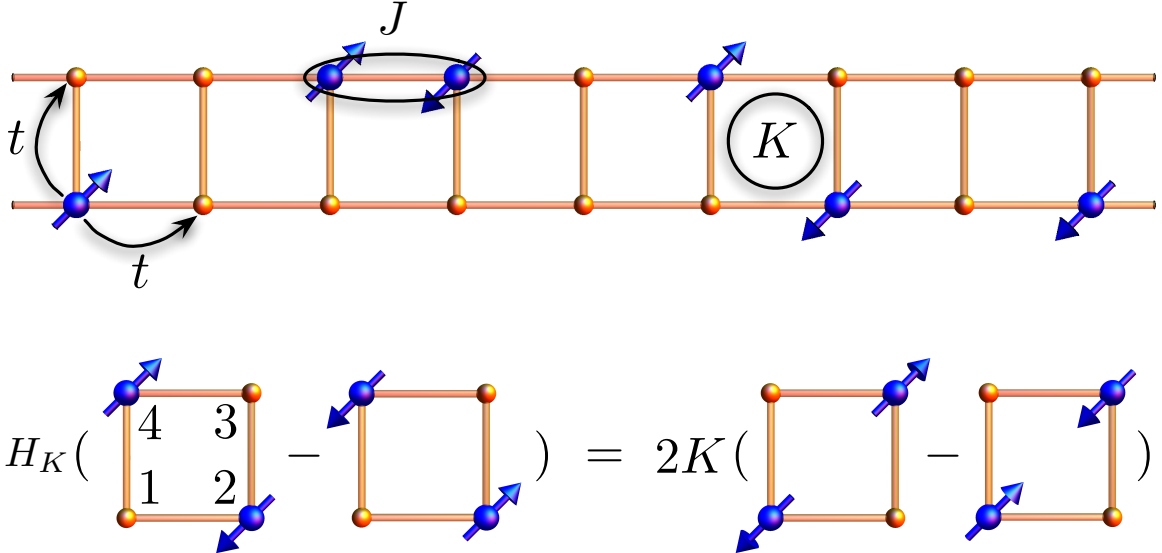


Figure 4.1: *Schematic of the t - J - K model Hamiltonian.* Top: Picture of the full t - J - K model, Eq. (4.6), on the two-leg ladder. In this work, we use periodic boundary conditions in the long (\hat{x}) direction for all calculations. Bottom: Action of the ring term H_K , Eq. (4.8), on a single plaquette, elucidating its “singlet-rotation” nature.

metal wave function [92] plays the role of Laughlin’s $\nu = 1/2$ bosonic state [137]. Just as Laughlin’s wave function imprints a nontrivial complex phase pattern on the Slater determinant, the DBM wave function imprints a nontrivial d -wave sign structure, hence our designation “ d -wave metal”. As we explore in detail below, there are many physical signatures associated with putting the chargons into the DBM phase, making the d -wave metal dramatically distinguishable from the traditional Landau Fermi liquid.

4.3 Microscopic Ring-Exchange Model

The t - J - K model Hamiltonian which we propose to stabilize the d -wave metal phase is given by

$$H = H_{tJ} + H_K, \quad (4.6)$$

$$H_{tJ} = -t \sum_{\langle i,j \rangle, s=\uparrow,\downarrow} \left(c_{is}^\dagger c_{js} + \text{H.c.} \right) + J \sum_{\langle i,j \rangle} \mathbf{S}_i \cdot \mathbf{S}_j, \quad (4.7)$$

$$H_K = 2K \sum_{\square} (\mathcal{S}_{13}^\dagger \mathcal{S}_{24} + \text{H.c.}), \quad (4.8)$$

where $\langle i, j \rangle$ and \square indicate sums over all nearest-neighbor bonds and all elementary plaquettes of the 2D square lattice, respectively. In the spirit of the t - J model, we choose to work in the subspace of no doubly occupied sites, but for simplicity, we do ignore the term $-\frac{J}{4}n_i n_j$ present in typical definitions of the t - J model [34]. In Eq. (4.8), we have defined a singlet creation operator on two sites as $\mathcal{S}_{ij}^\dagger = \frac{1}{\sqrt{2}}(c_{i\uparrow}^\dagger c_{j\downarrow}^\dagger - c_{i\downarrow}^\dagger c_{j\uparrow}^\dagger)$, so that H_K can be viewed as a four-site singlet-rotation term (see Fig. 4.1). For $K > 0$, the ground state of H_K on a single plaquette with two electrons is a d_{xy} -orbital spin-singlet; thus, loosely speaking, H_K has a tendency to build in d -wave correlations in the system and qualitatively alter the sign structure of the electronic ground state. Further arguments for studying this model in our search for the d -wave metal can be found in the Supplementary Information of Ref. [82].

While not being particularly conventional, our ring-exchange term H_K (which should not be confused with four-site cyclic spin-exchange; see Refs. [192, 58, 59] and Chapter 3) is in fact present when projecting the continuum many-body Hamiltonian for screened Coulomb-interacting electrons into a narrow, tight-binding band [193] (see the Supplementary Information of Ref. [82]). In fact, estimating the strength of K , or coefficients on related terms, in real materials such as $\text{La}_{2-x}\text{Sr}_x\text{CuO}_4$ is an interesting open question.

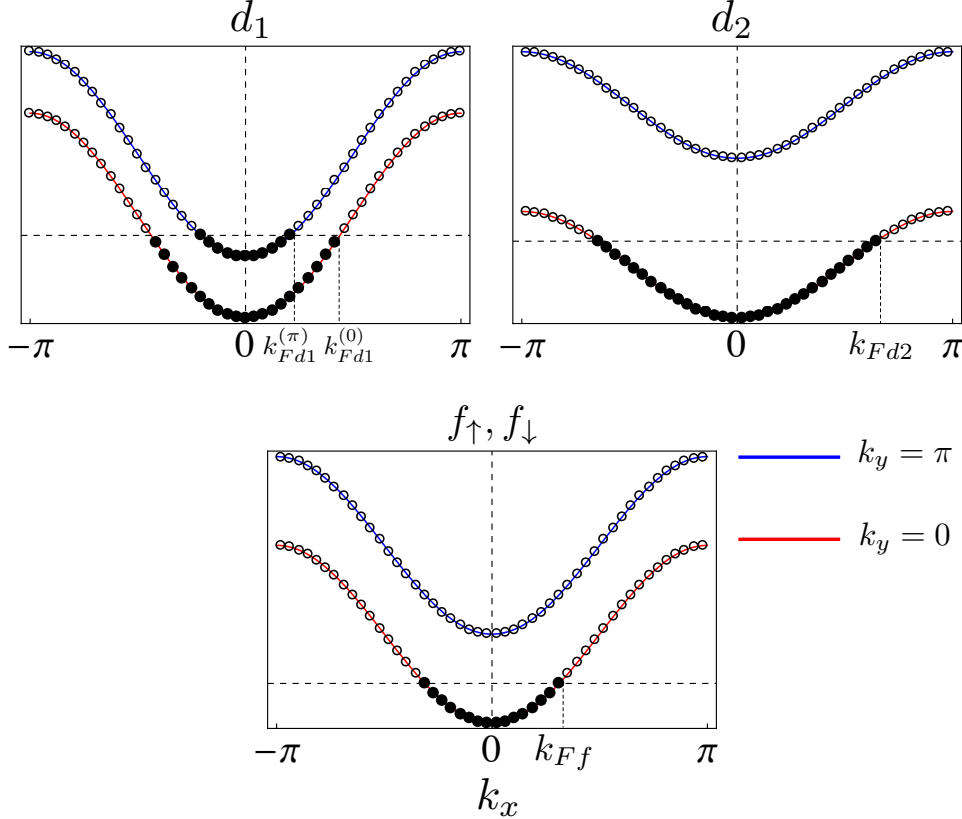


Figure 4.2: *Picture of the parton bands for the d -wave metal phase.* We show orbitals for a 48×2 system, showing partially occupied bonding ($k_y = 0$) and antibonding ($k_y = \pi$) bands for d_1 and partially occupied bonding bands for d_2 and $f_{\uparrow/\downarrow}$; that is, each Slater determinant in Eq. (4.5) consists of momentum-space orbitals as depicted here. The total electron number is $N_e = N_{c\uparrow} + N_{c\downarrow} = N_{d1} = N_{d2} = N_{f\uparrow} + N_{f\downarrow} = 32$, with $N_{f\uparrow} = N_{f\downarrow} = 16$ so that $S_{\text{tot}} = 0$; the longitudinal boundary conditions are periodic for d_1 and antiperiodic for d_2 and $f_{\uparrow/\downarrow}$. This is precisely the same d -wave metal configuration for which we display characteristic measurements in Fig. 4.5.

4.4 Two-Leg Study: DMRG and VMC

Unfortunately, as with any interacting fermionic model, our t - J - K Hamiltonian suffers from the so-called “fermionic sign problem”, rendering quantum Monte Carlo calculations inapplicable [113]. We thus follow the heretofore successful [84, 58, 85, 59, 86] approach of accessing 2D gapless phases by studying their *quasi-1D descendants* on ladder geometries, relying heavily on large-scale DMRG calculations. In fact, we have already established [84,

85, 86] that for two, three, and four legs, the DBM phase itself is the stable ground state of a boson ring-exchange model analogous to Eq. (4.6). Here, we take the important first step of placing the electron ring t - J - K model on the two-leg ladder in search of a two-leg descendant of the d -wave metal.

For concreteness, we now consider the model, Eq. (4.6), on the two-leg ladder (see Fig. 4.1) at a generic electron density of $\rho = N_e/(2L_x) = 1/3$, where $N_e = N_{c\uparrow} + N_{c\downarrow}$ is the total number of electrons and L_x is the length of our two-leg ladder (i.e., the system has $L_x \times 2$ total sites). At this density, $\rho = 1/3 < 1/2$, on the two-leg ladder, the noninteracting ground state is a spin-singlet wherein electrons of each spin partially fill the bonding band ($k_y = 0$), leaving the antibonding band ($k_y = \pi$) empty. Thus, for $t \gg K$, we expect the system to be in a simple one-band metallic state, which is a two-leg analog of the Fermi liquid. Formally speaking, this phase is a conventional Luttinger liquid with two one-dimensional (1D) gapless modes (central charge $c = 2$). For moderate values of ring exchange, $K \gtrsim t$, we anticipate the unconventional non-Fermi liquid d -wave metal to be a candidate ground state. On the two-leg ladder at this density, the d -wave metal phase has characteristic band filling configurations for the d_1 , d_2 , and $f_{\uparrow/\downarrow}$ partons as shown in Fig. 4.2: d_1 partially fills both bonding and antibonding bands, while d_2 and $f_{\uparrow/\downarrow}$ only fill the bonding band. (The d_1 and d_2 configurations constitute the phase denoted “DBL[2,1]” in Ref. [84].) In a mean-field approximation in which the partons do not interact, the system has five 1D gapless modes corresponding to the five total partially filled bands. However, in the strong-coupling limit of the full quasi-1D gauge theory (see the Supplementary Information of Ref. [82] and Appendix D of this dissertation), two orthonormal linear combinations of the original five modes are rendered massive, leaving an *unconventional*

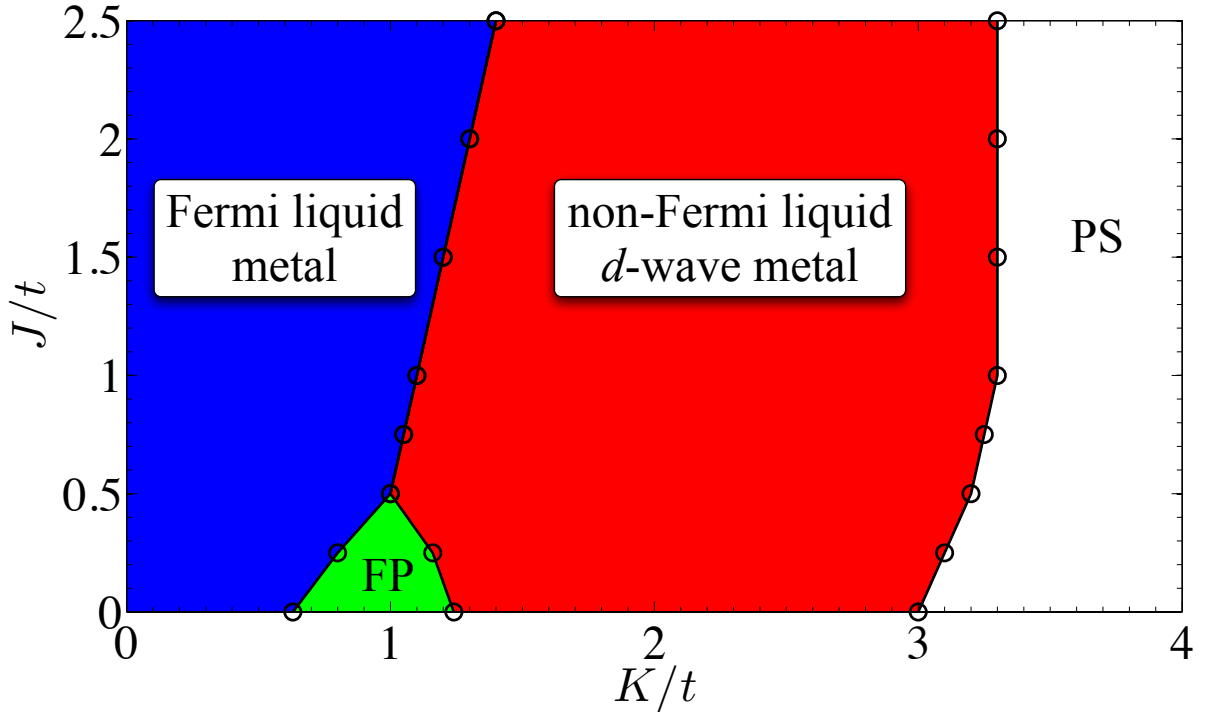


Figure 4.3: *Phase diagram of the t - J - K electron ring-exchange model at electron density $\rho = 1/3$ on the two-leg ladder.* In addition to the conventional one-band metal (“Fermi liquid metal”) and exotic “non-Fermi liquid d -wave metal”, there are two other realized phases. For small J , there is an intermediate phase with fully polarized electrons (region labeled “FP”). For large K , due to the inherently attractive nature of ring-exchange interactions [84], the system generally phase separates along the ladder (region labeled “PS”).

Luttinger liquid with $c = 3$ gapless modes.

We now provide extensive numerical evidence that this two-leg descendant of the d -wave metal exists as the ground state of the t - J - K model over a wide region of the phase diagram. We summarize these results in Fig. 4.3 by presenting the full phase diagram in the parameters K/t vs. J/t as obtained by DMRG calculations on length $L_x = 24$ and 48 systems at electron density $\rho = 1/3$. For small K , we find a conventional one-band (spinful) Luttinger liquid phase which is a two-leg analog of the “Fermi liquid metal”, hence the label in Fig. 4.3. For moderate J and upon increasing K , the system goes into the unconventional “non-Fermi liquid d -wave metal” phase, which is the main focus of this work. The phase boundaries in Fig. 4.3, all of

which represent strong first-order transitions, were determined by measuring several standard momentum-space correlation functions in the DMRG (see Appendix A.3 for details): the electron momentum distribution function $\langle c_{\mathbf{q}s}^\dagger c_{\mathbf{q}s} \rangle$, the density-density structure factor $\langle \delta n_{\mathbf{q}} \delta n_{-\mathbf{q}} \rangle$, and the spin-spin structure factor $\langle \mathbf{S}_{\mathbf{q}} \cdot \mathbf{S}_{-\mathbf{q}} \rangle$.

For concreteness, we now focus on the cut along $J/t = 2$ in Fig. 4.3 for a 48×2 system with $N_e = 32$ electrons. We take one point deep within the conventional one-band metal at $K/t = 0.5$ and the other point deep within the exotic d -wave metal at $K/t = 1.8$. First focusing on the former case, we show in Fig. 4.4 DMRG measurements characteristic of the conventional Luttinger liquid. The ground state is a spin-singlet with a sharp singularity in the electron momentum distribution function at $q_y = 0$ and $q_x = k_F = \pi N_{c\uparrow}/L_x = 8 \cdot 2\pi/48$, which is a usual Fermi wavevector determined solely from the electron density. The density-density and spin-spin structure factors at $q_y = 0$ also exhibit familiar features at $q_x = 0$ and $q_x = 2k_F = 16 \cdot 2\pi/48$, both characteristic of an ordinary one-band metallic state with gapless charge and spin modes [4]. We stress that, even with the constraint of no double-occupancy and nonzero $K/t = 0.5$ and $J/t = 2$, the interacting electronic system is still qualitatively very similar to the two-leg free Fermi gas; analogously, the 2D Fermi liquid is in many ways qualitatively similar to the 2D free Fermi gas. In both cases, the main differences are basically quantitative and are well-understood [4, 3].

We turn now to the characteristic point within the d -wave metal phase at $J/t = 2$ and $K/t = 1.8$. In Fig. 4.5, we show a set of DMRG measurements at this point, as well as measurements corresponding to a variational wave function chosen such that its singular features best reproduce the DMRG data (see the Supplementary Information of Ref. [82] for details

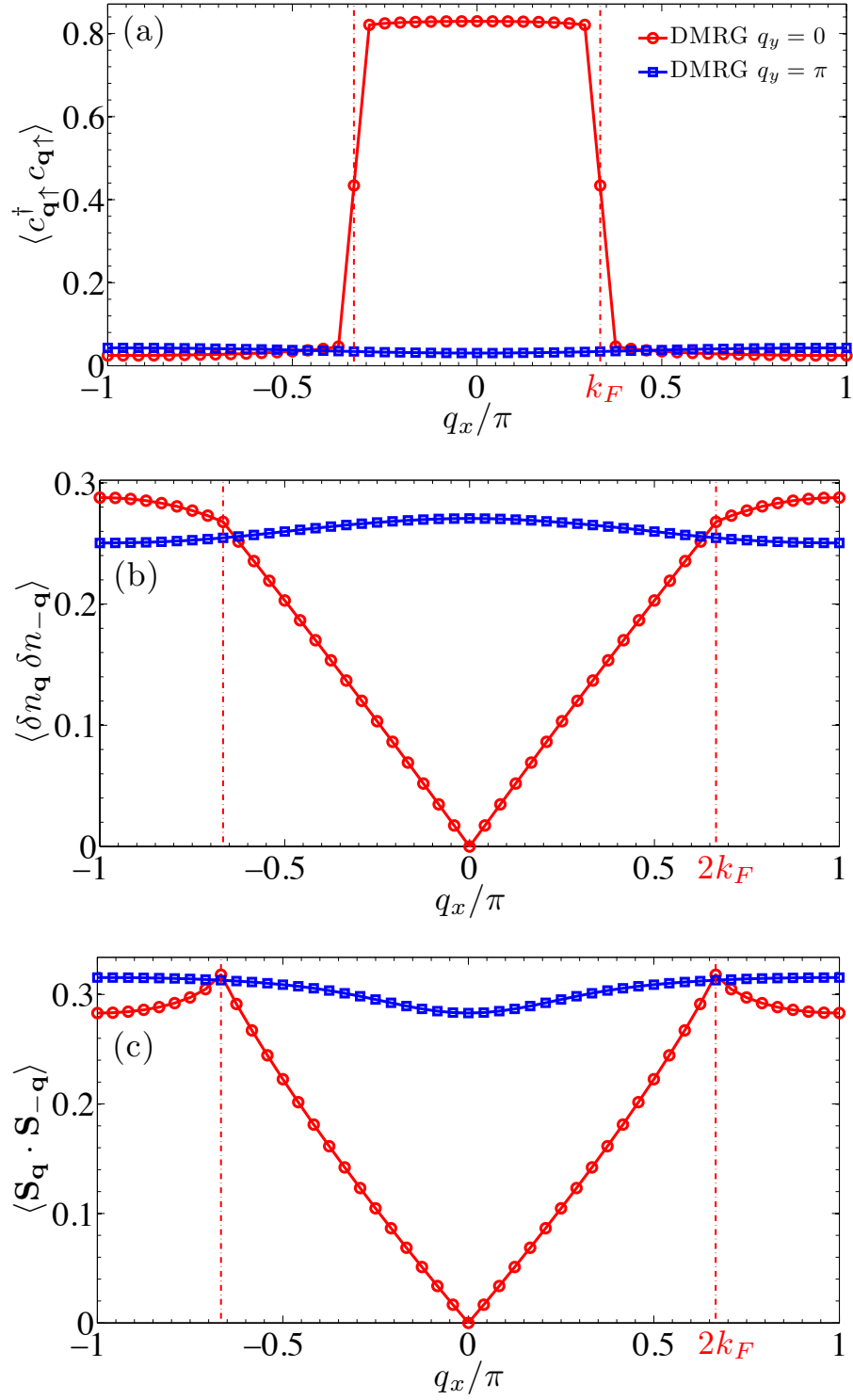


Figure 4.4: *DMRG measurements in the conventional Luttinger liquid phase at $J/t = 2$ and $K/t = 0.5$. We show (a) the electron momentum distribution function, (b) the density-density structure factor, and (c) the spin-spin structure factor. The important wavevectors k_F and $2k_F$, as described in the text, are highlighted by vertical dashed-dotted lines.*

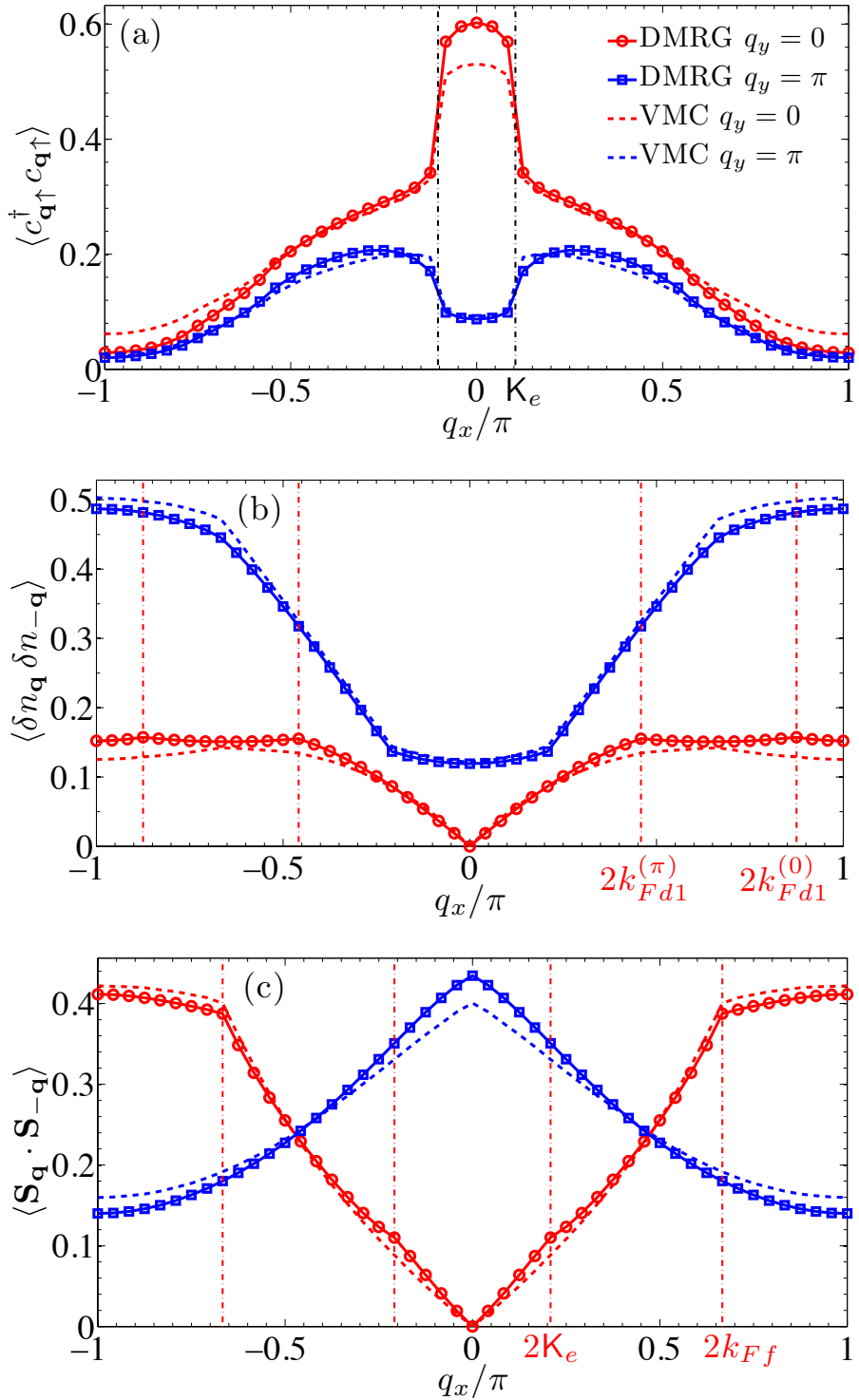


Figure 4.5: *DMRG measurements in the unconventional d -wave metal phase at $J/t = 2$ and $K/t = 1.8$. We show the same quantities as in Fig. 4.4. Here, we also show the matching VMC measurements using a d -wave metal trial wave function depicted in Fig. 4.2.*

of our VMC methods). The selected d -wave metal wave function is depicted schematically in Fig. 4.2. Specifically, we have the following parton Fermi wavevectors: $2k_{Fd1}^{(0)} = 21 \cdot 2\pi/48$, $2k_{Fd1}^{(\pi)} = 11 \cdot 2\pi/48$, $2k_{Fd2} = 32 \cdot 2\pi/48$, and $2k_{Ff} = 16 \cdot 2\pi/48$. The overall agreement between the DMRG and VMC measurements is very compelling, and we now summarize our understanding of these results from the perspective of the d -wave metal theory.

In sharp contrast to the conventional Luttinger liquid, the electron momentum distribution function now has singularities for both $q_y = 0$ and $q_y = \pi$ at a wavevector $q_x = K_e \equiv [k_{Fd1}^{(0)} - k_{Fd1}^{(\pi)}]/2$. This wavevector corresponds to a composite electron made from a combination of parton fields consisting of a right-moving d_1 parton, a left-moving d_2 parton, and a right-moving spinon: $d_{1R}^{(q_y)} d_{2L} f_{\uparrow R}$. In fact, these “enhanced electrons” can be guessed from simple “Amperian rules” [34, 54, 55] in our quasi-1D gauge theory as described in detail in the Supplementary Information of Ref. [82].

The corresponding density-density and spin-spin structure factors, displayed in Fig. 4.5(b)-(c), also show nontrivial behavior. We expect the density-density structure factor to be sensitive to each parton configuration individually and thus have singular features at various “ $2k_F$ ” parton wavevectors (see Refs. [92, 85] and the Supplementary Information of Ref. [82]). In the DMRG measurements, the most noticeable features are at $q_y = 0$ and $q_x = 2k_{Fd1}^{(0)}, 2k_{Fd1}^{(\pi)}$, which allow us to directly read off the realized d_1 parton configuration (see Fig. 4.2). The lack of these features in the VMC data, as well as the lack of analogous features at $q_x = 2k_{Fd2}$ in the DMRG data, can be understood within our gauge theory framework as presented in the Supplementary Information of Ref. [82], where we also note that our wave function is only a caricature of the full theory. Finally, the spin-spin structure factor at $q_y = 0$ not only has a

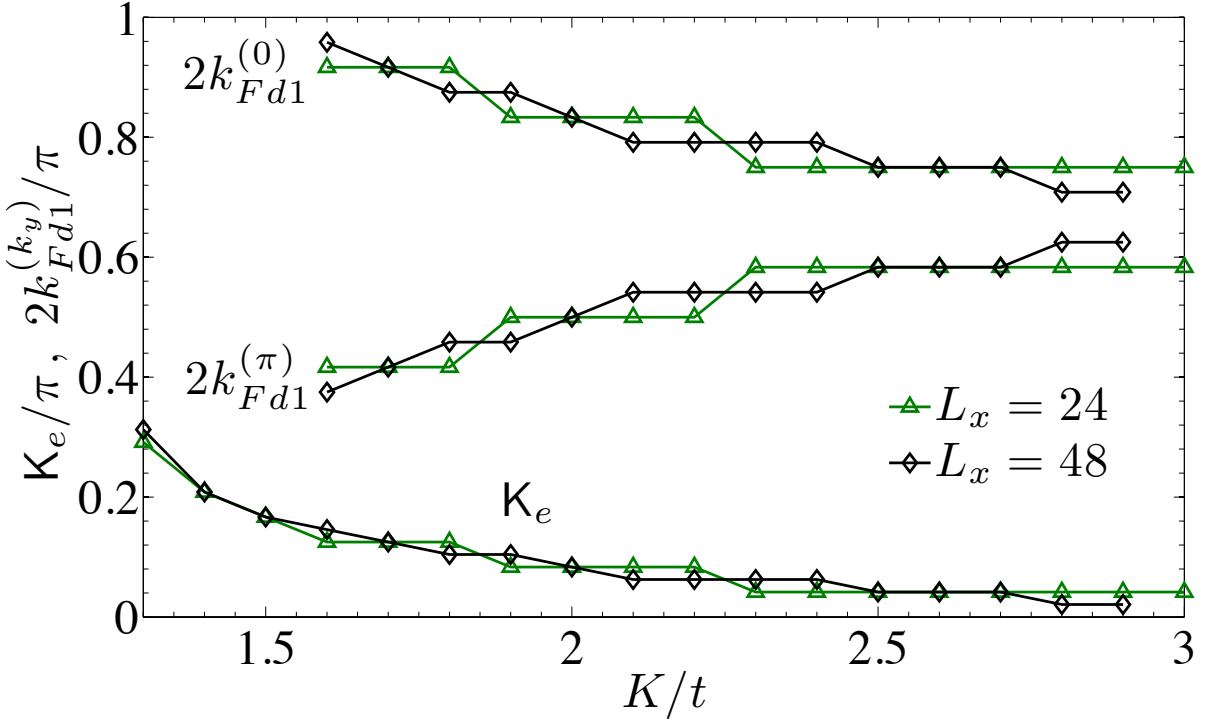


Figure 4.6: *Evolution of singular wavevectors in the d-wave metal phase.* At fixed $J/t = 2$ and varying K/t , we show the location of the dominant singular wavevector K_e in the electron momentum distribution function [see Fig. 4.5(a)], as well as the wavevectors identified as $2k_{Fd1}^{(0)}$ and $2k_{Fd1}^{(\pi)}$ in the density-density structure factor [see Fig. 4.5(b)]. These calculations were done with DMRG.

familiar, expected feature at $q_x = 2k_{Ff}$ coming from the spinon, but also remarkably contains a feature at $q_x = 2K_e$ that can be thought of as a “ $2k_F$ ” wavevector from the dominant “electron” in Fig. 4.5(a). All in all, as we detail thoroughly in the Supplementary Information of Ref. [82], the DMRG measurements are amazingly consistent, even on a fine quantitative level, with being in a stable non-Fermi liquid d -wave metal phase.

It is important to note that the wavevector K_e depends on the interaction strength K/t since the wavevectors $k_{Fd1}^{(0)}$ and $k_{Fd1}^{(\pi)}$ vary with ring exchange [84]. In Fig. 4.6, we show at $J/t = 2$ evolution with K/t of the wavevector K_e , i.e., the location of the sharp steps in the electron momentum distribution function [see Fig. 4.5(a)], as determined by DMRG. Since

the momentum-space “volume” enclosed by these singular features depends on the interaction K/t and is not simply determined by the total density of electrons, we may confidently say that the d -wave metal violates Luttinger’s volume theorem [7]. In fact, the very notion of a single “Fermi surface” is actually ambiguous in the d -wave metal phase. We also show in Fig. 4.6, for those values of K/t at which they are discernible, the wavevectors $2k_{Fd1}^{(0)}$ and $2k_{Fd1}^{(\pi)}$ as identified by features in the DMRG-measured density-density structure factor at $q_y = 0$ [see Fig. 4.5(b)]. For all points, the locations of the identified features satisfy the nontrivial identity $K_e = [2k_{Fd1}^{(0)} - 2k_{Fd1}^{(\pi)}]/4$, as predicted by our theory.

A remarkable property of the d -wave metal state found in the DMRG is that it has prominent critical d -wave Cooper pairs residing on the diagonals, as anticipated earlier from the ring energetics. We detail these findings in the Supplementary Information of Ref. [82], while here we only mention that such Cooper pair correlations have the slowest power law decay among all the discussed observables, including the electron Green’s function. This is in stark contrast with the conventional metal and suggests that the d -wave metal phase has some incipient d -wave superconductivity in two dimensions.

As a final piece of “smoking gun” evidence that the realized DMRG phase is in fact the d -wave metal, we have measured the number of 1D gapless modes, i.e., the effective central charge c , via scaling of the bipartite entanglement entropy [128, 194] in the DMRG and VMC [195, 22] wave functions. As explained above, we expect $c = 2$ in the conventional Luttinger liquid and $c = 3$ in the d -wave metal. A detailed comparison of the DMRG and VMC entropy measurements is presented in the Supplementary Information of Ref. [82], where the DMRG-VMC agreement is just as impressive as it is for the more traditional measurements of

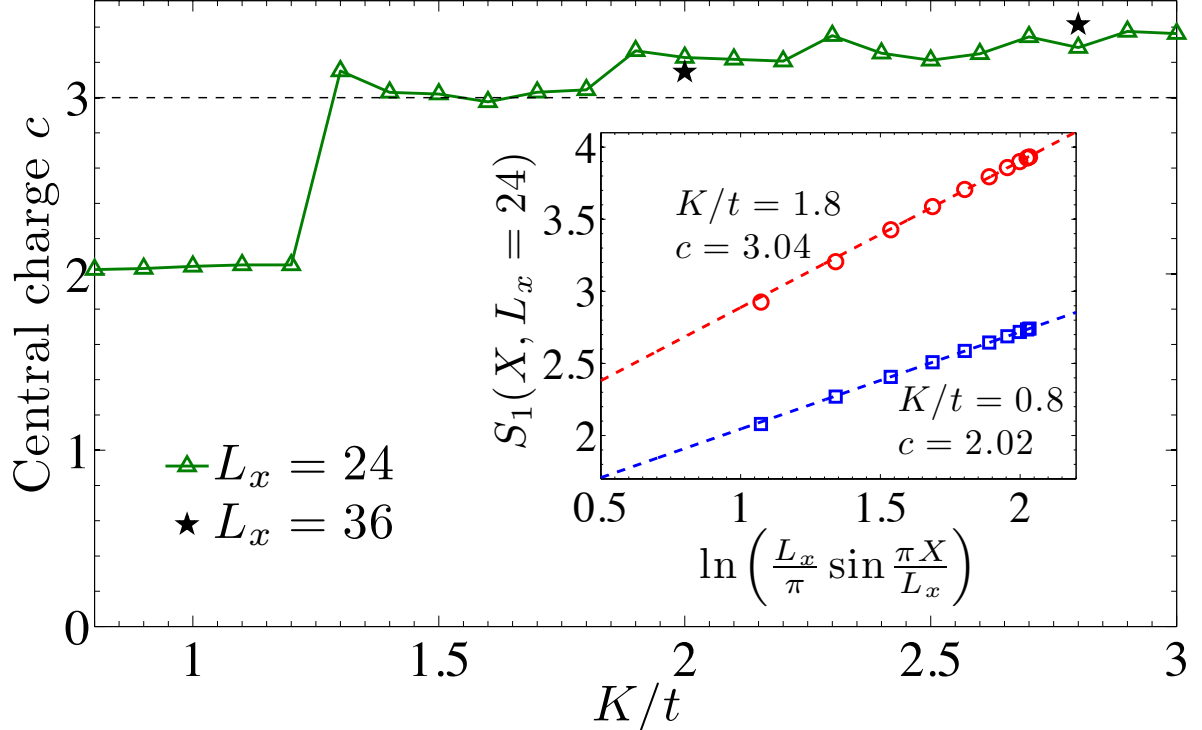


Figure 4.7: *Central charge c as a function of interaction K/t .* By measuring the von Neumann entanglement entropy S_1 in the DMRG, we calculate the effective central charge c at fixed $J/t = 2$ and varying K/t . There is a dramatic jump from $c \simeq 2$ to $c \simeq 3$ at the transition, as predicted by our theory. Data for two example points, $K/t = 0.8$ and 1.8 , is shown in the inset, where X is the number of rungs in each bipartition.

Fig. 4.5. The effective central charge versus K/t at $J/t = 2$ as determined by the DMRG is shown in Fig. 4.7. Indeed, these measurements indicate that $c \simeq 2$ in the conventional one-band metal, while $c \simeq 3$ in the exotic d -wave metal. Since $c = 3 > 2$, our putative d -wave metal phase clearly cannot be understood as an instability out of the conventional one-band metal, but also, since $c = 3 < 4$, the critical bonding and antibonding electrons in Fig. 4.5(a) cannot be reproduced by *any* perturbative treatment starting from free electrons [108]. In the following section, we elaborate on these important points in more detail.

4.5 Eliminating Conventional Luttinger Liquid Scenarios in Favor of the *d*-wave Metal

In light of the remarkable success to date of describing 1D and quasi-1D interacting quantum systems with conventional Luttinger liquid theory [4], it is natural to ask whether the results in our putative *d*-wave metal phase can be reproduced with such a conventional weak-coupling approach [108]. Clearly, since the number of gapless modes in the putative *d*-wave metal ($c = 3$) is larger than in the conventional one-band metal ($c = 2$), the former cannot be understood as an instability of the latter. However, there are more complicated scenarios that one may envision that involve strong Fermi surface renormalization, as well as electron pairing, but that still lie within the *conventional* Luttinger framework and still assume a free electron starting point.

For instance, one could first imagine the K term renormalizing the free electron band structure such that the antibonding band eventually gets populated (as if K had the effect of simply renormalizing the interchain hopping t_{\perp} towards zero—this is admittedly somewhat natural given that H_K conserves the number of electrons in each chain). If we denote a conventional Luttinger liquid with α gapless charge modes and β gapless spin modes as C α S β (see Ref. [108] and Chapter 2), then this free electron state would be some C2S2 metal with $c = 4$ gapless modes, say a charge (ρ) and spin (σ) mode for each band ($0/\pi$): $\theta_{\rho/\sigma}^{(0/\pi)}$. In principle, a spin gap in the antibonding band could be opened through relevance of an allowed backscattering term involving a cosine of only the $\theta_{\sigma}^{(\pi)}$ field [108] [see Eq. (B.84)], giving a C2S1 metal with $c = 3$ gapless modes. However, this possibility can be immediately ruled out in our puta-

tive d -wave metal region by noting that the DMRG state unambiguously has a critical Green's function for the antibonding electrons: See the sharp step in $\langle c_{\mathbf{q}s}^\dagger c_{\mathbf{q}s} \rangle$ at $\mathbf{q} = (q_x, q_y) = (\mathbf{K}_e, \pi)$ in Fig. 4.5(a), as well as the discussion in the Supplementary Information of Ref. [82] of the slow power law decay of the Green's function in real space. Pinning of the $\theta_\sigma^{(\pi)}$ field, on the other hand, directly implies that the electron Green's function would decay *exponentially* at $q_y = \pi$, in clear contradiction with our DMRG data.

Other aspects of the DMRG data are also markedly inconsistent with this C2S1 scenario. For example, throughout the d -wave metal phase at, say, $J/t = 2$ (to avoid small polarization observed at smaller J/t), we observe an enhanced feature in the spin-spin structure factor $\langle \mathbf{S}_{\mathbf{q}} \cdot \mathbf{S}_{-\mathbf{q}} \rangle$ at $\mathbf{q} = (2\pi\rho, 0)$ for all K/t . The location of this feature is fixed by the electron density and is readily explainable by our d -wave metal theory. In the C2S1 state discussed above, however, the only singularity in $\langle \mathbf{S}_{\mathbf{q}} \cdot \mathbf{S}_{-\mathbf{q}} \rangle$ at $q_y = 0$ would be at $q_x = 2k_F^{(0)}$, where $\pm k_F^{(0)}$ denotes the Fermi points for the bonding electrons assumed to be gapless. This wavevector is not fixed by the electron density and is more akin to our observed feature at $q_x = 2\mathbf{K}_e$. Hence, presence of the feature at $\mathbf{q} = (2\pi\rho, 0)$ in $\langle \mathbf{S}_{\mathbf{q}} \cdot \mathbf{S}_{-\mathbf{q}} \rangle$ [see Fig. 4.5(c)] is not consistent with a conventional C2S1. The C2S1 state also fails to explain things like why $\langle c_{\mathbf{q}s}^\dagger c_{\mathbf{q}s} \rangle$ has substantial weight outside the main “step” for the bonding electrons, whereas this observation is very naturally explained by the d -wave metal theory as shown explicitly by the VMC calculations in Fig. 4.5(a). There are yet more features in our data that are clearly inconsistent with this scenario which we do not mention further.

Having now eliminated the possibility that our putative $c = 3$ d -wave metal could instead be some conventional C2S1 obtained through band renormalization and pairing, we now con-

sider an even more complicated “standard” Luttinger scenario. Rather than focusing on the fact that we measure central charge $c = 3$ in the putative d -wave metal region, we can instead try to directly accommodate the obtained electron momentum distribution function $\langle c_{\mathbf{q}s}^\dagger c_{\mathbf{q}s} \rangle$ of Fig. 4.5(a) by postulating a band structure in which the antibonding electrons fill two disconnected Fermi segments, while the bonding electrons fill a single segment centered about $q_x = 0$. That is, consider a C3S3 metal with a Fermi sea $[-k_F^{(0)}, +k_F^{(0)}]$ in the bonding band and Fermi seas $[-k_{F2}^{(\pi)}, -k_{F1}^{(\pi)}]$, $[+k_{F1}^{(\pi)}, +k_{F2}^{(\pi)}]$ in the antibonding band ($k_{F2}^{(\pi)} > k_{F1}^{(\pi)} > 0$). Such a band structure could arise, for example, if the K term renormalizes the antibonding electrons to have substantial next-nearest-neighbor hopping. Furthermore, to be consistent with the DMRG data, we must take $k_F^{(0)} = k_{F1}^{(\pi)} \equiv K_e$, which would of course not generally be true for such a band structure, but such a fine-tuned state could at least exist in principle.

There exist many possible phases obtainable by gapping out various modes in the $c = 6$ C3S3 state. However, to reproduce the DMRG data within this framework, we must retain gapless electron fields at $\pm k_F^{(0)}$ and $\pm k_{F1}^{(\pi)}$ which directly implies $c \geq 4$. Thus, due to our measurement of $c = 3 < 4$ with the DMRG (see Fig. 4.7) we can eliminate *on very general grounds* any weak-coupling scenario that ends with critical electrons in both the bonding and antibonding bands.

All in all, the above weak-coupling scenarios clearly have severe difficulty describing the DMRG data obtained in the putative d -wave metal region of the phase diagram. Of course, we cannot rule out every single weak-coupling scenario, including even more complicated and contrived ones, but the above two possibilities would be the most natural in our view, and they are clearly not working. On the other hand, we stress that our d -wave metal framework can

basically describe the *entire* DMRG data set in a very natural, unified fashion, giving us a high degree of confidence that our novel *nonperturbative* d -wave metal theory is indeed correct. In addition, as discussed in the Supplementary Information of Ref. [82], the structure of the d -wave metal gauge theory itself gives us reason to at least anticipate that the t - J - K model Hamiltonian may harbor the non-Fermi liquid d -wave metal phase.

4.6 Discussion and Outlook

In this paper, we have presented exceptionally strong evidence for stability of a two-leg descendant of our exotic strange metal-type phase, the d -wave metal, and we conclude here with an outlook on exciting future work. Firstly, it would be desirable to march towards two dimensions by studying systems with more legs, where our present two-leg d -wave metal treatment is readily extendable. One of the main purposes of Ref. [86] was to establish stability of the d -wave Bose metal, the main ingredient of the d -wave metal, on three- and four-leg ladders, and this was indeed achieved. Thus, we do not envision any conceptual obstacles in the way of realizing a similar result for the d -wave metal. However, we do anticipate that going to more legs will be very challenging numerically for the DMRG due to the large amount of spatial entanglement present in the d -wave metal and Fermi liquid—this is also the current limitation preventing modern 2D tensor network state methods from attacking such problems [135]. A first step along these lines is to stay on the two-leg ladder, but increase the electron density such that the spinons potentially form a *two-band* metallic state (cf. the one-band state of the present chapter). This would lead to an exotic $c = 5$ mode d -wave metal phase and would itself constitute a significant step towards a putative two-dimensional realization of the d -wave metal.

While we leave such a complete DMRG study for future work, in Appendix D we present a bosonization analysis of this unconventional $c = 5$ mode Luttinger liquid and show that it is at least in principle a stable quantum phase.

With the goal of connecting to experiment, it would also be interesting to perform a detailed energetics study of the t - J - K model in two dimensions and explore applicability of such models to strongly correlated materials. By studying 2D variational wave functions based on the d -wave metal, it should be possible to compare physical properties with experimentally observed strange metals, such as that in the cuprates. This could include various instabilities of the d -wave metal, e.g., spinon pairing as a model of a pseudogap metal or chargon pairing as a model of an “orthogonal metal” discussed recently [196]. It would be particularly exciting to investigate incipient d -wave superconductivity of the cuprate variety—this is rather natural given the d -wave sign structure already inherent in the nonsuperconducting parent d -wave metal. Finally, while we have thus far stressed its Luttinger volume violation as a characteristic non-Fermi liquid property of the d -wave metal, we note that the 2D phase will also have no Landau quasiparticle as well as exhibit non-Fermi-liquid-like thermodynamics and transport. Comparing these predictions with properties of real strange metals would be an interesting endeavor. In the end, however, we would like to stress the conceptual nature of the present study, and we hope that our ideas may open up new avenues for thinking about non-Fermi liquid electronic fluids.

Chapter 5

Concluding Remarks

Strongly correlated electron systems present many outstanding theoretical challenges, one of the most difficult being developing a framework for highly entangled gapless systems in two dimensions which lack a weakly interacting description. In Chapters 2 and 4, we addressed two fundamental and experimentally important problems which fall under this most challenging realm: the continuous Mott metal-insulator transition and conducting non-Fermi liquid metals. In each case, we performed fully controlled studies of directly analogous problems on quasi-one-dimensional two-leg ladders, and although the two-leg system is admittedly a long ways from full two dimensions, we believe our results are beginning to shed light on what may eventually happen in 2D. In the future, it will clearly be desirable to go beyond two legs and see if the “exotic” behavior survives as we approach 2D. This is an exceedingly challenging DMRG task for the itinerant electron systems at the focus of Chapters 2 and 4; however, closely related spin and hard-core boson models indicate that the interesting physics indeed survives up to four-leg systems [59, 86], which is very encouraging. Still, it is clear that we need to be-

gin employing new numerical algorithms to make truly meaningful progress. The “multiscale entanglement renormalization ansatz” (MERA) of Vidal and coworkers [197, 198, 134, 136] seems well-suited for these most highly entangled gapless problems, and it would be most interesting to apply such methods to similar model Hamiltonians to those studied in this dissertation in both quasi-1D and eventually in full 2D.

In Chapter 3, we proposed a new low-energy theory for the two triangular lattice organic spin liquid candidate materials κ -(BEDT-TTF)₂Cu₂(CN)₃ and EtMe₃Sb[Pd(dmit)₂]₂. Our new $d + id$ state with quadratic band touching (QBT) has very appealing phenomenology with respect to the available experimental data and does surprisingly well variationally in an appropriate Heisenberg spin model supplemented with four-site cyclic ring exchange. Going forward, it will be interesting to look at this state in yet more detail both field theoretically and numerically with the VMC. The QBT state of Chapter 3 and the spin Bose metal state of Chapter 2 are very different quantum phases, yet both have many appealing characteristics in regard to the organics. Only with future experimental data will we be able to determine if either one is the ultimately correct theoretical description¹. All in all, future progress will clearly require, now more than ever, significant contributions from and close interrelationships among all three branches of condensed matter physics—theory, numerics, and experiment—making for a very exciting and challenging time in our field.

¹Neutron scattering measurements would likely settle the issue, but unfortunately, such experiments are infeasible in κ -(BEDT-TTF)₂Cu₂(CN)₃ and EtMe₃Sb[Pd(dmit)₂]₂ for several reasons.

5.1 Speculations on Future Directions

We conclude by making some speculative remarks on where the field of condensed matter physics, and specifically strongly correlated electrons, might be headed in the coming years. On the theoretical front, it is clear that we should always put *wave functions* front and center. As stressed in Sec. 1.4, doing so has been instrumental in attacking fundamental problems such as conventional superconductivity [35, 36] and the fractional quantum Hall effect [137, 199]. While it remains to be seen whether or not such an approach will work for the most challenging of problems such as nonperturbatively strongly interacting non-Fermi liquids, if such states can be true zero-temperature quantum phases², they *must* be describable by wave functions. In the cuprates themselves, realizing such a beautiful description in terms of a simple wave function is probably asking too much, as there seem to be too many complicated materials considerations at play, but we could still hope! Other materials may eventually be discovered which offer a cleaner window into such physics. And hopefully one day, systems of ultracold atoms or molecules will be able to make meaningful progress “simulating” novel strongly correlated phenomena; at present this is far from a sure thing even given the maturity of that area [200], although some situations are more well-suited to this approach than others. In any case, looking ahead it seems important that theorists put considerable effort towards further improving and refining their wave functions to model exotic phases; for example, by going beyond simple Gutzwiller projection and somehow including spatial fluctuations of the corresponding gauge field [141].

It is interesting to ponder what the field of condensed matter physics would look like if

²It is still not obvious that this is the case, but it is perfectly plausible.

someone were to someday³ solve the fermionic sign problem—an admittedly very unlikely scenario [113]. People often say things like “the sign problem is what keeps people in our field employed”. However, this notion is simply false. If we did in fact have some numerical algorithm which works in dimensions $d > 1$ as efficiently as does DMRG in 1D, it would lead to an explosion of activity in the field permeating all sectors: numerics, theory, and experiment. The main point is that by numerically solving for the ground state of a given model Hamiltonian we have not necessarily learned all that much. For one, we need to be able to *interpret* the data. Imagine trying to understand the DMRG measurements in the non-Fermi liquid region of the t - J - K model phase diagram of Chapter 4 without having the d -wave metal construction in mind. It would be a hopeless task to make sense of the abundance of incommensurate singular structure present. That is, to understand numerical data—just like to understand experimental data—we need good theory. In addition, there would be a premium placed on *ab initio* methods to provide accurate model Hamiltonians when attempting to connect to a given experimental system. A solution of the simplest Hubbard model or t - J model or Heisenberg model might not be particularly informative when trying to understand experimental data. Indeed, relatively simple perturbations (like our ring exchange term in Chapter 4) may change the physics in an extremely dramatic way. Ultimately, it would be remarkable if we could devise numerical algorithms which would somehow give hints about the nature of the *theoretical* construction of the low-lying excitations of a given phase. For example, would it be possible to “detect” partons even if we are not expecting them? While such a dream manifested in any kind of generality is clearly still many years off, especially in higher dimensions, exciting recent work in 1D [201] indicates that it may not be complete fantasy.

³Say, next week!

As alluded to in various parts of this dissertation, a real emerging theoretical and numerical frontier is to be able to better understand and eventually fully classify *gapless* phases of quantum matter in two dimensions, of which the spin Bose metal and *d*-wave metal are two concrete examples. Numerically, such states are very hard to access with 2D tensor network state methods [132], and this is especially true for states such as the spin Bose metal and *d*-wave metal which exhibit an entire *surface* of gapless excitations. These states are expected [130, 202, 22] to have an anonymously⁴ large amount of spatial entanglement, $S \sim L^{d-1} \log L$, thus rendering typical formulations of tensor network states completely incapable of solving the problem [133, 134, 135, 136]. In essence, the fermion sign problem has a cousin which has appeared in recent years: the fermion “entanglement problem”; and it will be interesting to see if these two fundamental problems are related to each other on a formal level, which is surprisingly far from obvious at the moment. Analytical control over such states is equally challenging [99]. However, gapless phases are at the very heart of some of the most unconventional and mysterious, yet important, experimental systems of our time, e.g., the cuprates and the organics. This should be contrasted with long-range entangled *gapped* phases of matter, over which we have much better numerical [21] and analytical [19, 206] control, but as of yet there are no real good experimental candidates which realize them. It thus seems that with *gapless* phases nature has given us a grand challenge, one that should keep us busy for years and decades to come.

⁴For Fermi liquids, the coefficient in front of the $L^{d-1} \log L$ term is expected to be universal in the sense that it depends only on the shape of the Fermi surface but not on interactions [202, 203, 204]. Therefore, in analogy with detection of topological order via measurement of the topological entanglement entropy [21], measurement of this leading coefficient in a ground state wave function for conducting electrons may potentially be a robust *positive* definition for the presence of a non-Fermi liquid metal [205].

Appendix A

Details of the Numerical Calculations

In this appendix, we discuss various details of the numerical calculations pertinent to the results presented in Chapters 2-4.

A.1 DMRG on the Extended t - t' Hubbard Model (Chapter 2)

In Chapter 2, we use large-scale DMRG calculations to calculate ground state properties of our model Hamiltonian, Eqs. (2.1)-(2.2), on finite-size chains of length L sites. While we have performed simulations with both open and periodic boundary conditions, we find the latter to be preferable for our model in spite of the well-known more challenging convergence properties with periodic boundaries in DMRG calculations. The long-ranged nature of our interaction potential [Eq. (2.2)], however, makes open boundaries problematic. The issue is that all interactions up to fourth neighbor are chosen to scale with the overall Hubbard strength U , so that, at least for the parameters chosen in our study, it is energetically favorable for the end sites of an open chain to become doubly occupied at large U/t . That is, even though the

system then has to pay very large on-site U on the end sites, it gains significant energy by not having to pay as substantial V_1 to V_4 . Therefore, for the calculations on the extended Hubbard model presented in Chapter 2, we have employed periodic boundary conditions.

To numerically characterize the ground state properties of the system with the DMRG, we calculate the density structure factor $\langle \delta n_q \delta n_{-q} \rangle$, the spin structure factor $\langle \mathbf{S}_q \cdot \mathbf{S}_{-q} \rangle$, the dimer structure factor $\langle \mathcal{B}_q \mathcal{B}_{-q} \rangle$, and the electron momentum distribution function $\langle c_{q\alpha}^\dagger c_{q\alpha} \rangle$ (where $\alpha = \uparrow, \downarrow$ with no implied summation). In each case, the structure factor is defined as the Fourier transform of the associated two-point function. Specifically, we have

$$\langle \delta n_q \delta n_{-q} \rangle = \frac{1}{L} \sum_{x,x'} e^{-iq(x-x')} \langle \delta n(x) \delta n(x') \rangle, \quad (\text{A.1})$$

$$\langle \mathbf{S}_q \cdot \mathbf{S}_{-q} \rangle = \frac{1}{L} \sum_{x,x'} e^{-iq(x-x')} \langle \mathbf{S}(x) \cdot \mathbf{S}(x') \rangle, \quad (\text{A.2})$$

$$\langle \mathcal{B}_q \mathcal{B}_{-q} \rangle = \frac{1}{L} \sum_{x,x'} e^{-iq(x-x')} \langle \mathcal{B}(x) \mathcal{B}(x') \rangle, \quad (\text{A.3})$$

$$\langle c_{q\alpha}^\dagger c_{q\alpha} \rangle = \frac{1}{L} \sum_{x,x'} e^{-iq(x-x')} \langle c_\alpha^\dagger(x) c_\alpha(x') \rangle, \quad (\text{A.4})$$

where $n(x) \equiv \sum_{\alpha=\uparrow,\downarrow} c_\alpha^\dagger(x) c_\alpha(x)$ is the number operator [with $\delta n(x) \equiv n(x) - \langle n(x) \rangle$], $\mathbf{S}(x) \equiv \frac{1}{2} \sum_{\alpha,\beta} c_\alpha^\dagger(x) \boldsymbol{\sigma}_{\alpha\beta} c_\beta(x)$ is the spin operator, and $\mathcal{B}(x) \equiv \mathbf{S}(x) \cdot \mathbf{S}(x+1)$ is the bond energy operator. For simplicity, we set $\langle \mathcal{B}(x) \mathcal{B}(x') \rangle = 0$ if $\mathcal{B}(x)$ and $\mathcal{B}(x')$ share common sites [58]. When presenting all structure factor measurements, we only show data for $q \geq 0$ since the measurements are symmetric about $q = 0$.

For the dimer structure factor in Eq. (A.3), we do not subtract a product of local averages from the $\langle \mathcal{B}(x) \mathcal{B}(x') \rangle$ correlations as we do, e.g., for the density structure factor in Eq. (A.1). The main reason for this choice is that at large $U/t \gtrsim 5.0$ our DMRG calculations, even with periodic boundary conditions, have a tendency to get “stuck” in one of the two possible

symmetry broken period-2 VBS patterns, giving a rather strong period-2 signal in the local expectation value $\langle \mathcal{B}(x) \rangle = \langle \mathbf{S}(x) \cdot \mathbf{S}(x+1) \rangle$. This is likely due to the somewhat awkward way in which periodic boundaries are implemented in a traditional DMRG setup which treats the end sites on a different footing. Fourier transforming $\langle \mathcal{B}(x)\mathcal{B}(x') \rangle - \langle \mathcal{B}(x) \rangle \langle \mathcal{B}(x') \rangle$ then washes out the Bragg peaks present at $q = \pi$. Hence, we just use $\langle \mathcal{B}(x)\mathcal{B}(x') \rangle$ as the real-space two-point function and exclude plotting $\langle \mathcal{B}_q \mathcal{B}_{-q} \rangle$ at $q = 0$. This both well captures the obvious Bragg peaks at $q = \pi$ in the C0S0 and also gives very clear power-law singularities at the various “ $2k_F$ ” wavevectors as expected in the C1S2 insulator (see Fig. 2.5, Sec. B.3, and Ref. [58]).

More generally, we find that the averaging done in our Fourier transforms when summing over both x and x' in Eqs. (A.1)-(A.3) does an effective job of representing the structure factors in cases where, due to slight lack of convergence in the DMRG ground state, the two-point functions depend on both the separation distance $x - x'$ and the “origin” x' . (Of course, for a perfectly translationally invariant state the two-point functions depend only on $x - x'$.)

In our DMRG calculations, we keep up to $m = 6000$ states and perform at least 6 finite-size sweeps which results in a density matrix truncation error of on the order of 10^{-5} or smaller. All measurements are well-converged to the extent necessary to establish the statements made in Chapter 2. To get a feel for the difficulty encountered in obtaining highly accurate data on the stiffness parameters $g_{\rho+}$ and $g_{\sigma+}$ (see Chapter 2 and Appendix B below), one can observe the data in the insets of Figs. 2.3 and 2.4 at the free electron point $U/t = 0$ —basically the most challenging point for the DMRG. For free electrons, we should have $g_{\rho+} = g_{\sigma+} = 1$. We see that there is a rather severe error at the first allowed momentum $q = 2\pi/L$, yet the error for

momenta $q > 2\pi/L$ is very acceptable, on the order of 1% or less.

A.2 VMC on the Heisenberg Model Plus Ring Exchange (Chapter 3)

For the variational Monte Carlo results presented in Chapter 3, we typically used $\sim 10^6$ equilibrium sweeps, and averaged over 2000 spin configurations obtained from $\sim 10^6$ measurement sweeps. In estimating the error of our measurements, we used a binning analysis with ~ 20 samples per bin. In our plots, all errors are either on the order of or smaller than the symbol size, or explicitly depicted with one-sigma error bars.

To avoid degeneracies or singularities in the spin liquid wave functions, we work with a mean-field Hamiltonian, Eq. (3.2), with spinon boundary conditions periodic in one direction and antiperiodic in the other direction; this ensures a spin wave function with fully periodic boundary conditions. We have carefully checked that our measurements, e.g., $\langle \vec{S}_i \cdot \vec{S}_j \rangle$ and $\langle P_{ijkl} + \text{H.c.} \rangle$, are converged in the system size $L_x \times L_y$ and do not depend on the spinon boundary conditions. The final energetics data presented in Fig. 3.1, as well as that in Figs. 3.2 and 3.3, was taken on a 30×30 lattice.

For the ordered states, we use three-sublattice 120° antiferromagnetic (AFM) [41, 49] and four-sublattice [176] states that are suggested within a spin-wave analysis of the model at $K = 0$. Such ground state ordering patterns (120° AFM and collinear) were also found in exact diagonalization calculations on small lattice clusters [176, 177, 207, 173]. Furthermore, we have checked the possibility of spiral orders with arbitrary wavevectors (commensurate with

the system size).

We note that quadratic fermion Hamiltonians similar to Eq. (3.2) can be used to construct states exhibiting magnetic order [138, 139, 171]. However, it turns out that such Gutzwiller projected spin-density wave states do not give good variational energies. In our case of triangular lattice spin-1/2 antiferromagnets, much better wave functions can be obtained by applying spin-Jastrow factors to product states, as pioneered in [41]. We use such Huse-Elser wave functions with first- and second-neighbor Jastrow factors to compare their energies with those of the spin liquid states, and to map out the variational phase diagram of the model.

The variational phase diagram we obtain for the parameter range and states considered is shown in Fig. 3.4. On the line $K = 0$, we find that the 120° AFM state is stable up to $J_2 \lesssim 0.05$, at which point a nodal d -wave spin liquid starts to have the lowest energy within our set of wave functions. It should be noted that on the line $K = 0$, spin-wave calculations predict a transition from the 120° AFM state to a collinear phase at $J_2 = 0.125$ [176]. Exact diagonalization results seem to support a scenario without an intermediate spin liquid phase [177]. It is therefore possible that our variational approach overestimates the spin liquid regions with respect to the ordered states, especially in the case of the nodal d -wave spin liquid. Also, we have not considered spin liquids obtained by spinon hopping patterns with finite fluxes, as the ring term strongly disfavors such states [49] (although Motrunich [208] has found the time-reversal invariant “ $U1B$ ” state with alternating 0 and π fluxes through the triangles to be a promising ground state candidate for $K \simeq 0$ and $J_2 \gtrsim 0$). Interestingly, the zero-flux U(1) spin liquid at $K \gtrsim 0.25$ is quite stable with respect to second-neighbor interaction J_2 , and it is not destroyed within the parameter range and states we considered.

Finally, on the line $J_2 = 0$, Motrunich [49, 208] found a transition to a spin liquid phase at $K \gtrsim 0.14$. This small discrepancy with the transition point we find in the present paper may be traced back to the fact that we did not keep as many variational parameters in our Huse-Elser wave functions, and that he considered a more restricted set of spin liquid states. We leave a systematic study of the effect of more parameters in all our wave functions for future work. However, we expect that the spin liquid phase space may only slightly shrink, and that the basic conclusions of our study remain unchanged.

Let us briefly discuss other variational quantum spin liquid wave functions that we have also considered, but that were not mentioned thus far. We have generalized s - and d -wave states by allowing three independent real singlet pairings $\Delta_{rr'}$ on first-neighbor links. Furthermore, we have checked the possibility of finite-momentum pairing instabilities of the U(1) spin liquid as proposed in Ref. [209] with the “Amperean pairing” state. However, we could not find convincing evidence that such states are realized in our model, Eq. (3.1).

Finally, in order to further improve the energy of the QBT $d + id$ state, we set the hopping $t_{rr'} = 0$ and added a second-neighbor pairing amplitude $\Delta^{(2)}$ to the trial Hamiltonian, Eq. (3.2). However, we found that the optimal parameter is always essentially $\Delta^{(2)}/\Delta^{(1)} \simeq 0$ for the model considered.

A.3 DMRG on the Two-Leg t - J - K Electron Ring-Exchange Model (Chapter 4)

In Chapter 4, we determine the ground state phase diagram of the t - J - K model, Eq. (4.6), by large-scale DMRG calculations. We consider square lattice clusters with total number of sites $L_x \times L_y$. Here, we study the two-leg ladder system, i.e., $L_y = 2$, and use periodic boundary conditions along the \hat{x} direction.

Our DMRG calculations generally keep between $m = 5,000$ and $20,000$ states in each DMRG block. This is found to give excellent convergence in the measurements such as the ground state energy and various correlation functions defined below, with small errors which can be neglected safely for our sizes up to $L_x = 48$. The phase boundaries in the $(J/t, K/t)$ -parameter space are determined by extensive scans of the derivatives of the ground state energy and by monitoring the correlation functions. On the other hand, even with such a large m , we can converge the entanglement entropy only for sizes up to $L_x = 36$.

To characterize the ground state properties of the system, as well as properties of the variational wave functions, we calculate the electron Green's function

$$G_e(\mathbf{r}_i - \mathbf{r}_j) = \langle c_{is}^\dagger c_{js} \rangle, \quad (\text{A.5})$$

where $e = c_s$ with $s = \uparrow, \downarrow$ the electron spin (there is no implied summation over s). For our electron Green's function calculations and analysis, we fix s to one of the two possible flavors of spin, say $s = \uparrow$, which in the spin-singlet states considered in this work, gives the same Green's function as the other flavor of spin. The Fourier transform gives us the electron

momentum distribution function

$$\langle c_{\mathbf{q}s}^\dagger c_{\mathbf{q}s} \rangle = \frac{1}{L_x L_y} \sum_{ij} e^{i\mathbf{q}\cdot(\mathbf{r}_i - \mathbf{r}_j)} \langle c_{is}^\dagger c_{js} \rangle. \quad (\text{A.6})$$

Similarly, we calculate the electron density-density structure factor in momentum space

$$\langle \delta n_{\mathbf{q}} \delta n_{-\mathbf{q}} \rangle = \frac{1}{L_x L_y} \sum_{ij} e^{i\mathbf{q}\cdot(\mathbf{r}_i - \mathbf{r}_j)} \langle (n_i - \rho)(n_j - \rho) \rangle, \quad (\text{A.7})$$

where $n_i = \sum_s c_{is}^\dagger c_{is}$ is the electron number operator at site i and ρ is the electron density. To characterize the magnetic properties of the system, we also study the spin structure factor

$$\langle \mathbf{S}_{\mathbf{q}} \cdot \mathbf{S}_{-\mathbf{q}} \rangle = \frac{1}{L_x L_y} \sum_{ij} e^{i\mathbf{q}\cdot(\mathbf{r}_i - \mathbf{r}_j)} \langle \mathbf{S}_i \cdot \mathbf{S}_j \rangle, \quad (\text{A.8})$$

where the spin operator is defined as $\mathbf{S}_i = \frac{1}{2} \sum_{s,s'} c_{is}^\dagger \boldsymbol{\sigma}_{ss'} c_{is'}$.

Appendix B

Interacting Electrons on the Two-Leg

Triangular Strip: Luttinger Liquid

Description and Solution by Bosonization

In this appendix, we spell out the effective low-energy description of the C2S2 metal and C1S2 spin Bose metal and intervening Kosterlitz-Thouless (KT)-like Mott transition, focusing on those aspects of the theory most relevant to the DMRG results presented in Chapter 2. Some aspects of our presentation follow that of Refs. [58] and [151].

B.1 Long-Wavelength Description of C2S2 Metal and C1S2

Spin Bose Metal

Consider noninteracting electrons at half-filling on the two-leg triangular strip (see Fig. 2.1).

When viewed as a 1D chain with first-neighbor and second-neighbor hopping, t and t' , the electron dispersion is given by (see also Fig. 2.2)

$$\epsilon(q) = -2t \cos(q) - 2t' \cos(2q) - \mu. \quad (\text{B.1})$$

For $t'/t > 0.5$, which is the case of interest here, the ground state consists of two disconnected Fermi seas (bands) which we label by $a = 1, 2$. We take the convention that the Fermi velocities v_{Fa} are positive (negative) for electrons moving near k_{Fa} ($-k_{Fa}$), corresponding to right and left movers, respectively. Furthermore, taking the system to be at half-filling gives the sum rule $k_{F1} + k_{F2} = -\pi/2 \bmod 2\pi$.

As usual [4], we take the low-energy continuum limit and expand the electron operator in terms of slowly varying continuum fields at the four Fermi points:

$$c_\alpha(x) = \sum_{a,P} e^{iP k_{Fa} x} c_{Pa\alpha}, \quad (\text{B.2})$$

where $\alpha = \uparrow, \downarrow$ denotes the electron spin, and the sum runs over $a = 1, 2$ for the two Fermi seas and $P = R/L = +/ -$ for the right and left moving electrons at the Fermi points of each Fermi sea. Although not written explicitly, the continuum fields of course depend on position x : $c_{Pa\alpha} = c_{Pa\alpha}(x)$.

Next, we bosonize [4] the continuum fields according to

$$c_{Pa\alpha} = \eta_{a\alpha} e^{i(\varphi_{a\alpha} + P\theta_{a\alpha})}, \quad (\text{B.3})$$

where $\varphi_{a\alpha}$ and $\theta_{a\alpha}$ are the canonically conjugate bosonic phase and phonon fields, respectively.

Specifically, we have

$$[\varphi_{a\alpha}(x), \varphi_{b\beta}(x')] = [\theta_{a\alpha}(x), \theta_{b\beta}(x')] = 0, \quad (\text{B.4})$$

$$[\varphi_{a\alpha}(x), \theta_{b\beta}(x')] = i\pi\delta_{ab}\delta_{\alpha\beta}\Theta(x - x'). \quad (\text{B.5})$$

The fields $\eta_{a\alpha}$ are the Klein factors, i.e., Majorana fermions $\{\eta_{a\alpha}, \eta_{b\beta}\} = 2\delta_{ab}\delta_{\alpha\beta}$, which are necessary to ensure the correct anticommutation relations among different fermionic species $a\alpha$. Finally, the slowly varying component of the electron density is given by the derivative of the $\theta_{a\alpha}$ fields: $\rho_{a\alpha} = \sum_{P=\pm} c_{Pa\alpha}^\dagger c_{Pa\alpha} = \partial_x \theta_{a\alpha}/\pi$, where $c_{Pa\alpha}^\dagger c_{Pa\alpha} = \partial_x(\theta_{a\alpha} + P\varphi_{a\alpha})/(2\pi)$. Hence, Eq. (B.5) is essentially a statement of the density-phase uncertainty relation: $[\rho(x), \varphi(x')] = i\delta(x - x')$.

Next, we linearize about the Fermi points and express the problem in terms of the bosonized fields introduced above. Working in the Euclidean path integral formalism, the low-energy continuum Lagrangian density for the two-band noninteracting electron gas then reads:

$$\mathcal{L}_{\text{free}} = \mathcal{H}_{\text{free}} + \sum_{a,\alpha} \frac{i}{\pi} (\partial_x \theta_{a\alpha})(\partial_\tau \varphi_{a\alpha}), \quad (\text{B.6})$$

where

$$\mathcal{H}_{\text{free}} = \sum_{a,\alpha} \frac{v_{Fa}}{2\pi} [(\partial_x \theta_{a\alpha})^2 + (\partial_x \varphi_{a\alpha})^2]. \quad (\text{B.7})$$

We now introduce the “charge” and “spin” modes for each band:

$$\theta_{a\rho/\sigma} \equiv \frac{1}{\sqrt{2}} (\theta_{a\uparrow} \pm \theta_{a\downarrow}), \quad (\text{B.8})$$

and the “overall” and “relative” combinations with respect to the two bands:

$$\theta_{\mu\pm} \equiv \frac{1}{\sqrt{2}} (\theta_{1\mu} \pm \theta_{2\mu}), \quad (\text{B.9})$$

where $\mu = \rho, \sigma$. Fields analogous to Eqs. (B.8) and (B.9) are also defined for the φ 's. These newly defined fields satisfy the same canonical commutation relations as the original fields [Eqs. (B.4)-(B.5)]. The free-electron Lagrangian $\mathcal{L}_{\text{free}}$ then as usual decouples into charge and spin sectors:

$$\mathcal{L}_{\text{free}} = \mathcal{L}_{\text{free}}^\rho + \mathcal{L}_{\text{free}}^\sigma, \quad (\text{B.10})$$

where

$$\mathcal{L}_{\text{free}}^\mu = \mathcal{H}_{\text{free}}^\mu + \sum_a \frac{i}{\pi} (\partial_x \theta_{a\mu})(\partial_\tau \varphi_{a\mu}), \quad (\text{B.11})$$

$$\mathcal{H}_{\text{free}}^\mu = \sum_a \frac{v_{Fa}}{2\pi} [(\partial_x \theta_{a\mu})^2 + (\partial_x \varphi_{a\mu})^2]. \quad (\text{B.12})$$

We are finally in position to discuss interactions. In the interacting C2S2 Luttinger liquid, the fixed-point theory is similar to Eq. (B.10), i.e.,

$$\mathcal{L}_{\text{C2S2}} = \mathcal{L}_{\text{C2S2}}^\rho + \mathcal{L}_{\text{C2S2}}^\sigma, \quad (\text{B.13})$$

except we have general mode velocities and, in the charge sector, nontrivial Luttinger parameters. For convenience in the discussion that follows, in the charge sector we work in the $\rho\pm$ basis of Eq. (B.9) and write the most general charge sector Lagrangian as

$$\mathcal{L}_{\text{C2S2}}^\rho = \mathcal{H}_{\text{C2S2}}^\rho + \frac{i}{\pi} \partial_x \Theta^T \cdot \partial_\tau \Phi, \quad (\text{B.14})$$

$$\mathcal{H}_{\text{C2S2}}^\rho = \frac{1}{2\pi} [\partial_x \Theta^T \cdot \mathbf{A} \cdot \partial_x \Theta + \partial_x \Phi^T \cdot \mathbf{B} \cdot \partial_x \Phi], \quad (\text{B.15})$$

where $\Theta^T \equiv (\theta_{\rho+}, \theta_{\rho-})$ and $\Phi^T \equiv (\varphi_{\rho+}, \varphi_{\rho-})$; \mathbf{A} and \mathbf{B} are symmetric, positive-definite 2×2 matrices which encode interactions. Note that even for free electrons, if $v_{F1} \neq v_{F2}$, the charge sector is not diagonal in the $\rho\pm$ basis, i.e., $A_{12} = A_{21} \neq 0$, $B_{12} = B_{21} \neq 0$, and in general the interacting C2S2 metal will have coupled $\rho+$ and $\rho-$ modes [151].

For the spin sector, we stay in the band basis $a = 1, 2$ and write

$$\mathcal{L}_{\text{C2S2}}^\sigma = \mathcal{H}_{\text{C2S2}}^\sigma + \sum_a \frac{i}{\pi} (\partial_x \theta_{a\sigma}) (\partial_\tau \varphi_{a\sigma}), \quad (\text{B.16})$$

$$\mathcal{H}_{\text{C2S2}}^\sigma = \sum_a \frac{v_{a\sigma}}{2\pi} \left[\frac{1}{g_{a\sigma}} (\partial_x \theta_{a\sigma})^2 + g_{a\sigma} (\partial_x \varphi_{a\sigma})^2 \right]. \quad (\text{B.17})$$

SU(2) invariance dictates only trivial Luttinger parameters in the spin sector, i.e., $g_{1\sigma} = g_{2\sigma} = 1$ (see Sec. B.3), but we keep them general in Eq. (B.17) for further analysis below. Our representation of the spin sector here is somewhat schematic in that allowed strictly marginal chiral interactions will couple the bare spin modes [Eq. (B.8)] in the quadratic part of the C2S2 action. However, the resulting $\mathcal{H}_{\text{C2S2}}^\sigma$ is symmetric under interchanging $\theta_{a\sigma} \leftrightarrow \varphi_{a\sigma}$ and so can easily be brought back to diagonal form via a simple orthogonal transformation which acts identically on the $\theta_{a\sigma}$ and $\varphi_{a\sigma}$ fields, hence keeping the Luttinger parameters at their trivial values. Thus, for the quadratic part of the C2S2 fixed-point theory, Eq. (B.17) is completely general for our purposes. Interestingly, the full C2S2 fixed-point theory also contains a strictly marginal chiral interband scattering term of the form $(\mathcal{H}_{\text{chiral}}^\sigma)_\perp \sim \cos(2\varphi_{\sigma-}) \cos(2\theta_{\sigma-})$, which is nonharmonic [162]. However, we expect that the presence of this, presumably exactly marginal, nonharmonic chiral interaction will not quantitatively alter the spin sector at the C2S2 (and C1S2; see below) fixed point—at least with respect to the Luttinger parameters and contributions to the scaling dimensions of various operators (see Sec. B.3). In fact, assuming that $(\mathcal{H}_{\text{chiral}}^\sigma)_\perp$ is exactly marginal already *implies* trivial spin sector Luttinger parameters, $g_{1\sigma} = g_{2\sigma} = 1$, which is encouraging.

In addition to such strictly marginal interactions, there are many nonchiral interactions allowed by symmetry which may be added to Eq. (B.13) and potentially destabilize the C2S2 theory described above. To connect to a given microscopic Hamiltonian, a common approach

is to employ a weak-coupling renormalization group (RG) scheme. That is, one can project the microscopic interactions onto all continuum symmetry-allowed interactions and read off initial conditions for all such couplings; these initial conditions can then be subsequently used in a controlled RG analysis valid for weak microscopic coupling $U/t \ll 1$. Then, bosonizing the four-fermion interactions—particularly those that may flow to strong coupling, hence destabilizing the “mother” C2S2—emits a direct physical interpretation of the resulting phase. This is the approach pioneered many years ago in Ref. [108], where it was shown (see also Ref. [157]) that for the on-site $t-t'-U$ Hubbard model, the C2S2 metal is generally unstable at weak repulsive interactions to the opening of a spin gap. The basic idea is that the RG flow equations—which are indeed rather complicated for the two-band system and in general require a detailed numerical analysis—have a tendency to eventually drive *attractive* divergent couplings in the spin sector (e.g., the terms denoted $g_{a\sigma}$ in Ref. [108] or, equivalently, λ_{aa}^σ in Ref. [151]). These divergent couplings conspire to gap out all modes except the overall conducting charge mode $\theta_{\rho+}$, leaving a one-mode C1S0 conducting Luttinger liquid, essentially the quasi-1D analog of a superconductor.

However, this spin-gap tendency is not unavoidable. For example, one can fight such pairing tendencies by adding longer-ranged repulsion to the model Hamiltonian. This approach was recently explored systematically in Ref. [151], where it was shown that the C2S2 metal occupies a substantial portion of the weak-coupling phase diagram for the model considered in our work: Eqs. (2.1)-(2.2). Stability of the C2S2 metal at weak coupling indeed seems to be a necessary component for realizing the C2S2→C1S2 Mott transition presented numerically in Chapter 2, and we buttress off the weak-coupling phase diagram presented in Ref. [151] when

selecting the specific parameters of our model Hamiltonian.

Finally, as stressed in Chapter 2, our Mott transition is driven at strong interactions by an *eight-fermion* umklapp term wherein both spin-up and spin-down electrons are scattered across each Fermi sea (see Fig. 2.2):

$$\mathcal{H}_8 = u(c_{R1\uparrow}^\dagger c_{R1\downarrow}^\dagger c_{R2\uparrow}^\dagger c_{R2\downarrow}^\dagger c_{L1\uparrow} c_{L1\downarrow} c_{L2\uparrow} c_{L2\downarrow} + \text{H.c.}), \quad (\text{B.18})$$

which when written in terms of the bosonized fields simply becomes a cosine of the overall charge field $\theta_{\rho+}$:

$$\mathcal{H}_8 = 2u \cos(4\theta_{\rho+}). \quad (\text{B.19})$$

The C1S2 spin Bose metal spin liquid corresponds to relevance of \mathcal{H}_8 so that u flows to strong coupling. That is, the field content of the C1S2 fixed-point theory looks identical to that of C2S2 but with a massive overall charge mode $\theta_{\rho+}$. Specifically, we have

$$\mathcal{L}_{\text{C1S2}} = \mathcal{L}_{\text{C1S2}}^\rho + \mathcal{L}_{\text{C1S2}}^\sigma, \quad (\text{B.20})$$

where the “charge sector” now only contains the $\rho-$ mode:

$$\mathcal{L}_{\text{C1S2}}^\rho = \mathcal{H}_{\text{C1S2}}^\rho + \frac{i}{\pi}(\partial_x \theta_{\rho-})(\partial_\tau \varphi_{\rho-}), \quad (\text{B.21})$$

$$\mathcal{H}_{\text{C1S2}}^\rho = \frac{v_{\rho-}}{2\pi} \left[\frac{1}{g_{\rho-}} (\partial_x \theta_{\rho-})^2 + g_{\rho-} (\partial_\tau \varphi_{\rho-})^2 \right], \quad (\text{B.22})$$

which physically represents gapless local current fluctuations, and the spin sector formally reads the same as before:

$$\mathcal{L}_{\text{C1S2}}^\sigma = \mathcal{L}_{\text{C2S2}}^\sigma, \quad (\text{B.23})$$

still with trivial Luttinger parameters, $g_{1\sigma} = g_{2\sigma} = 1$. For an extensive discussion of the C1S2 phase with respect to its features and stability, we refer the reader to Ref. [58].

B.2 Renormalization Group Analysis of the C2S2→C1S2 Mott Transition

We now present the details of the critical theory describing our Mott transition. The theory is KT-like with a complication arising because the field $\theta_{\rho+}$, which is being gapped out, is coupled to the field $\theta_{\rho-}$ in the Gaussian fixed-point action for the C2S2 [see Eq. (B.15)], and $\theta_{\rho-}$ is massless on both sides of the transition.

From the above considerations, the charge sector Lagrangian describing the transition between the C2S2 metal and C1S2 spin Bose metal reads

$$\mathcal{L} = \mathcal{L}_0 + \mathcal{L}_{\cos}, \quad (\text{B.24})$$

where

$$\mathcal{L}_0 = \frac{1}{2\pi} [\partial_x \Theta^T \cdot \mathbf{C} \cdot \partial_x \Theta + \partial_\tau \Theta^T \cdot \mathbf{D} \cdot \partial_\tau \Theta] \quad (\text{B.25})$$

is just $\mathcal{L}_{\text{C2S2}}^\rho$ from Eq. (B.14) with the φ 's integrated out, $\Theta^T \equiv (\theta_{\rho+}, \theta_{\rho-})$, and

$$\mathcal{L}_{\cos} = 2u \cos(n\theta_{\rho+}) \quad (\text{B.26})$$

with $n = 4$ is our eight-fermion umklapp term. It is convenient to diagonalize the quadratic part of the theory \mathcal{L}_0 in a fashion similar to that described in Ref. [151], thus obtaining for the full theory

$$\mathcal{L}_0 = \frac{1}{2\pi} \sum_{i=1,2} \left[\frac{1}{v_i} (\partial_\tau \theta_i)^2 + v_i (\partial_x \theta_i)^2 \right], \quad (\text{B.27})$$

$$\mathcal{L}_{\cos} = 2u \cos(n_1 \theta_1 + n_2 \theta_2), \quad (\text{B.28})$$

where we have absorbed the nontrivial Luttinger parameters of the two normal modes, θ_1 and θ_2 , into the real coefficients n_1 and n_2 via a rescaling of the fields. While θ_1 and θ_2 are specific

linear combinations of $\theta_{\rho+}$ and $\theta_{\rho-}$, e.g., $n\theta_{\rho+} = n(c_1\theta_1 + c_2\theta_2) = n_1\theta_1 + n_2\theta_2$, we do not spell out the details here, but instead refer the reader to the Appendix of Ref. [151] for a similar calculation. Ultimately, this linear combination, as well as the velocities and Luttinger parameters of the normal modes in the diagonalized system, are rather complicated, but still analytic, functions of the original parameters **C** and **D** of the coupled system.

We have performed a renormalization group (RG) analysis of the above two-mode system, obtaining the following leading-order KT-like (see below) flow equations for all couplings:

$$\frac{dC_{11}}{d\ell} = \frac{\pi n^2}{\Lambda^4 v_1} I\left(\frac{v_2}{v_1}, \frac{n_2^2}{4}\right) u^2, \quad (\text{B.29})$$

$$\frac{dD_{11}}{d\ell} = \frac{\pi n^2}{\Lambda^4 v_1^3} \left(\frac{v_2}{v_1}\right)^{-2n_2^2/4} I\left(\frac{v_1}{v_2}, \frac{n_2^2}{4}\right) u^2, \quad (\text{B.30})$$

$$\frac{du}{d\ell} = \left[2 - \left(\frac{n_1^2}{4} + \frac{n_2^2}{4}\right)\right] u, \quad (\text{B.31})$$

where

$$I(\alpha, \beta) \equiv \int_0^{2\pi} d\theta \frac{\cos^2 \theta}{(\cos^2 \theta + \alpha^2 \sin^2 \theta)^\beta} \geq 0. \quad (\text{B.32})$$

As with ordinary KT, the coupling u renormalizes according to the scaling dimension of the cosine with respect to the quadratic action,

$$\Delta[\cos(n\theta_{\rho+})] = \Delta[\cos(n_1\theta_1 + n_2\theta_2)] = \frac{n_1^2}{4} + \frac{n_2^2}{4}, \quad (\text{B.33})$$

and obtaining its beta function, Eq. (B.31), can proceed in a textbook Wilsonian fashion [4]. However, renormalizing the parameters in \mathcal{L}_0 is significantly more involved and depends on the specific regularization scheme employed. First, note that since \mathcal{L}_{\cos} contains only the field $\theta_{\rho+}$, it cannot possibly renormalize any terms containing $\theta_{\rho-}$ to any order in perturbation theory; hence, the only nonzero beta functions are those for the couplings C_{11} and D_{11} . The respective beta functions, Eqs. (B.29) and (B.30), were obtained using a field-theoretic approach [159] in

which we consider insertions into correlation functions of the form $\langle \partial_x \theta_i(x) \partial_x \theta_j(y) \rangle$, where x and y are points in our (1+1)D space-time. At $\mathcal{O}(u^2)$, one has to integrate over two 2D points from two u insertions, say z and z' . Indeed, as $z - z'$ becomes small, the integral diverges logarithmically, and we cut it off at a short-distance scale Λ^{-1} . We then compute corrections to $\langle \partial_x \theta_i(x) \partial_x \theta_j(y) \rangle$ from posited ‘‘counterterms’’ in \mathcal{L}_0 which are chosen to exactly cancel the aforementioned logarithmic divergence. This allows us, after an altogether somewhat lengthy calculation, to arrive at the above RG flow equations for C_{11} and D_{11} .

The case of vanishing $\theta_{\rho+}\text{-}\theta_{\rho-}$ coupling in Eq. (B.25) corresponds to the limit $n_2 \rightarrow 0$, so that $\theta_1 \propto \theta_{\rho+}$ and C_{11} and D_{11} renormalize at the same rate (up to an overall scale of v_1^2). This of course corresponds to ordinary Kosterlitz-Thouless RG wherein only one parameter in \mathcal{L}_0 renormalizes: $\frac{d(g^{-1})}{d\ell} \sim u^2$, with g the single-mode Luttinger parameter [4].

In the general case, the beta functions for C_{11} and D_{11} involve highly nonuniversal content, and thus we have not attempted a detailed study of the flows. Still, the transition is KT-like in nature except that two parameters (as opposed to one) in \mathcal{L}_0 are renormalized by the single cosine, and the transition occurs when the scaling dimension of the cosine equals the space-time dimension: $\Delta[\cos(n\theta_{\rho+})] = \frac{n_1^2}{4} + \frac{n_2^2}{4} = 2$, where n_1 and n_2 are functions of the parameters C and D.

We can formally argue for the KT-like nature as follows. From the start, we focus only on the flowing parameters C_{11} , D_{11} , and u . Let us denote the (non-negative) factors multiplying u^2 in the beta functions for C_{11} and D_{11} as $A(C_{11}, D_{11})$ and $B(C_{11}, D_{11})$, respectively, and also denote the coefficient of u in the beta function for u as $\Gamma(C_{11}, D_{11})$. We emphasize that A , B , and Γ are functions of C_{11} and D_{11} , which, while perhaps complicated functions, are

analytical and not special. As we vary in the (C_{11}, D_{11}) plane, we generically expect to find a line where $\Gamma = 0$ separating regions where a small u perturbation is relevant or irrelevant. Let us consider one point on this line, $(C_{11}^{(0)}, D_{11}^{(0)})$, and study small deviations $(\delta C_{11}, \delta D_{11})$ from this point. The RG equations are, to leading order,

$$\frac{d\delta C_{11}}{d\ell} = A^{(0)}u^2, \quad (\text{B.34})$$

$$\frac{d\delta D_{11}}{d\ell} = B^{(0)}u^2, \quad (\text{B.35})$$

$$\frac{du}{d\ell} = (\alpha^{(0)}\delta C_{11} + \beta^{(0)}\delta D_{11}) u, \quad (\text{B.36})$$

where $A^{(0)}$ and $B^{(0)}$ are the A and B functions evaluated at $(C_{11}^{(0)}, D_{11}^{(0)})$, while $\alpha^{(0)}$ and $\beta^{(0)}$ are derivatives $\partial\Gamma/\partial C_{11}$ and $\partial\Gamma/\partial D_{11}$ evaluated at the same point. Deviations satisfying $\alpha^{(0)}\delta C_{11} + \beta^{(0)}\delta D_{11} = 0$ correspond to moving along the $\Gamma = 0$ line, while generic deviations will cut across this line. Formally, we can change variables to $r = \alpha^{(0)}\delta C_{11} + \beta^{(0)}\delta D_{11}$, $s = -\beta^{(0)}\delta C_{11} + \alpha^{(0)}\delta D_{11}$, which flow as

$$\frac{dr}{d\ell} = (\alpha^{(0)}A^{(0)} + \beta^{(0)}B^{(0)}) u^2, \quad (\text{B.37})$$

$$\frac{ds}{d\ell} = (-\beta^{(0)}A^{(0)} + \alpha^{(0)}B^{(0)}) u^2, \quad (\text{B.38})$$

$$\frac{du}{d\ell} = ru. \quad (\text{B.39})$$

Thus, the flow equations for the r and u variables have familiar KT-like form and subsequent standard analysis can kick in. On the other hand, the flow of the s variable is simply slaved to u and does not affect the KT analysis.

In principle, one should be able to confirm the KT universality class from the numerical DMRG data, for example, by performing Weber-Minnhagen [160] style fits to finite-size estimates of the scaling dimension of the cosine in the metallic phase (essentially the stiffness in

the XY model context; see also Sec. B.3 below). However, this requires highly accurate data on large system sizes in the scaling regime, which is currently prohibitive for our multimode electronic system (see Appendix A.1). Also, it is not unreasonable to expect that the presence of two renormalizing parameters in \mathcal{L}_0 , instead of one, might make the finite-size effects more severe. In the end though, this is a rather nonuniversal matter which we do not pursue further.

B.3 Observables and Stiffness Parameters

To characterize the system, we have focused on the density structure factor, the spin structure factor, the dimer structure factor, and the electron momentum distribution function as presented in Chapter 2 and as defined in Appendix A.1. In this section, we lay out the details of the bosonization treatment which allows us to use these measurements, both at finite and zero wavevectors, to probe the nature of the Luttinger liquid phases realized by our model Hamiltonian.

B.3.1 Establishing the Result $\Delta[\mathcal{H}_8] = 4g_{\rho+}$

As stressed in Chapter 2, we can directly measure the scaling dimension of the eight-fermion umklapp term [see Eqs. (2.3) and (B.19)] responsible for driving our Mott transition by measuring the slope of the density structure factor at $q = 0$ momentum [see Eq. (2.4)]. We now spell out how these two quantities, $\Delta[\mathcal{H}_8]$ and $g_{\rho+}$, are formally related.

The former is defined through the corresponding two-point function:

$$\langle e^{i4\theta_{\rho+}(x)} e^{-i4\theta_{\rho+}(0)} \rangle \sim \frac{1}{|x|^{2\Delta[\mathcal{H}_8]}}, \quad (\text{B.40})$$

where, for simplicity, we work at equal (imaginary) time such that x is a spatial coordinate only. Assuming that the system is in the C2S2 phase so that the charge sector is described by the quadratic Lagrangian $\mathcal{L}_{\text{C2S2}}^\rho$ of Eq. (B.14), we can use a standard identity [4] and write

$$\langle e^{i4\theta_{\rho+}(x)} e^{-i4\theta_{\rho+}(0)} \rangle = e^{-\frac{4^2}{2} \langle [\theta_{\rho+}(x) - \theta_{\rho+}(0)]^2 \rangle}. \quad (\text{B.41})$$

Now, the slowly varying component of the total electron density (measured relative to the average density) is given by $\delta n(x) = 2\partial_x \theta_{\rho+}/\pi$, so that the long-wavelength contribution to the density-density correlation function in real space is given by

$$\langle \delta n(x) \delta n(0) \rangle = \frac{4}{\pi^2} \partial_x \partial_{x'} \langle \theta_{\rho+}(x) \theta_{\rho+}(x') \rangle|_{x'=0} + \dots. \quad (\text{B.42})$$

The right-hand side can be obtained from Eq. (B.41) via straightforward manipulations, which after invoking Eq. (B.40) gives

$$\langle \delta n(x) \delta n(0) \rangle = -\frac{\Delta[\mathcal{H}_8]}{2\pi^2} \frac{1}{x^2} + \dots. \quad (\text{B.43})$$

On the other hand, we define the slope of the momentum-space density structure factor as $q \rightarrow 0$ according to Eq. (2.4), i.e.,

$$\langle \delta n_q \delta n_{-q} \rangle = \frac{2g_{\rho+}}{\pi} |q|, \quad (\text{B.44})$$

such that $g_{\rho+} = 1$ corresponds to a two-band noninteracting electron gas. After Fourier transformation, Eqs. (B.43) and (B.44) imply that

$$\Delta[\mathcal{H}_8] = 4g_{\rho+}, \quad (\text{B.45})$$

which is the desired result. Note that $g_{\rho+}$ is not generally a genuine Luttinger parameter due to the coupling between the $\rho+$ and $\rho-$ sectors in the C2S2 phase, but should instead be viewed as a direct measurement of $\Delta[\mathcal{H}_8]$ through the density structure factor.

In Chapter 2, we relied heavily upon Eq. (B.45) to distinguish between metallic and insulating behavior, where measured $g_{\rho+} > 1/2$ ($g_{\rho+} < 1/2$) implies that \mathcal{H}_8 is irrelevant (relevant) so that the system is metallic (insulating). Of course, if $\Delta[\mathcal{H}_8] < 2$, the system is necessarily insulating and Eq. (B.44) no longer applies; instead we have $\langle \delta n_q \delta n_{-q} \rangle \sim q^2$ as $q \rightarrow 0$. That is, measured $g_{\rho+} < 1/2$ via Eq. (B.44) on a finite-size system corresponds in the thermodynamic limit to $g_{\rho+} \rightarrow 0$. In Fig. 2.3, even well into the insulating phase of our model as determined by the above arguments, we see on our $L = 96$ site system that apparently $\langle \delta n_q \delta n_{-q} \rangle \sim |q|$; however, with \mathcal{H}_8 relevant, this must be a finite-size effect due to the large charge correlation length present in our weak Mott insulating C1S2.

B.3.2 Bosonized Representation of Operators at Finite Wavevectors

We now give the bosonized expressions for the spin and density operators at finite “ $2k_F$ ” wavevectors and mathematically establish the Amperean enhancement mechanism summarized in Chapter 2. Expanding the spin operator as $\mathbf{S}(x) = \sum_Q \mathbf{S}_Q e^{iQx}$, we can easily write the slowly varying part of the spin operator at various wavevectors, i.e., $\mathbf{S}_Q = \mathbf{S}_Q(x)$, in terms of the right and left moving electron operators defined in Sec. B.1:

$$\mathbf{S}_{2k_{Fa}} = \frac{1}{2} c_{La\alpha}^\dagger \boldsymbol{\sigma}_{\alpha\beta} c_{Ra\beta}, \quad (\text{B.46})$$

$$\mathbf{S}_{\pi/2} = \frac{1}{2} c_{R1\alpha}^\dagger \boldsymbol{\sigma}_{\alpha\beta} c_{L2\beta} + \frac{1}{2} c_{R2\alpha}^\dagger \boldsymbol{\sigma}_{\alpha\beta} c_{L1\beta}, \quad (\text{B.47})$$

$$\mathbf{S}_{k_{F2}-k_{F1}} = \frac{1}{2} c_{R1\alpha}^\dagger \boldsymbol{\sigma}_{\alpha\beta} c_{R2\beta} + \frac{1}{2} c_{L2\alpha}^\dagger \boldsymbol{\sigma}_{\alpha\beta} c_{L1\beta}. \quad (\text{B.48})$$

Similarly, for the density operator, we have

$$\delta n_{2k_{Fa}} = c_{La\alpha}^\dagger c_{Ra\alpha}, \quad (\text{B.49})$$

$$\delta n_{\pi/2} = c_{R1\alpha}^\dagger c_{L2\alpha} + c_{R2\alpha}^\dagger c_{L1\alpha}, \quad (\text{B.50})$$

$$\delta n_{k_{F2}-k_{F1}} = c_{R1\alpha}^\dagger c_{R2\alpha} + c_{L2\alpha}^\dagger c_{L1\alpha}. \quad (\text{B.51})$$

In each case, summations over spin indices are implied, and $\mathbf{S}_{-Q} = \mathbf{S}_Q^\dagger$ and $\delta n_{-Q} = \delta n_Q^\dagger$.

Throughout, our use of denoting wavevectors with either Q or q is an attempt to distinguish the long-wavelength component of an operator, O_Q , from the actual exact operator used in the DMRG, O_q .

Bosonizing the above electron bilinears using Eq. (B.3) results in the following expressions for the spin:

$$S_{2k_{Fa}}^x = -i\eta_{a\uparrow}\eta_{a\downarrow}e^{i\theta_{\rho+}}e^{\pm i\theta_{\rho-}}\sin(\sqrt{2}\varphi_{a\sigma}), \quad (\text{B.52})$$

$$S_{2k_{Fa}}^y = -i\eta_{a\uparrow}\eta_{a\downarrow}e^{i\theta_{\rho+}}e^{\pm i\theta_{\rho-}}\cos(\sqrt{2}\varphi_{a\sigma}), \quad (\text{B.53})$$

$$S_{2k_{Fa}}^z = -e^{i\theta_{\rho+}}e^{\pm i\theta_{\rho-}}\sin(\sqrt{2}\theta_{a\sigma}), \quad (\text{B.54})$$

$$\begin{aligned} S_{\pi/2}^x &= e^{-i\theta_{\rho+}} \left[-i\eta_{1\uparrow}\eta_{2\downarrow}e^{-i\theta_{\sigma-}}\sin(\varphi_{\rho-} + \varphi_{\sigma+}) \right. \\ &\quad \left. - i\eta_{1\downarrow}\eta_{2\uparrow}e^{i\theta_{\sigma-}}\sin(\varphi_{\rho-} - \varphi_{\sigma+}) \right], \end{aligned} \quad (\text{B.55})$$

$$\begin{aligned} S_{\pi/2}^y &= e^{-i\theta_{\rho+}} \left[-i\eta_{1\uparrow}\eta_{2\downarrow}e^{-i\theta_{\sigma-}}\cos(\varphi_{\rho-} + \varphi_{\sigma+}) \right. \\ &\quad \left. + i\eta_{1\downarrow}\eta_{2\uparrow}e^{i\theta_{\sigma-}}\cos(\varphi_{\rho-} - \varphi_{\sigma+}) \right], \end{aligned} \quad (\text{B.56})$$

$$\begin{aligned} S_{\pi/2}^z &= e^{-i\theta_{\rho+}} \left[-i\eta_{1\uparrow}\eta_{2\uparrow}e^{-i\theta_{\sigma+}}\sin(\varphi_{\rho-} + \varphi_{\sigma-}) \right. \\ &\quad \left. + i\eta_{1\downarrow}\eta_{2\downarrow}e^{i\theta_{\sigma+}}\sin(\varphi_{\rho-} - \varphi_{\sigma-}) \right], \end{aligned} \quad (\text{B.57})$$

$$\begin{aligned} S_{k_{F2}-k_{F1}}^x &= e^{-i\theta_{\rho-}} \left[-i\eta_{1\uparrow}\eta_{2\downarrow}e^{-i\theta_{\sigma+}}\sin(\varphi_{\rho-} + \varphi_{\sigma+}) \right. \\ &\quad \left. - i\eta_{1\downarrow}\eta_{2\uparrow}e^{i\theta_{\sigma+}}\sin(\varphi_{\rho-} - \varphi_{\sigma+}) \right], \end{aligned} \quad (\text{B.58})$$

$$S_{k_{F2}-k_{F1}}^y = e^{-i\theta_{\rho-}} \left[-i\eta_{1\uparrow}\eta_{2\downarrow}e^{-i\theta_{\sigma+}}\cos(\varphi_{\rho-} + \varphi_{\sigma+}) \right.$$

$$+ i\eta_{1\downarrow}\eta_{2\uparrow}e^{i\theta_{\rho+}} \cos(\varphi_{\rho-} - \varphi_{\sigma+}) \Big], \quad (\text{B.59})$$

$$\begin{aligned} S_{k_{F2}-k_{F1}}^z = e^{-i\theta_{\rho-}} & \left[-i\eta_{1\uparrow}\eta_{2\uparrow}e^{-i\theta_{\sigma-}} \sin(\varphi_{\rho-} + \varphi_{\sigma-}) \right. \\ & \left. + i\eta_{1\downarrow}\eta_{2\downarrow}e^{i\theta_{\sigma-}} \sin(\varphi_{\rho-} - \varphi_{\sigma-}) \right], \end{aligned} \quad (\text{B.60})$$

and for the density:

$$\delta n_{2k_{Fa}} = 2ie^{i\theta_{\rho+}}e^{\pm i\theta_{\rho-}} \cos(\sqrt{2}\theta_{a\sigma}), \quad (\text{B.61})$$

$$\begin{aligned} \delta n_{\pi/2} = 2e^{-i\theta_{\rho+}} & \left[-i\eta_{1\uparrow}\eta_{2\uparrow}e^{-i\theta_{\sigma+}} \sin(\varphi_{\rho-} + \varphi_{\sigma-}) \right. \\ & \left. - i\eta_{1\downarrow}\eta_{2\downarrow}e^{i\theta_{\sigma+}} \sin(\varphi_{\rho-} - \varphi_{\sigma-}) \right], \end{aligned} \quad (\text{B.62})$$

$$\begin{aligned} \delta n_{k_{F2}-k_{F1}} = 2e^{-i\theta_{\rho-}} & \left[-i\eta_{1\uparrow}\eta_{2\uparrow}e^{-i\theta_{\sigma-}} \sin(\varphi_{\rho-} + \varphi_{\sigma-}) \right. \\ & \left. - i\eta_{1\downarrow}\eta_{2\downarrow}e^{i\theta_{\sigma-}} \sin(\varphi_{\rho-} - \varphi_{\sigma-}) \right], \end{aligned} \quad (\text{B.63})$$

where for expressions with \pm in the exponent, $+$ refers to band $a = 1$, while $-$ refers to band $a = 2$.

Perhaps the most important point to take away is that all operators at $Q = 2k_{Fa}, \pi/2$ are proportional to $e^{\pm i\theta_{\rho+}}$. Therefore, the fluctuating field content of these operators is reduced upon gapping out (pinning of) $\theta_{\rho+}$ when crossing the Mott transition from the C2S2 metal to C1S2 insulator. This leads to lowering of the associated scaling dimensions and subsequent enhancement of the structure factor singularities. To illustrate this concretely, assume for the moment that the $\rho+$ and $\rho-$ sectors are decoupled in the charge sector Lagrangian for the C2S2, i.e., $A_{12} = A_{21} = B_{12} = B_{21} = 0$ in Eq. (B.15), with corresponding Luttinger parameters $g_{\rho+}$ and $g_{\rho-}$. We then have the following for the scaling dimensions of the above operators:

$$\Delta[\mathbf{S}_{2k_{Fa}}] = \Delta[\delta n_{2k_{Fa}}] = \frac{1}{2} + \frac{g_{\rho-}}{4} + \frac{g_{\rho+}}{4}, \quad (\text{B.64})$$

$$\Delta[\mathbf{S}_{\pi/2}] = \Delta[\delta n_{\pi/2}] = \frac{1}{2} + \frac{1}{4g_{\rho-}} + \frac{g_{\rho+}}{4}, \quad (\text{B.65})$$

$$\Delta[\mathbf{S}_{k_{F2}-k_{F1}}] = \Delta[\delta n_{k_{F2}-k_{F1}}] = \frac{1}{2} + \frac{1}{4g_{\rho-}} + \frac{g_{\rho+}}{4}, \quad (\text{B.66})$$

where we have assumed SU(2) invariance, $g_{1\sigma} = g_{2\sigma} = 1$ (see the next section). Right at the Mott transition $g_{\rho+} = 1/2$, while immediately on the insulating side $g_{\rho+} \rightarrow 0$. Therefore, the dimensions in Eqs. (B.64) and (B.65) corresponding to operators at $Q = 2k_{Fa}, \pi/2$ should indeed *decrease* at the transition (by an amount of 1/8 in the decoupled approximation). Such an enhancement of the associated spin structure factor singularities on the insulating side of the Mott transition is in fact dramatically seen in the DMRG data of Fig. 2.4.

Furthermore, stability of the C1S2 insulator requires $g_{\rho-} < 1$ (see Ref. [58]), which implies $\Delta[\mathbf{S}_{\pi/2}] > \Delta[\mathbf{S}_{2k_{Fa}}]$ (and similarly for δn_Q). Thus, for the structure factors in the C1S2 phase, the features at $q = 2k_{Fa}$ should be more pronounced than those at $q = \pi/2$. Indeed, this is observed in the spin structure factor data of Fig. 2.4 on the insulating side of the Mott transition in our model. More generally, the presence of clear power-law singularities in $\langle \mathbf{S}_q \cdot \mathbf{S}_{-q} \rangle$ at finite wavevectors in both the metal and weak Mott insulator points strongly towards the presence of gapless spin excitations in both phases (see also Sec. B.3.3).

Note that the density operator at $Q = 2k_{Fa}, \pi/2, k_{F2} - k_{F1}$ still remains power law when $\theta_{\rho+}$ gets pinned, i.e., δn_Q does not contain the wildly fluctuating field $\varphi_{\rho+}$. In fact, for $Q = 2k_{Fa}, \pi/2$ the density also contains directly $\theta_{\rho+}$ [see Eqs. (B.61), (B.62)] and has the same scaling dimension as the spin operator: $\Delta[\delta n_Q] = \Delta[\mathbf{S}_Q]$! Therefore, such Friedel oscillations should actually be enhanced in the Mott insulator [91]. This enhancement is difficult to see in the density structure factor DMRG data of Fig. 2.3, but that is likely due to the small amplitudes of the features. The power-law nature, however, is still apparent, at least around

$$q = 2k_{F1}, k_{F2} - k_{F1}.$$

The bilinears that get enhanced, i.e., those at $Q = 2k_{Fa}, \pi/2$, can be predicted by simple “Amperean rules”. Specifically, in the (1+1)D U(1) gauge theory formulation of the C1S2 spin Bose metal phase [58], $\theta_{\rho+}$ corresponds to the mode that is pinned upon inclusion of gauge fluctuations which implements at long wavelengths the constraint of one spinon per site (in this language, the up and down spinons carry the same gauge charge). We then expect that the bilinears that get enhanced upon introducing the gauge fluctuations are those composed from operators that produce parallel gauge currents, so-called Amperean attraction [34, 58]. This is indeed the case for the spin and density operators at $Q = 2k_{Fa}, \pi/2$ which involve a particle and hole moving in opposite directions. In contrast, the bilinears at $Q = k_{F2} - k_{F1}$ involve operators with antiparallel gauge currents and are therefore not enhanced; indeed these operators do not contain $\theta_{\rho+}$ at all. We remark that in our electronic model, the above “gauge constraint” is implemented dynamically by electron repulsion upon pinning of the overall conducting charge mode $\theta_{\rho+}$.

In Chapter 2, we have also used the dimer correlations, as defined and detailed in Appendix A.1, to characterize the ground state. Following Ref. [58], we can approximate the bond energy as the electron hopping energy, i.e., $\mathcal{B}(x) \sim -t \sum_{\alpha} [c_{\alpha}^{\dagger}(x)c_{\alpha}(x+1) + \text{H.c.}]$. In fact, in our DMRG measurements it would have been reasonable to use this as the definition of $\mathcal{B}(x)$, but we instead implemented the full $\mathcal{B}(x) = \mathbf{S}(x) \cdot \mathbf{S}(x+1)$, which makes the two-point function $\langle \mathcal{B}(x)\mathcal{B}(x') \rangle$ a four-spin (eight-electron) measurement. In any case, expansion in continuum fields reveals

$$\mathcal{B}_Q \sim e^{iQ/2} \delta n_Q, \quad (\text{B.67})$$

which holds for all $Q \neq \pi$. Hence, we expect features at the same wavevectors in measurements of both $\langle \delta n_q \delta n_{-q} \rangle$ and $\langle \mathcal{B}_q \mathcal{B}_{-q} \rangle$. This is indeed observed in Figs. 2.3 and 2.5, where in the putative C1S2 insulator the power-law nature of the features is, as expected, much more apparent in the dimer correlations than in the density correlations.

We further note that $\langle \mathcal{B}_q \mathcal{B}_{-q} \rangle$ very clearly picks up a feature at $q = 4k_{F2} = -4k_{F1}$, while this feature is much weaker, though still present, in $\langle \delta n_q \delta n_{-q} \rangle$. As mentioned in Chapter 2, the wavevector $4k_{F2} = -4k_{F1}$ is a four-fermion contribution to the density/bond energy. Specifically,

$$\delta n_{4k_{F1}} : c_{L1\uparrow}^\dagger c_{L1\downarrow}^\dagger c_{R1\uparrow} c_{R1\downarrow} \sim e^{i2\theta_{\rho+}} e^{i2\theta_{\rho-}}, \quad (\text{B.68})$$

$$\delta n_{-4k_{F2}} : c_{R2\uparrow}^\dagger c_{R2\downarrow}^\dagger c_{L2\uparrow} c_{L2\downarrow} \sim e^{-i2\theta_{\rho+}} e^{i2\theta_{\rho-}}, \quad (\text{B.69})$$

both contribute with independent numerical prefactors, and have scaling dimensions in the decoupled $\rho\pm$ approximation of

$$\Delta[\delta n_{4k_{F2}}] = \Delta[\mathcal{B}_{4k_{F2}}] = g_{\rho+} + g_{\rho-}. \quad (\text{B.70})$$

In the C1S2, $g_{\rho+} \rightarrow 0$ so that $\Delta[\mathcal{B}_{4k_{F2}}] = g_{\rho-}$. Gaplessness of the spin sector requires $g_{\rho-} < 1$ (see Refs. [58, 151]). Hence, the singularity at $q = 4k_{F2}$ in $\langle \mathcal{B}_q \mathcal{B}_{-q} \rangle$ should be stronger than a slope discontinuity (unit scaling dimension of the associated operator)—this indeed appears to be the case in our dimer structure factor data of Fig. 2.5.

There is yet another important four-fermion contribution to the spin and density/bond energy at wavevector $Q = \pi$. We here focus on the latter, where for the bond energy we get contributions such as [58] $\mathcal{B}_\pi : i\delta n_{2k_{F1}} \delta n_{2k_{F2}} + \text{H.c.}$, which when bosonized gives

$$\mathcal{B}_\pi \sim [\cos(2\theta_{\sigma+}) + \cos(2\theta_{\sigma-})] \sin(2\theta_{\rho+}) + \dots \quad (\text{B.71})$$

This operator has unit scaling dimension at the C1S2 fixed point ($\Delta[\mathcal{B}_\pi] = 1$) and should thus correspond to a slope discontinuity in $\langle \mathcal{B}_q \mathcal{B}_{-q} \rangle$ at $q = \pi$. Remarkably, this appears to be consistent with e.g. our characteristic C1S2 data point at $U/t = 4.0$ as presented in Fig. 2.5. Furthermore, inspecting Eq. (B.71) reveals that this feature will only be present in the C1S2 if the pinning of $\theta_{\rho+}$ due to relevance of $\mathcal{H}_8 = 2u \cos(4\theta_{\rho+})$ is such that $\sin(2\theta_{\rho+}) \neq 0$. This is precisely what we would expect if the pinned value of $\theta_{\rho+}$ occurs at $4\theta_{\rho+} = \pi \bmod 2\pi$, which corresponds to the *minima* of $\cos(4\theta_{\rho+})$. We thus conclude that $u > 0$ in our eight-fermion umklapp interaction, as might initially be expected for repulsively interacting electrons [58]. On the other hand, $u < 0$ would lead to pinning of $\theta_{\rho+}$ such that $4\theta_{\rho+} = 0 \bmod 2\pi$, i.e., $\sin(2\theta_{\rho+}) = 0$, thus killing the feature in $\langle \mathcal{B}_q \mathcal{B}_{-q} \rangle$ at $q = \pi$.

At wavevector $Q = \pi$, the bond-centered density \mathcal{B}_π is odd under mirror symmetry ($x \rightarrow -x$), while the site-centered density δn_π is even. Contributions to the latter include $\delta n_\pi : \delta n_{2k_F1} \delta n_{2k_F2} + \text{H.c.}$, which in terms of the bosonized fields reads

$$\delta n_\pi \sim [\cos(2\theta_{\sigma+}) + \cos(2\theta_{\sigma-})] \cos(2\theta_{\rho+}) + \dots \quad (\text{B.72})$$

Hence, the pinning condition $4\theta_{\rho+} = \pi \bmod 2\pi$ inferred above implies $\cos(2\theta_{\rho+}) = 0$. Indeed, the DMRG data shows no feature in $\langle \delta n_q \delta n_{-q} \rangle$ at $q = \pi$ within the putative C1S2 phase (see Fig. 2.3). Again, we conclude that for our system with repulsively interacting electrons, we must have $u > 0$ in \mathcal{H}_8 .

Finally, presence of a feature at $q = \pi$ in $\langle \delta n_q \delta n_{-q} \rangle$ in the C1S2 weak Mott insulator would lead to long-range period-2 (site-centered) charge density wave order in the C0S0 strong Mott insulator at very large U/t . This is indeed very unnatural in our model where the on-site U term is the largest interaction energy scale in the Hamiltonian. Instead, the strong Mott insula-

tor realized in our model develops period-2 long-range order in the *bond-centered* density, as evidenced by the Bragg peak in $\langle \mathcal{B}_q \mathcal{B}_{-q} \rangle$ at $q = \pi$. The power-law feature at the same wavevector in the weak Mott insulator [see Eq. (B.71)] is the precursor of this eventual long-range VBS order at large U/t .

We finally discuss the electron operator itself [Eq. (B.3)], which is of course the most primitive operator of all. When written in terms of “ ρ^\pm ” and “ $a\sigma$ ” modes, we have

$$c_{Pa\alpha} = \eta_{a\alpha} \exp \left\{ \frac{i}{\sqrt{2}} \left[\frac{1}{\sqrt{2}} (\varphi_{\rho+} \pm \varphi_{\rho-}) \pm \varphi_{a\sigma} \right] + \frac{iP}{\sqrt{2}} \left[\frac{1}{\sqrt{2}} (\theta_{\rho+} \pm \theta_{\rho-}) \pm \theta_{a\sigma} \right] \right\}, \quad (\text{B.73})$$

where the first \pm on each line refers to $a = 1, 2$, while the second refers to $\alpha = \uparrow, \downarrow$. Of course, once the $\theta_{\rho+}$ field is pinned, the electron Green’s function $\langle c_\alpha^\dagger(x) c_\alpha(0) \rangle$ is expected to decay exponentially at all wavevectors. Mathematically, this is due to its conjugate field $\varphi_{\rho+}$ also being present in the bosonized representation of the electron operator: By the uncertainty principle, pinning of $\theta_{\rho+}$ will cause $\varphi_{\rho+}$ to fluctuate wildly leading to exponential decay of the Green’s function. While it is somewhat difficult to ascertain this exponential decay within the putative C1S2 phase for the electron momentum distribution function DMRG data of Fig. 2.6, we again believe this is due to the excessively large charge correlation lengths present in our electronic spin Bose metal.

From Eq. (B.73), we also see that gapping of a spin mode will cause the associated electron Fermi point to gap out, and thus the electron Green’s function can in principle detect spin-gap behavior. However, this is rather difficult in practice [158], and in the following section we discuss a better approach as employed in Chapter 2.

B.3.3 Assessing Gaplessness of the Spin Sector Through $g_{\sigma+}$

Inspection of the bosonized expressions for the different components of the spin operator at wavevectors $Q = 2k_{Fa}$ in Eqs. (B.52)-(B.54), reveals that in the fixed-point theory for either the C2S2 metal or C1S2 insulator we must have only trivial Luttinger parameters in the spin sector: $g_{1\sigma} = g_{2\sigma} = 1$. Specifically, for arbitrary $g_{a\sigma}$ as in Eq. (B.17) and decoupled $\rho+$ and $\rho-$ modes as in the illustrative discussion in Sec. B.3.2 above, we have

$$\Delta[S_{2k_{Fa}}^x] = \Delta[S_{2k_{Fa}}^y] = \frac{g_{\rho+}}{4} + \frac{g_{\rho-}}{4} + \frac{1}{2g_{a\sigma}}, \quad (\text{B.74})$$

$$\Delta[S_{2k_{Fa}}^z] = \frac{g_{\rho+}}{4} + \frac{g_{\rho-}}{4} + \frac{g_{a\sigma}}{2}, \quad (\text{B.75})$$

where in the C1S2 insulator we have $g_{\rho+} \rightarrow 0$. Therefore, SU(2) spin invariance manifest through isotropic spin-spin correlations functions at wavevectors $2k_{Fa}$, i.e., $\Delta[S_{2k_{Fa}}^x] = \Delta[S_{2k_{Fa}}^y] = \Delta[S_{2k_{Fa}}^z]$, indeed dictates that

$$g_{1\sigma} = g_{2\sigma} = 1, \quad (\text{B.76})$$

which constitutes a simple generalization of the well-known one-mode case [4] (see also Ref. [162]).

We now show how measurement of the spin structure factor at zero momentum can assess the condition in Eq. (B.76). The slowly varying part of the spin density is $S^z(x) = \partial_x \theta_{\sigma+}/\pi$, hence the long-wavelength part of the real-space spin-spin correlation function evaluated in the fixed-point theory for either the C2S2 or C1S2 [see Eq. (B.17)] reads

$$\langle S^z(x)S^z(0) \rangle = -\frac{g_{\sigma+}}{2\pi^2} \frac{1}{x^2} + \dots, \quad (\text{B.77})$$

where we have defined

$$g_{\sigma+} \equiv \frac{g_{1\sigma} + g_{2\sigma}}{2}. \quad (\text{B.78})$$

Equation (B.77) gives for the spin structure factor as $q \rightarrow 0$:

$$\langle S_q^z S_{-q}^z \rangle = \frac{g_{\sigma+}}{2\pi} |q|, \quad (\text{B.79})$$

which we use in Chapter 2 to estimate the parameter $g_{\sigma+}$ [see Eq. (2.5) and the inset of Fig. 2.4].

Clearly then within the fixed-point theory we should have $g_{\sigma+} = 1$, while in the presence of a spin gap $\langle S_q^z S_{-q}^z \rangle \sim q^2$, so that $g_{\sigma+} \rightarrow 0$. Note that, as with $g_{\rho+}$ above, $g_{\sigma+}$ is not a genuine Luttinger parameter as even free electrons are not generally diagonal in the $\sigma\pm$ basis.

The above considerations are valid for the fixed point in the thermodynamic limit. However, there are several marginal interactions that need to be irrelevant for the spin sector to remain gapless and the C2S2 and C1S2 to be stable phases. Thus, the presence of such marginally irrelevant interactions will affect measurement of $g_{\sigma+}$ on finite-size systems. In the case of our C2S2 and C1S2, the residual interactions in the spin sector that mix right and left movers read

$$\mathcal{H}_{RL}^\sigma = - \sum_{a,b} (w_{ab}^\sigma \mathbf{J}_{Rab} \cdot \mathbf{J}_{Lab} + \lambda_{ab}^\sigma \mathbf{J}_{Raa} \cdot \mathbf{J}_{Lbb}), \quad (\text{B.80})$$

where $\mathbf{J}_{Pab} \equiv \frac{1}{2} c_{Paa}^\dagger \boldsymbol{\sigma}_{\alpha\beta} c_{Pb\beta}$. In the C2S2 and C1S2, the w_{ab}^σ terms are strictly irrelevant, while the λ_{ab}^σ terms are only marginally irrelevant [58, 151]. Bosonizing the latter interactions gives

$$\tilde{\mathcal{H}}_{RL}^\sigma = V_z + V_\perp, \quad (\text{B.81})$$

$$V_z = \sum_a \frac{\lambda_{aa}^\sigma}{8\pi^2} [(\partial_x \varphi_{a\sigma})^2 - (\partial_x \theta_{a\sigma})^2] \quad (\text{B.82})$$

$$+ \frac{\lambda_{12}^\sigma}{4\pi^2} [(\partial_x \varphi_{1\sigma})(\partial_x \varphi_{2\sigma}) - (\partial_x \theta_{1\sigma})(\partial_x \theta_{2\sigma})], \quad (\text{B.83})$$

$$V_\perp = \sum_a \lambda_{aa}^\sigma \cos(2\sqrt{2}\theta_{a\sigma}) \quad (\text{B.84})$$

$$+ 2\lambda_{12}^\sigma \hat{\Gamma} \cos(2\theta_{\sigma+}) \cos(2\varphi_{\sigma-}), \quad (\text{B.85})$$

where $\hat{\Gamma} \equiv \eta_{1\uparrow}\eta_{1\downarrow}\eta_{2\uparrow}\eta_{2\downarrow}$.

A necessary condition for the spin to be gapless is that the couplings λ_{ab}^σ be initially positive, corresponding to the system being overall repulsive in the spin sector. Ultimate stability of the C2S2 and C1S2 corresponds to λ_{ab}^σ renormalizing to zero via slow marginal flows. It should in principle be possible to calculate precise flows (and finite-size scaling behavior) of our effective $g_{\sigma+}$ parameter by analyzing the behavior of the zero-momentum piece of the spin structure factor perturbatively in the λ_{ab}^σ . We do not pursue this here, but instead to get a rough, initial feel for the trends within our Abelian bosonization, imagine for the moment naively ignoring the V_\perp cosines and λ_{12}^σ cross terms. Then, the quadratic V_z terms effectively feed into renormalizing the $g_{a\sigma}$ Luttinger parameters above (below) unity for λ_{aa}^σ positive (negative), hence effectively corresponding to $g_{\sigma+} > 1$ ($g_{\sigma+} < 1$) on a finite-size system. This is indeed the expected trend for overall repulsion in the spin sector.

On the other hand, the flows for the C1S0 superconductor (the main instability of the C2S2) correspond to λ_{aa}^σ eventually becoming negative (attraction in the spin sector) and then diverging to $-\infty$. All modes then eventually get gapped out except the overall conducting $\rho+$ mode [108, 157], so that for the spin structure factor we have $\langle S_q^z S_{-q}^z \rangle \sim q^2$ as $q \rightarrow 0$, i.e., $g_{\sigma+} \rightarrow 0$. On a finite-size system, we thus expect the spin gap to be manifest as a measured $g_{\sigma+} < 1$. Note, though, that due to *initial* repulsion in the spin sector [$\lambda_{ab}^\sigma(\ell = 0) > 0$], even an eventual C1S0 may exhibit “stiffening” of the spin sector on relatively short length scales, i.e., measured $g_{\sigma+} > 1$. These considerations highlight why it is so difficult to detect spin-gap behavior in models such as the t - t' - U Hubbard model [158]. We stress, however, that in our model with longer-ranged repulsion—a model which is known to be spin gapless at weak cou-

pling ($U/t \ll 1$) for our chosen parameters [151]—measurements of $g_{\sigma+}$ still strongly indicate spin gaplessness all the way up to $U/t \simeq 5.0$, well past the Mott critical value of $U/t = 1.6$. In the next section, we contrast this with the behavior of the on-site t - t' - U Hubbard model at $\kappa = 0$ in which the metal and insulator are presumably both spin gapped.

Finally, we again mention that the observed power-law singularities in the spin structure factor at the various “ $2k_F$ ” wavevectors (see Fig. 2.4 and Sec. B.3.2) provide complementary evidence that the spin sector is gapless in both the metal (C2S2) and weak Mott insulator (C1S2) of our model.

B.4 Further Analysis of $g_{\sigma+}$ DMRG Data

Here we present more data of our DMRG measurements of the parameter $g_{\sigma+}$ discussed in the previous section. Specifically, we define a finite-size estimate of $g_{\sigma+}$ via Eq. (2.5) by evaluating the slope of the spin structure factor at a momentum $q = n\frac{2\pi}{L}$ with n a small integer:

$$g_{\sigma+}(L, n) \equiv \frac{L}{3n} \langle \mathbf{S}_q \cdot \mathbf{S}_{-q} \rangle \Big|_{q=n\frac{2\pi}{L}}, \quad (\text{B.86})$$

where in what follows we choose $n = 2$.

In Figs. B.1 and B.2, we show $g_{\sigma+}(L, n = 2)$ versus U/t on several system sizes L for the extended Hubbard model as presented in the Chapter 2 [Eqs. (2.1)-(2.2) with $t'/t = 0.8$, $\kappa = 0.5$, $\gamma = 0.2$] and the on-site t - t' - U Hubbard model [Eqs. (2.1)-(2.2) with $t'/t = 0.8$, $\kappa = 0$], respectively. In the former case, we use periodic boundary conditions due to the reasons discussed in Appendix A.1, while in the latter case we use standard open boundary conditions. Note that the $L = 96$ data in Fig. B.1 corresponds to the second ($q = 2\frac{2\pi}{96}$) data

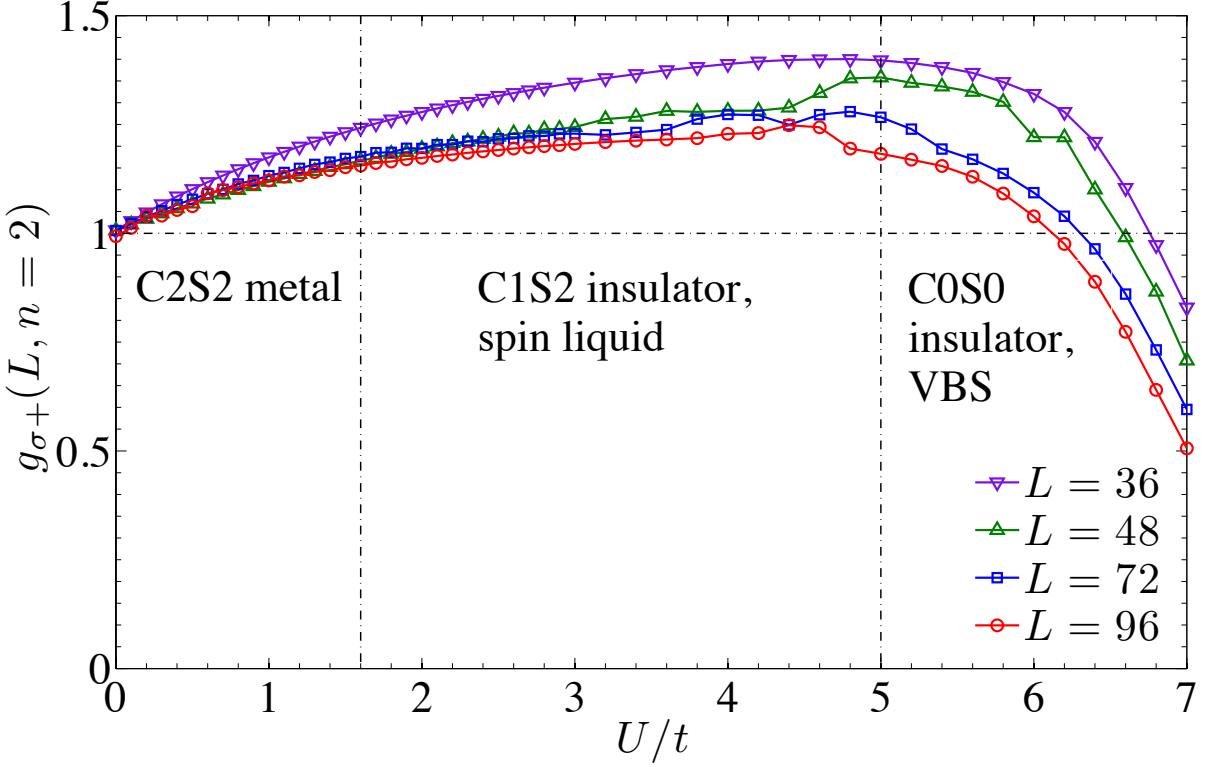


Figure B.1: Finite-size estimates of $g_{\sigma+}$ [see Eq. (B.86)] versus U/t : Extended Hubbard model for the same parameters used in Chapter 2. The putative realized phases (see text) are labeled with separating vertical dashed-dotted lines. At $U/t = 0$, our DMRG calculations give $g_{\sigma+}(L, n = 2) = 1$ to within 1% for all sizes; this serves as a very useful check on our convergence since free electrons are, ironically, very challenging to converge in the DMRG.

points in the inset of Fig. 2.4.

We first focus on the extended Hubbard model data as shown in Fig. B.1. Here, $g_{\sigma+}(L)$ increases above unity as we turn on U/t and continues to do so well past the putative Mott transition from the C2S2 metal to C1S2 insulator at $U/t = 1.6$. Rather remarkably, the data does not start renormalizing visibly downwards until $U/t \gtrsim 4.0$. Around $U/t \simeq 5.0$, the system starts showing signs of spin-gap behavior (e.g., a Bragg peak in the dimer structure factor; see Fig. 2.5) near which $g_{\sigma+}(L)$ finally starts bending downward. While the data points on the large sizes are still not fully converged due to the periodic boundary conditions and inherent difficulty involved in converging such a quantity at small momenta, we believe that as

$L \rightarrow \infty$ we would find $g_{\sigma+} = 1$ for $U/t \lesssim 5.0$ and $g_{\sigma+} = 0$ for $U/t \gtrsim 5.0$ (see the previous section).

We here mention that we are not generally able to converge perfectly to a spin-singlet in our DMRG simulations. To assess this, we can measure the total spin S_{tot} in the ground state (we work only in the $S_{\text{tot}}^z = 0$ sector in the DMRG) by evaluating the computed spin structure factor at $q = 0$:

$$\langle \mathbf{S}_q \cdot \mathbf{S}_{-q} \rangle|_{q=0} = \frac{1}{L} \langle \mathbf{S}_{\text{tot}}^2 \rangle = \frac{1}{L} S_{\text{tot}}(S_{\text{tot}} + 1). \quad (\text{B.87})$$

In simulations of Eqs. (2.1)-(2.2) with periodic boundary conditions, we often find for S_{tot} some small noninteger value on the order of unity. For example, on $L = 96$ sites with $m = 6000$ states, at the free electron point $U/t = 0$, we find $S_{\text{tot}} = 0.60$, and at the characteristic C1S2 spin Bose metal point $U/t = 4.0$, we find $S_{\text{tot}} = 0.46$. However, we believe this is just a benign effect of our inability to fully converge the DMRG and the eventual ground state at $m \rightarrow \infty$ will be a spin-singlet with $S_{\text{tot}} = 0$. We know this to be true at $U/t = 0$, while all indications point toward a spin-singlet C1S2 for $1.6 < U/t \lesssim 5.0$, e.g., the features at $2k_{F1}$ and $2k_{F2}$ are symmetrically located about $q = \pi/2$ in measurements of $\langle \mathbf{S}_q \cdot \mathbf{S}_{-q} \rangle$ (see Fig. 2.4). In fact, this convergence difficulty is to be expected in our parameter regime of $t'/t = 0.8$, as realization of the two-band spin Bose metal in a pure spin model with ring exchanges (Ref. [58]) found similar DMRG convergence problems in the corresponding parameter regime of that model.

Also, these difficulties are likely responsible for the small “jumps” in the data in Fig. B.1, since measured finite total spin will have a small, somewhat unpredictable, quantitative effect on our $g_{\sigma+}(L, n)$ values. For instance, we are able to converge to a singlet for all U/t on

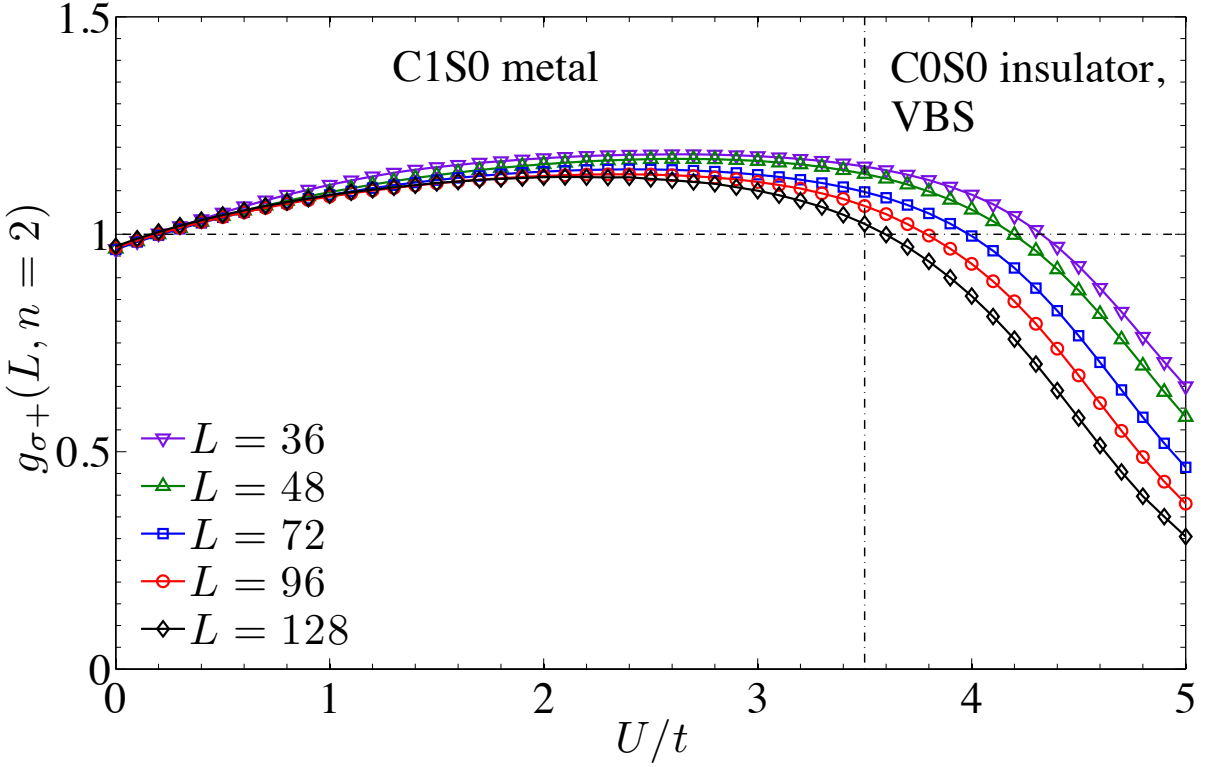


Figure B.2: Finite-size estimates of $g_{\sigma+}$ [see Eq. (B.86)] versus U/t : On-site t - t' - U Hubbard model at $t'/t = 0.8$. The vertical dashed-dotted line at $U/t = 3.5$ indicates our estimate of the Mott transition between the C1S0 metal and C0S0 period-2 VBS insulator from $g_{\rho+}$ measurements (not shown; see Ref. [210]). This value is in good agreement with earlier studies of the half-filled t - t' - U Hubbard model [158, 164]. Here, we use open boundary conditions which gives very good convergence, though at the expense of some small systematic error in determining $g_{\sigma+}$ from the momentum-space structure factor; e.g., $g_{\sigma+}(L, n = 2)$ is slightly less than one at $U/t = 0$ which is due entirely to the usage of open boundary conditions.

the $L = 36$ site system, and hence its curve is smooth. On the other hand, on the $L = 48$ site system, the measured total spin starts abruptly dropping toward zero near $U/t = 4.4$, and we believe this behavior is responsible for the corresponding feature in the $L = 48$ curve of Fig. B.1. Ultimately, however, these convergence problems will almost certainly have no qualitative effect on our conclusions being drawn from the $g_{\sigma+}$ data.

In Fig. B.2, we show analogous $g_{\sigma+}(L, n = 2)$ measurements for the ordinary on-site t - t' - U Hubbard model at $t'/t = 0.8$. This model has a spin gap at weak coupling $U/t \ll 1$ (see,

e.g., Refs. [108, 157]) so that at small finite interaction strengths we expect the system to be in a spin-gapped C1S0 phase. However, the RG flows which describe the opening of this spin gap are rather intricate. Specifically, due to the repulsive Hubbard U , the system is initially repulsive (stable) in the spin sector, while the eventual gapping out of both the spin modes and the “ $\rho-$ ” mode happens due to a delicate interplay of all channels (see Fig. 3 of Ref. [151]). We believe this initial repulsion in the spin sector is responsible for measured $g_{\sigma+} > 1$ (see also discussion in the previous section), while it will drop below unity for large enough sizes. On the other hand, if the spin sector is initially attractive (unstable), then we observe $g_{\sigma+} < 1$ for all sizes. This occurs, e.g., in electronic models with explicit Heisenberg coupling $J \mathbf{S}_i \cdot \mathbf{S}_j$ that favors a spin-gapped (Luther-Emery) liquid (see Ref. [210]).

The Mott transition in the t - t' - U Hubbard model will also be driven by the same eight-fermion umklapp term discussed above. By measuring its scaling dimension in the same fashion as we have done for the extended model (see Fig. 2.3 and Sec. B.3), we have determined that for the U -only Hubbard model at $t'/t = 0.8$ the Mott transition occurs near $U/t = 3.5$, after which period-2 VBS order sets in immediately (see Ref. [210] for more details). We see, however, that $g_{\sigma+}(L)$ already starts bending downward well before then. We stress that this is in sharp contrast to the data of Fig. B.1 in which our model with longer-ranged repulsion shows no signs of a spin gap until *well past* the Mott transition. In that case, the intervening phase is the spin gapless C1S2 spin liquid insulator.

Appendix C

Determinantal Representation of BCS-type Wave Functions

In this appendix, we spell out the technical details pertinent to representing N -particle BCS-type wave functions by simple determinants. The material presented here was used in Chapter 3, where we performed a VMC study of the Heisenberg model with ring exchange on the triangular lattice, Eq. (3.1), using spin liquid wave functions obtained by projecting out doubly-occupied sites from such BCS wave functions at half filling.

We begin with a mean-field Hamiltonian describing spin-1/2 spinons on some lattice with sites labeled r [see also Eq. (3.2)]:

$$H_{\text{MF}} = - \sum_{r,r'} \left[t_{rr'}^\alpha f_{r\alpha}^\dagger f_{r'\alpha} + (\Delta_{rr'} f_{r\uparrow}^\dagger f_{r'\downarrow}^\dagger + \text{H.c.}) \right], \quad (\text{C.1})$$

where $t_{r'r}^\alpha = (t_{rr'}^\alpha)^*$ (from Hermiticity) and either $\Delta_{r'r} = \Delta_{rr'}$ (singlet channel pairing) or $\Delta_{r'r} = -\Delta_{rr'}$ (triplet channel pairing). In the first term, there is an implicit sum over spin indices $\alpha = \uparrow, \downarrow$. Here we are allowing for spin-dependent hopping patterns $t_{rr'}^\alpha$, which for

$t_{rr'}^\uparrow \neq t_{rr'}^\downarrow$ breaks the global SU(2) symmetry, but can be useful for constructing interesting mean-field states which have gapless Fermi pockets coexisting with paired spinons [211, 212] (see Sec. C.2 below). In Sec. C.1, we formulate the Bogoliubov-de Gennes (BdG) solution to Eq. (C.1) and calculate the corresponding pair wave function *entirely in real space*, which is convenient for numerical implementation; for this we will eventually assume spin-independent hopping, $t_{rr'}^\uparrow = t_{rr'}^\downarrow = t_{rr'}$, as pertinent to Chapter 3. In Sec. C.2, on the other hand, we will discuss an alternative form of the determinantal representation of the ground state of Eq. (C.1), which through a particle-hole transformation on the $f_{r\downarrow}$ spinon, avoids the BdG transformation entirely; while being numerically less efficient for subsequent VMC calculations, this approach is very numerically stable and robust for *any* physically relevant hopping and pairing patterns, $t_{rr'}^\alpha$ and $\Delta_{rr'}$.

C.1 Calculating the Pair Wave Function in Real Space: Bogoliubov-de Gennes Approach

It is well-known [213] that when projected onto the N -particle sector unpolarized superconducting BCS wave functions can be written as a single $N/2 \times N/2$ determinant:

$$\psi_{\text{BCS}} \left(\left\{ R_i^\uparrow \right\}, \left\{ R_i^\downarrow \right\} \right) = \left\langle \left\{ R_i^\uparrow \right\}, \left\{ R_i^\downarrow \right\} \middle| \text{BCS} \right\rangle_N = \det \left[\phi \left(R_i^\uparrow, R_j^\downarrow \right) \right], \quad (\text{C.2})$$

where $\{R_i^\alpha\}$ is the set of particle positions for species $\alpha = \uparrow, \downarrow$ with $i = 1, 2, \dots, N/2$ ($N_\uparrow = N_\downarrow = N/2$). This first-quantized form of the BCS wave function nicely elucidates the fact that a superconducting wave function can be thought of as a condensate of Cooper pairs each described by the two-particle *pair wave function* $\phi(R_i^\uparrow, R_j^\downarrow)$. For a translationally invariant

system, $\phi(r, r') = \phi(r - r')$, and calculating ϕ by going to momentum space is a textbook exercise in BCS theory [37]. Here, we calculate $\phi(r, r')$ for generally nontranslationally invariant systems in terms of the inputs to the mean-field theory in real space: $t_{rr'}^\uparrow = t_{rr'}^\downarrow = t_{rr'}$ and $\Delta_{rr'}$.

To proceed, we write Eq. (C.1) for a finite-size system of L sites as

$$H_{\text{MF}} = \vec{F}^\dagger \cdot \mathcal{H} \cdot \vec{F} = \left(\vec{F}^\dagger \right)_{ra} \mathcal{H}_{rr'}^{ab} \left(\vec{F} \right)_{r'b}, \quad (\text{C.3})$$

where $\vec{F}^\dagger = (f_{1\uparrow}^\dagger, f_{1\downarrow}^\dagger, f_{2\uparrow}^\dagger, f_{2\downarrow}^\dagger, \dots, f_{L\uparrow}^\dagger, f_{L\downarrow}^\dagger)$ is a row vector of $2L$ fermionic operators and \mathcal{H} is a $2L \times 2L$ matrix filled out by elements of the 2×2 matrices

$$\mathcal{H}_{rr'} = \begin{pmatrix} -t_{rr'} & \Delta_{rr'} \\ \pm\Delta_{rr'}^* & t_{rr'}^* \end{pmatrix}, \quad (\text{C.4})$$

with the rows (a) and columns (b) corresponding the $a, b = \uparrow, \downarrow = 1, 2$; for pairing in the singlet (triplet) channel, we take $+$ ($-$) on the $a = 2, b = 1$ element in Eq. (C.4). \mathcal{H} is a Hermitian matrix and can thus be diagonalized by a unitary transformation:

$$U^\dagger \cdot \mathcal{H} \cdot U = \mathcal{D} \leftrightarrow \mathcal{H} = U \cdot \mathcal{D} \cdot U^\dagger, \quad (\text{C.5})$$

so $H_{\text{MF}} = \vec{\Gamma}^\dagger \cdot \mathcal{D} \cdot \vec{\Gamma}$, where $\vec{\Gamma}^\dagger = \vec{F}^\dagger \cdot U = (\gamma_{1\uparrow}^\dagger, \gamma_{1\downarrow}^\dagger, \gamma_{2\uparrow}^\dagger, \gamma_{2\downarrow}^\dagger, \dots, \gamma_{L\uparrow}^\dagger, \gamma_{L\downarrow}^\dagger)$ is a row vector of our $2L$ Bogoliubov quasiparticle operators $\gamma_{n\alpha}$ which obey canonical fermionic anticommutation relations and carry spin $\alpha = \uparrow, \downarrow$, and \mathcal{D} is a diagonal matrix containing the eigenenergies E_n .

The eigenvalue problem we are trying to solve reads

$$\mathcal{H}_{rr'}^{ab} \Psi_{r'b}^{E_n} = E_n \Psi_{ra}^{E_n}, \quad (\text{C.6})$$

where in what follows we parameterize the eigenstates with common “ (u, v) ”-type notation as

$$\vec{\Psi}_r^{E_n} = \begin{pmatrix} \Psi_{r1}^{E_n} \\ \Psi_{r2}^{E_n} \end{pmatrix} \equiv \begin{pmatrix} u_r^{E_n} \\ v_r^{E_n} \end{pmatrix}. \quad (\text{C.7})$$

It is simple to check that for $\mathcal{H}_{rr'}$ as defined in (C.4), we have the following “particle-hole” symmetry:

$$\tau^{y/x} \cdot \mathcal{H}_{rr'}^* \cdot \tau^{y/x} = -\mathcal{H}_{rr'}, \quad (\text{C.8})$$

where $\tau^{y/x}$ are Pauli matrices with τ^y (τ^x) corresponding to singlet (triplet) channel pairing.

Note that the simple form of this symmetry relies on spin-independent hopping, $t_{rr'}^\uparrow = t_{rr'}^\downarrow = t_{rr'}$, as assumed above. Equation (C.8) allows us to relate positive and negative energy eigenstates of \mathcal{H} . Specifically, given an eigenstate with energy $E_n > 0$, Eq. (C.8) guarantees a corresponding eigenstate with energy $-E_n < 0$:

$$\vec{\Psi}_r^{-E_n} = \begin{pmatrix} \Psi_{r1}^{-E_n} \\ \Psi_{r2}^{-E_n} \end{pmatrix} = \begin{pmatrix} \Psi_{r2}^{E_n*} \\ \mp \Psi_{r1}^{E_n*} \end{pmatrix} = \begin{pmatrix} v_r^{E_n*} \\ \mp u_r^{E_n*} \end{pmatrix}. \quad (\text{C.9})$$

We can then organize the unitary matrix U which diagonalizes \mathcal{H} as follows:

$$U = \begin{pmatrix} \vdots & \vdots & \vdots & \vdots \\ \Psi_{ra}^{E_1} & \Psi_{ra}^{-E_1} & \dots & \Psi_{ra}^{E_L} & \Psi_{ra}^{-E_L} \\ \vdots & \vdots & \vdots & \vdots & \vdots \end{pmatrix} = \begin{pmatrix} u_1^{E_1} & v_1^{E_1*} & \dots & u_1^{E_L} & v_1^{E_L*} \\ v_1^{E_1} & \mp u_1^{E_1*} & \dots & v_1^{E_L} & \mp u_1^{E_L*} \\ \vdots & \vdots & \ddots & \vdots & \vdots \end{pmatrix}, \quad (\text{C.10})$$

where in the last expression we have explicitly shown only the first two rows corresponding to the first lattice site, $r = 1$. Up to a constant, our original Hamiltonian can now be written purely in terms of Bogoliubov quasiparticle number operators all with positive energies $E_n > 0$:

$$H_{\text{MF}} = \vec{\Gamma}^\dagger \cdot \mathcal{D} \cdot \vec{\Gamma} = \sum_{n,\alpha} E_n \gamma_{n\alpha}^\dagger \gamma_{n\alpha}. \quad (\text{C.11})$$

That is, the ground state of H_{MF} , which we denote $|\text{BCS}\rangle$, is the familiar *vacuum of Bogoliubov quasiparticles*:

$$\gamma_{n\alpha} |\text{BCS}\rangle = 0 \quad \forall n = 1, 2, \dots, L; \alpha = \uparrow, \downarrow. \quad (\text{C.12})$$

For simplicity, we are here assuming no zero modes in the spectrum of \mathcal{H} , i.e., $E_n \neq 0$.

While such modes can be accounted for in the above framework (they lead to degeneracies in the ground state), for the types of problems we are interested in solving (see Chapter 3), one can in practice always choose appropriate spinon boundary conditions which leave the spectrum void of zero modes. Perhaps most importantly, zero modes lead to singularities in the pair wave function calculation in what follows, so they are best avoided if possible. The methods described in Sec. C.2, on the other hand, are completely robust to the presence of zero modes.

By standard BCS arguments [37, 38], we know that we can write $|BCS\rangle$ in the following form:

$$|BCS\rangle = e^{-\sum_{r,r'} f_{r\uparrow}^\dagger \phi(r,r') f_{r'\downarrow}^\dagger} |0\rangle = e^{-(\vec{F}_\uparrow^\dagger)^T \cdot \Phi \cdot \vec{F}_\downarrow^\dagger} |0\rangle, \quad (\text{C.13})$$

where $|0\rangle$ is the vacuum of the f particles, and we have defined the L -component column vectors $(\vec{F}_\alpha)_r \equiv f_{r\alpha}$ and $(\vec{F}_\alpha^\dagger)_r \equiv f_{r\alpha}^\dagger$ and the $L \times L$ ‘‘pairing matrix’’ $\Phi_{rr'} \equiv \phi(r, r')$ which is precisely the pair wave function of Eq. (C.2). At this point, we basically take (C.13) as an ansatz and require (C.12) via an appropriate choice of Φ . To this end, we write the quasiparticle operators $\gamma_{n\alpha}$ in terms of the eigenvectors of \mathcal{H} :

$$\gamma_{n\uparrow} = \sum_r \left[u_r^{E_n*} f_{r\uparrow} + v_r^{E_n*} f_{r\downarrow}^\dagger \right] = (\vec{u}_n^*)^T \cdot \vec{F}_\uparrow + (\vec{v}_n^*)^T \cdot \vec{F}_\downarrow^\dagger, \quad (\text{C.14})$$

$$\gamma_{n\downarrow} = \sum_r \left[v_r^{E_n*} f_{r\uparrow}^\dagger \mp u_r^{E_n*} f_{r\downarrow} \right] = (\vec{v}_n^*)^T \cdot \vec{F}_\uparrow^\dagger \mp (\vec{u}_n^*)^T \cdot \vec{F}_\downarrow, \quad (\text{C.15})$$

where we have introduced L -component column vectors containing the u ’s and v ’s, $(\vec{u}_n)_r \equiv u_r^{E_n}$ and $(\vec{v}_n)_r \equiv v_r^{E_n}$. We now require $\gamma_{n\uparrow}|BCS\rangle = \gamma_{n\downarrow}|BCS\rangle = 0$. Here, we focus on the case $\gamma_{n\uparrow}|BCS\rangle = 0$ (requiring $\gamma_{n\downarrow}|BCS\rangle = 0$ gives an identical result). Using Eqs. (C.14) and

(C.13), we have

$$\gamma_{n\uparrow}|\text{BCS}\rangle = \left[(\vec{u}_n^*)^T \cdot \vec{F}_\uparrow + (\vec{v}_n^*)^T \cdot \vec{F}_\downarrow^\dagger \right] e^{-(\vec{F}_\uparrow^\dagger)^T \cdot \Phi \cdot \vec{F}_\downarrow^\dagger} |0\rangle = 0. \quad (\text{C.16})$$

Since $\gamma_{n\uparrow}$ changes the number of f particles by ± 1 and $|\text{BCS}\rangle$ contains terms with only even numbers of f particles (as can be seen by simple Taylor expansion), Eq. (C.16) can be broken up into sectors each containing an odd integer number of particles, $N = 2j - 1$ for positive integers $j = 1, 2, \dots$. The simplest case corresponds to $N = j = 1$ which gives

$$[(\vec{v}_n^*)^T - (\vec{u}_n^*)^T \cdot \Phi] \cdot \vec{F}_\downarrow^\dagger = 0, \quad (\text{C.17})$$

so that $(\vec{u}_n^*)^T \cdot \Phi = (\vec{v}_n^*)^T$. Requiring this for all $n = 1, 2, \dots, L$, gives a matrix equation $U_1^\dagger \cdot \Phi = V_1^\dagger$, where

$$U_1 \equiv \begin{pmatrix} \vec{u}_1 & \vec{u}_2 & \dots & \vec{u}_L \end{pmatrix}, \quad V_1 \equiv \begin{pmatrix} \vec{v}_1 & \vec{v}_2 & \dots & \vec{v}_L \end{pmatrix} \quad (\text{C.18})$$

are matrices formed from the column vectors \vec{u}_n and \vec{v}_n . We have thus derived an expression for Φ in terms of the \vec{u}_n and \vec{v}_n which are ultimately functions of the parameters $t_{rr'}$ and $\Delta_{rr'}$ through diagonalization of \mathcal{H} above. The final result is

$$\Phi = \left(U_1^\dagger \right)^{-1} \cdot V_1^\dagger, \quad \Phi_{rr'} = \phi(r, r'), \quad (\text{C.19})$$

which is the analog of the well-known expression for the pair wave function in momentum space [37, 213]: $\phi_k = v_k/u_k = \Delta_k/(\xi_k + \sqrt{\xi_k^2 + |\Delta_k|^2})$. Thus far we have focused only on the term $N = j = 1$; however, it is straightforward, though at a level of complete rigor somewhat tedious, to show that Eq. (C.19) is indeed the correct form of the pair wave function for all $N = 2j - 1$.

By a standard calculation [138, 213, 37], we can show that projecting $|BCS\rangle$ to N total particles results in the $N/2 \times N/2$ determinant quoted in Eq. (C.2) above:

$$\psi_{BCS} \left(\left\{ R_i^\uparrow \right\}, \left\{ R_i^\downarrow \right\} \right) = \left\langle \left\{ R_i^\uparrow \right\}, \left\{ R_i^\downarrow \right\} \middle| \left(\sum_{r,r'} \phi(r, r') f_{r\uparrow}^\dagger f_{r'\downarrow}^\dagger \right)^{N/2} \middle| 0 \right\rangle = \det \left[\phi \left(R_i^\uparrow, R_j^\downarrow \right) \right]. \quad (C.20)$$

We can subsequently perform VMC on such wave functions (perhaps in the presence of Gutzwiller projection) using well-established methods [138, 139, 140], as was done obtaining the results in Chapter 3 and Ref. [143]. We stress that the above method is simple to implement as its only inputs are the real-space hopping and pairing patterns, $t_{rr'}$ and $\Delta_{rr'}$, of the mean-field Hamiltonian, and it is numerically efficient in the VMC as it only requires updating a single $N/2 \times N/2$ determinant.

C.2 Avoiding Bogoliubov-de Gennes with a Particle-Hole

Transformation on $f_{r\downarrow}$

However, the above expression for the pair wave function, Eq. (C.19), is ill-conditioned if U_1 is a singular matrix, i.e., $\det(U_1) = 0$. In Fourier space, such singular behavior corresponds to zeros of the function $u_k = \xi_k + \sqrt{\xi_k^2 + |\Delta_k|^2}$, where $\xi_k = \epsilon_k - \mu$ is the Fourier transform of the hopping pattern $t_{rr'}$ with Fermi energy μ , and Δ_k is the Fourier transform of the pairing pattern $\Delta_{rr'}$. In practice, such zeros will arise from time to time, e.g., the nodal d -wave state of Chapter 3 is plagued by them with fully periodic boundary conditions, but usually one can alter the spinon boundary conditions to avoid them. Also, the above analysis is rather specific to unpolarized states ($N_\uparrow = N_\downarrow = N/2$) with spin-independent hopping ($t_{rr'}^\uparrow = t_{rr'}^\downarrow = t_{rr'}$). In

what follows, we will describe another approach which avoids these downfalls and limitations, albeit with a slight loss of numerical efficiency in the final VMC.

The idea is very simple. It starts by performing a particle-hole transformation on the \downarrow -spin spinon:

$$f_{r\uparrow} = d_1(r), \quad f_{r\downarrow} = d_2^\dagger(r), \quad (\text{C.21})$$

where the d notation is inspired from the d -wave Bose metal construction of Chapter 4. This transformation is canonical so that the anticommutation relations of the new $d_a(r)$ operators are the usual fermionic ones. That is, our d particles are just canonical fermions with “spin” or “orbital” index $a = 1, 2$. The main point here is that pairing in the f language then transforms to spin-flip hopping (“spin-orbit coupling”) in the d language:

$$\Delta_{rr'} f_{r\uparrow}^\dagger f_{r'\downarrow}^\dagger \rightarrow \Delta_{rr'} d_1^\dagger(r) d_2(r'), \quad (\text{C.22})$$

while hopping in the f language remains ordinary hopping the d language:

$$t_{rr'}^\uparrow f_{r\uparrow}^\dagger f_{r'\uparrow} \rightarrow t_{rr'} d_1^\dagger(r) d_1(r'), \quad (\text{C.23})$$

$$t_{rr'}^\downarrow f_{r\downarrow}^\dagger f_{r'\downarrow} \rightarrow -t_{rr'}^* d_2^\dagger(r) d_2(r'). \quad (\text{C.24})$$

Thus, under Eq. (C.21) our mean-field Hamiltonian, Eq. (C.1), is transformed into a *pure-hopping model* (with spin-orbit coupling), and obtaining the ground state $|\text{BCS}\rangle$ is as simple as diagonalizing the corresponding single-particle hopping Hamiltonian and filling up a Fermi sea of d fermions. Indeed, H_{MF} conserves the total number of d fermions, so filling up a Fermi sea is precisely the correct thing to do. On a lattice of L sites, the total number of d ’s composing the Fermi sea should be

$$N_{d,\text{tot}} = N_{d1} + N_{d2} = N_{f\uparrow} - N_{f\downarrow} + L = 2S_{\text{tot}}^z + L, \quad (\text{C.25})$$

for a fixed polarization $S_{\text{tot}}^z = (N_{f\uparrow} - N_{f\downarrow})/2$ in the f problem (H_{MF} conserves S_{tot}^z); this simply follows from (C.21) which implies $N_{f\uparrow} = N_{d1}$ and $N_{f\downarrow} = L - N_{d2}$. The d language thus very naturally accounts for finite polarization in the f problem.

Translating the projection to $N = N_{f,\text{tot}}$ total spinons, \mathcal{P}_N , as well as the subsequent Gutzwiller projection, \mathcal{P}_G , can also naturally be done within this framework. To address the former, we note that in terms of d particle numbers, the total number of f fermions is given by

$$N_{f,\text{tot}} = N_{f\uparrow} + N_{f\downarrow} = N_{d1} - N_{d2} + L = \Delta N_d + L. \quad (\text{C.26})$$

Therefore, fixing S_{tot}^z and $N_{f,\text{tot}}$ in Eqs. (C.25) and (C.26) gives unique quantum numbers $N_{d1} = N_{f\uparrow}$ and $N_{d2} = L - N_{f\downarrow}$. While we do not spell out all the details here, this can be straightforwardly accommodated for in first-quantization by fixing the number of particle positions corresponding to d_1 and d_2 fermions. Ultimately, we obtain a single Slater determinant of size $N_{d,\text{tot}} \times N_{d,\text{tot}}$ (for usual unpolarized states, $S_{\text{tot}}^z = 0$, this is simply $L \times L$) filled by orbitals obtained from diagonalizing the single-particle hopping problem for the d fermions (see above).

Gutzwiller projection is also straightforward to implement. For example, for the spin liquid wave functions considered in Chapter 3, we have $S_{\text{tot}}^z = 0$ and $N_{f,\text{tot}} = L$ and wish to project out all doubly-occupied sites in the f problem; this corresponds to projecting out all singly-occupied sites in the d problem:

$$\mathcal{P}_G : f_{r\uparrow}^\dagger f_{r\uparrow} + f_{r\downarrow}^\dagger f_{r\downarrow} = 1 \leftrightarrow d_1^\dagger(r) d_1(r) = d_2^\dagger(r) d_2(r). \quad (\text{C.27})$$

Thus, in the VMC we need only consider configurations with equivalent sets of positions for the d_1 and d_2 particles: $\{R_i^{(1)}\} = \{R_i^{(2)}\} = \{R_i\}$ for $i = 1, 2, \dots, L/2$. It is equally straight-

forward to project out doubly-occupied sites away from half filling, say to model a strongly correlated superconductor [138].

Conversely, one can run this dictionary the other way and project out all singly-occupied sites from the f problem, producing a wave function for hard-core bosons. An example where this would be useful is for representing wave functions associated with pairing instabilities of the d -wave Bose metal of Refs. [92, 84, 86]. There, we have two species of fermions, say f_{\uparrow} and f_{\downarrow} , on the square lattice with spin-dependent anisotropic Fermi seas rotated from each other by 90° . (Note that in Refs. [92, 84, 86] and in Chapter 4, we call the *original* fermionic partons d_1 and d_2 .) This anisotropy can be achieved, for example, by taking a nearest-neighbor hopping pattern with $t_x^{\uparrow} = t_y^{\downarrow}$ and $t_y^{\uparrow} = t_x^{\downarrow}$; we can parameterize the anisotropy by the dimensionless parameter $w \equiv t_x^{\uparrow}/t_y^{\uparrow} = t_y^{\downarrow}/t_x^{\downarrow}$. Without any pairing at the mean-field level, projecting out all singly-occupied sites, $\mathcal{P}_G : f_{r\uparrow}^{\dagger}f_{r\uparrow} = f_{r\downarrow}^{\dagger}f_{r\downarrow}$, gives precisely the d -wave Bose metal of Ref. [92]. One can then consider adding finite pairing, say of the s -wave form: $\Delta_{rr'} = \Delta_0\delta_{rr'}$. For strong enough pairing Δ_0 , all Bogoliubov quasiparticles will be gapped, which corresponds to an ordinary superconductor before projection, and a bosonic superfluid after projection. However, for weak to intermediate pairing and anisotropy w sufficiently different from unity, we have an interesting BdG solution which has ordinary paired, gapped fermions coexisting with interesting gapless Fermi pockets—essentially the state denoted “gapless superfluid” in Ref. [211]—which after projection we call superfluid* (SF*). The * represents the excess gapless excitations from the unpaired Fermi pockets. While a determinantal representation of these states can be formulated in analogy with the “boson-fermion mixed state” of Ref. [213], they can be computed in a more simple fashion using the framework outlined in this section, which

again results in an appropriately Gutzwiller projected single $L \times L$ determinant. In the end, however, we must leave a detailed numerical exploration of such wave functions for future work.

To conclude, a simple particle-hole transformation on the $f_{r\downarrow}$ operator [see Eq. (C.21)] allows us to find and represent by a single $(2S_{\text{tot}}^z + L) \times (2S_{\text{tot}}^z + L)$ determinant the ground state of Eq. (C.1) in a unified and robust way for basically any parameters, including for the interesting SF* state discussed above. For large-scale calculations, however, the BdG methods described in Sec. C.1 are preferable since in that representation the determinant is substantially smaller, e.g., for spin liquids the determinant is $L/2 \times L/2$ versus $L \times L$. For $N \times N$ determinants, the VMC algorithm scales asymptotically as $O(N^2)$ [139], so the efficiency difference can be noticeable. All results in Chapter 3 and Ref. [143] were obtained with the more conventional and numerically efficient approach of Sec. C.1.

Appendix D

Bosonization Analysis of a $c = 5$ Mode

d -wave Metal Phase on the Two-Leg Ladder

In Chapter 4, we presented extensive evidence for stability in a reasonable lattice model of a two-leg ladder descendant of an exotic two-dimensional conducting non-Fermi liquid metal, the d -wave metal. In our construction of the d -wave metal, we decompose the physical electron operator as a product of three slave fermions (“partons”):

$$c_s(\mathbf{r}) = d_1(\mathbf{r})d_2(\mathbf{r})f_s(\mathbf{r}), \quad (\text{D.1})$$

where we assign the spinon f_s to carry the spin $s = \uparrow, \downarrow$ of the electron. The d_1 and d_2 partons, on the other hand, compose the charge sector and are chosen to be in the so-called d -wave Bose metal phase of Refs. [92, 84, 86], where we take the d_1 (d_2) parton to hop preferentially in the \hat{x} (\hat{y}) direction. In order to model an actual electronic system, the decomposition (D.1) must

be supplemented with a constraint:

$$d_1^\dagger(\mathbf{r})d_1(\mathbf{r}) = d_2^\dagger(\mathbf{r})d_2(\mathbf{r}) = \sum_{s=\uparrow,\downarrow} f_s^\dagger(\mathbf{r})f_s(\mathbf{r}) = n_e(\mathbf{r}). \quad (\text{D.2})$$

Decompositions such as Eqs. (D.1)-(D.2) naturally, and necessarily, lead to gauge theory descriptions of the physical electronic system. In the specific case of the d -wave metal, we require *two* U(1) gauge fields, roughly corresponding to the first two equal signs in the constraint (D.2). On ladder systems such as that studied in Chapter 4, it is especially straightforward to include the U(1) gauge fluctuations which implement Eq. (D.2) on long wavelengths. Specifically, we know gauge fluctuations will render two orthonormal linear combinations of the original bosonized massless modes massive (see below and Refs. [84, 58, 86, 82]). The resulting phase is a highly unconventional Luttinger liquid with $c = c_{d1} + c_{d2} + c_f - 2$ gapless modes. In the d -wave metal phase presented in Chapter 4 at electron density $\rho = 1/3$ (see Fig. 4.2), the d_1 system partially fills two 1D bands so that $c_{d1} = 2$, while the d_2 system only fills one band so that $c_{d2} = 1$; the spinon f forms a simple one-band spinful metal with $c_f = 2$. All in all, we expect $c = 2 + 1 + 2 - 2 = 3$, a highly nontrivial prediction which was indeed compellingly realized in the DMRG data of Fig. 4.7.

However, the $\rho = 1/3$ system considered in Chapter 4 is rather dilute, and a qualitatively new two-leg d -wave metal phase can be envisioned for densities $\rho > 1/2$. In this putative phase which we depict in Fig. D.1, the d_2 partons will completely fill the bonding band, and, assuming spatially isotropic spinon hopping, the f 's will form a *two-band* spinful metal with $c_f = 4$ (basically the C2S2 phase discussed in Chapter 2 and Appendix B, but here on the two-leg *square* ladder [108]). With the inclusion of gauge fluctuations, this phase is an unconventional Luttinger liquid now with $c = 2 + 1 + 4 - 2 = 5$ gapless modes, and thus represents a significant

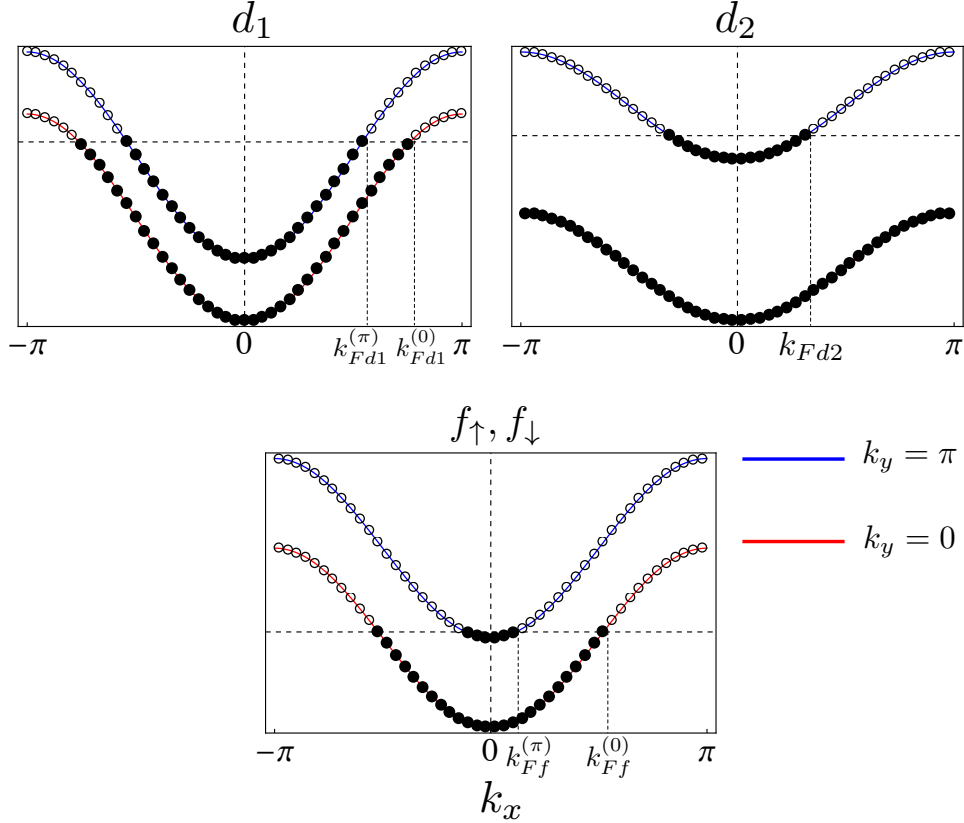


Figure D.1: Picture of the parton bands for the putative $c = 5$ mode d -wave metal phase on the two-leg ladder. In the d -wave metal state at densities $\rho > 1/2$ at the focus of this appendix, the d_1 system has partially filled bonding and antibonding bands, the d_2 system has a fully filled bonding band and a partially filled antibonding band, while the f_s system has partially filled (spinful) bonding and antibonding bands. The parton Fermi wavevectors must satisfy the sum rule $k_{Fd1}^{(0)} + k_{Fd1}^{(\pi)} = \pi + k_{Fd2} = 2(k_{Ff}^{(0)} + k_{Ff}^{(\pi)}) = 2\pi\rho$. By simple mode-counting arguments, after (before) inclusion of gauge fluctuations, this state has $c = 5$ ($c = 7$) 1D gapless modes.

step toward realization of the 2D d -wave metal with fewer one-dimensional pathologies. Initial DMRG results indicate that this $c = 5$ d -wave metal phase is likely unstable to the opening of a spin gap in the t - J - K ring model studied in Chapter 4, but this study is still ongoing. In this appendix, we present a bosonization analysis of the $c = 5$ state of Fig. D.1 and show that it can actually be a stable quantum phase, at least in principle. However, making specific predictions about a given microscopic model at strong coupling (e.g., our t - J - K model) within such a framework is exceedingly difficult, and thus we do not pursue that here.

D.1 Long-Wavelength Bosonized Description

We describe the low-energy physics of the phase depicted in Fig. D.1 in the usual way [4, 82] by introducing a pair of bosonic fields (θ_b, φ_b) for each of the seven partially filled 1D bands in the state: $b \in \{d_1^{(0)}, d_1^{(\pi)}, d_2, f_\uparrow^{(0)}, f_\downarrow^{(0)}, f_\uparrow^{(\pi)}, f_\downarrow^{(\pi)}\}$. At the mean-field level, we start by writing down a Lagrangian for seven independent 1D gapless modes:

$$\mathcal{L}_0 = \sum_{k_y=0,\pi} \frac{1}{2\pi g_{d1}^{(k_y)}} \left[\frac{1}{v_{d1}^{(k_y)}} (\partial_\tau \theta_{d1}^{(k_y)})^2 + v_{d1}^{(k_y)} (\partial_x \theta_{d1}^{(k_y)})^2 \right] \quad (\text{D.3})$$

$$+ \frac{1}{2\pi g_{d2}} \left[\frac{1}{v_{d2}} (\partial_\tau \theta_{d2})^2 + v_{d2} (\partial_x \theta_{d2})^2 \right] \quad (\text{D.4})$$

$$+ \sum_{k_y=0,\pi} \frac{1}{2\pi g_{f\rho}^{(k_y)}} \left[\frac{1}{v_{f\rho}^{(k_y)}} (\partial_\tau \theta_{f\rho}^{(k_y)})^2 + v_{f\rho}^{(k_y)} (\partial_x \theta_{f\rho}^{(k_y)})^2 \right] \quad (\text{D.5})$$

$$+ \sum_{k_y=0,\pi} \frac{1}{2\pi g_{f\sigma}^{(k_y)}} \left[\frac{1}{v_{f\sigma}^{(k_y)}} (\partial_\tau \theta_{f\sigma}^{(k_y)})^2 + v_{f\sigma}^{(k_y)} (\partial_x \theta_{f\sigma}^{(k_y)})^2 \right]. \quad (\text{D.6})$$

In the above, we have allowed some generality by encoding intraband forward scattering interactions into the Luttinger parameters g_b ; this is of course, however, not an exhaustive parameterization of all allowed density-density interactions in this system. We have also separated the spinon sector into charge (D.5) and spin (D.6) modes for each band:

$$\theta_{f\rho/\sigma}^{(k_y)} = \frac{1}{\sqrt{2}} (\theta_{f\uparrow}^{(k_y)} \pm \theta_{f\downarrow}^{(k_y)}), \quad (\text{D.7})$$

where SU(2) invariance dictates only trivial Luttinger parameters for the spin modes (see Appendix B.3.3): $g_{f\sigma}^{(0)} = g_{f\sigma}^{(\pi)} = 1$. Below it will be convenient to introduce “overall” and “relative” combinations with respect to the two bands:

$$\theta_{f\mu\pm} = \frac{1}{\sqrt{2}} (\theta_{f\mu}^{(0)} \pm \theta_{f\mu}^{(\pi)}), \quad (\text{D.8})$$

where $\mu = \rho, \sigma$. Finally, we have integrated out the φ_b fields from the full Lagrangian, which is convenient to do at this point for purposes of treating the full gauge theory in what follows.

Equations (D.3)-(D.6) describe some $c = 7$ mode Luttinger liquid with five nontrivial Luttinger parameters. We now wish to include gauge fluctuations so that our theory actually represents an *electronic* system on long wavelengths. To this end, we note that the slowly varying components of the parton densities (relative to the average densities) are given simply by $\rho_b = \partial_x \theta_b / \pi$. In this language, the *long-wavelength version* of the on-site constraint given in Eq. (D.2) reads

$$\rho_{d1}^{(0)} + \rho_{d1}^{(\pi)} = \rho_{d2} = \rho_{f\uparrow}^{(0)} + \rho_{f\downarrow}^{(0)} + \rho_{f\uparrow}^{(\pi)} + \rho_{f\downarrow}^{(\pi)}, \quad (\text{D.9})$$

so that, up to fixed constant shifts, the θ_b fields themselves must satisfy

$$\theta_{d1}^{(0)} + \theta_{d1}^{(\pi)} = \theta_{d2} = \theta_{f\uparrow}^{(0)} + \theta_{f\downarrow}^{(0)} + \theta_{f\uparrow}^{(\pi)} + \theta_{f\downarrow}^{(\pi)}. \quad (\text{D.10})$$

Our experience with such U(1) gauge theories in quasi-1D [84, 58, 86] teaches us that (1) we can always work in a gauge which eliminates all spatial components of the gauge fields and that (2) integrating out the (massive) temporal components leads to mass terms for certain linear combinations of the original fields, which upon pinning give precisely to the long-wavelength form of the “gauge constraint” [here Eq. (D.10)]. Therefore, in quasi-1D it is straightforward to implement gauge fluctuations in a very algebraic manner without ever explicitly writing out the full gauge theory. We take this approach in what follows.

Specifically, for the present case, we define the following orthonormal transformation of the original seven fields θ_b :

$$\theta_{f\sigma}^{(0)} = \frac{1}{\sqrt{2}} \left(\theta_{f\uparrow}^{(0)} - \theta_{f\downarrow}^{(0)} \right), \quad (\text{D.11})$$

$$\theta_{f\sigma}^{(\pi)} = \frac{1}{\sqrt{2}} \left(\theta_{f\uparrow}^{(\pi)} - \theta_{f\downarrow}^{(\pi)} \right), \quad (\text{D.12})$$

$$\theta_{f\rho-} = \frac{1}{\sqrt{2}} \left(\theta_{f\rho}^{(0)} - \theta_{f\rho}^{(\pi)} \right) = \frac{1}{2} \left(\theta_{f\uparrow}^{(0)} + \theta_{f\downarrow}^{(0)} - \theta_{f\uparrow}^{(\pi)} - \theta_{f\downarrow}^{(\pi)} \right), \quad (\text{D.13})$$

$$\theta_{d1-} = \frac{1}{\sqrt{2}} \left(\theta_{d1}^{(0)} - \theta_{d1}^{(\pi)} \right), \quad (\text{D.14})$$

$$\theta_{\rho\text{tot}} = \frac{1}{\sqrt{7}} \left[\frac{1}{2} \left(\theta_{f\uparrow}^{(0)} + \theta_{f\downarrow}^{(0)} + \theta_{f\uparrow}^{(\pi)} + \theta_{f\downarrow}^{(\pi)} \right) + \left(\theta_{d1}^{(0)} + \theta_{d1}^{(\pi)} + 2\theta_{d2} \right) \right], \quad (\text{D.15})$$

$$\theta_a = \frac{1}{\sqrt{3}} \left(\theta_{d1}^{(0)} + \theta_{d1}^{(\pi)} - \theta_{d2} \right), \quad (\text{D.16})$$

$$\theta_A = \sqrt{\frac{3}{14}} \left[\left(\theta_{f\uparrow}^{(0)} + \theta_{f\downarrow}^{(0)} + \theta_{f\uparrow}^{(\pi)} + \theta_{f\downarrow}^{(\pi)} \right) - \frac{1}{3} \left(\theta_{d1}^{(0)} + \theta_{d1}^{(\pi)} + 2\theta_{d2} \right) \right], \quad (\text{D.17})$$

with the same transformation applied the fields φ_b . By the above considerations, gauge fluctuations will render the fields θ_a and θ_A massive, so that we have $\theta_a, \theta_A \rightarrow \tilde{\theta}_a, \tilde{\theta}_A = \text{const.}$ up to gapped fluctuations. Indeed, pinning of θ_a corresponds to $\rho_{d1} = \rho_{d2}$ in Eq. (D.9), while pinning of θ_A corresponds to $\sum_{s=\uparrow,\downarrow} \rho_{fs} = \rho_{d2}$ ($= \rho_{d1}$), where $\rho_{d1} = \rho_{d1}^{(0)} + \rho_{d1}^{(\pi)}$ and $\rho_{fs} = \rho_{fs}^{(0)} + \rho_{fs}^{(\pi)}$. That is, roughly speaking the former corresponds to gluing together d_1 and d_2 to form the char-
gon $b = d_1 d_2$ (see Sec. 4.2), while the latter corresponds to gluing together b and f_s to form the electron $c_s = b f_s = d_1 d_2 f_s$.

In practice, pinning of θ_a and θ_A effectively sets them to zero in the quadratic part of the theory. The final fixed-point theory is then a $c = 5$ mode Luttinger liquid described by

$$\mathcal{L} = \mathcal{L}^\sigma + \mathcal{L}^\rho, \quad (\text{D.18})$$

where the spin sector theory reads [cf. Eq. (B.17) and the surrounding discussion]

$$\mathcal{L}^\sigma = \frac{1}{2\pi} \sum_{k_y=0,\pi} \left[\frac{1}{v_{f\sigma}^{(k_y)}} \left(\partial_\tau \theta_{f\sigma}^{(k_y)} \right)^2 + v_{f\sigma}^{(k_y)} \left(\partial_x \theta_{f\sigma}^{(k_y)} \right)^2 \right], \quad (\text{D.19})$$

while the charge sector theory reads

$$\mathcal{L}^\rho = \frac{1}{2\pi} \left[\partial_x \Theta^T \cdot \mathbf{A} \cdot \partial_x \Theta + \partial_\tau \Theta^T \cdot \mathbf{B} \cdot \partial_\tau \Theta \right], \quad (\text{D.20})$$

with $\Theta^T \equiv (\theta_{f\rho-}, \theta_{d1-}, \theta_{\rho\text{tot}})$; \mathbf{A} and \mathbf{B} can be general symmetric, positive-definite 3x3 matrices, which with the somewhat general (but not exhaustive) density-density interactions present

in Eqs. (D.3)-(D.5) have elements

$$A_{11} = \frac{1}{2} \left(\frac{v_{f\rho}^{(0)}}{g_{f\rho}^{(0)}} + \frac{v_{f\rho}^{(\pi)}}{g_{f\rho}^{(\pi)}} \right), \quad (\text{D.21})$$

$$A_{12} = A_{21} = 0, \quad (\text{D.22})$$

$$A_{13} = A_{31} = \frac{1}{2\sqrt{7}} \left(\frac{v_{f\rho}^{(0)}}{g_{f\rho}^{(0)}} - \frac{v_{f\rho}^{(\pi)}}{g_{f\rho}^{(\pi)}} \right), \quad (\text{D.23})$$

$$A_{22} = \frac{1}{2} \left(\frac{v_{d1}^{(0)}}{g_{d1}^{(0)}} + \frac{v_{d1}^{(\pi)}}{g_{d1}^{(\pi)}} \right), \quad (\text{D.24})$$

$$A_{23} = A_{32} = \frac{1}{\sqrt{14}} \left(\frac{v_{d1}^{(0)}}{g_{d1}^{(0)}} - \frac{v_{d1}^{(\pi)}}{g_{d1}^{(\pi)}} \right), \quad (\text{D.25})$$

$$A_{33} = \frac{1}{14} \left(2 \frac{v_{d1}^{(0)}}{g_{d1}^{(0)}} + 2 \frac{v_{d1}^{(\pi)}}{g_{d1}^{(\pi)}} + 8 \frac{v_{d2}}{g_{d2}} + \frac{v_{f\rho}^{(0)}}{g_{f\rho}^{(0)}} + \frac{v_{f\rho}^{(\pi)}}{g_{f\rho}^{(\pi)}} \right), \quad (\text{D.26})$$

and

$$B_{11} = \frac{1}{2} \left(\frac{1}{g_{f\rho}^{(0)} v_{f\rho}^{(0)}} + \frac{1}{g_{f\rho}^{(\pi)} v_{f\rho}^{(\pi)}} \right), \quad (\text{D.27})$$

$$B_{12} = B_{21} = 0, \quad (\text{D.28})$$

$$B_{13} = B_{31} = \frac{1}{2\sqrt{7}} \left(\frac{1}{g_{f\rho}^{(0)} v_{f\rho}^{(0)}} - \frac{1}{g_{f\rho}^{(\pi)} v_{f\rho}^{(\pi)}} \right), \quad (\text{D.29})$$

$$B_{22} = \frac{1}{2} \left(\frac{1}{g_{d1}^{(0)} v_{d1}^{(0)}} + \frac{1}{g_{d1}^{(\pi)} v_{d1}^{(\pi)}} \right), \quad (\text{D.30})$$

$$B_{23} = B_{32} = \frac{1}{\sqrt{14}} \left(\frac{1}{g_{d1}^{(0)} v_{d1}^{(0)}} - \frac{1}{g_{d1}^{(\pi)} v_{d1}^{(\pi)}} \right), \quad (\text{D.31})$$

$$B_{33} = \frac{1}{14} \left(\frac{2}{g_{d1}^{(0)} v_{d1}^{(0)}} + \frac{2}{g_{d1}^{(\pi)} v_{d1}^{(\pi)}} + \frac{8}{g_{d2} v_{d2}} + \frac{1}{g_{f\rho}^{(0)} v_{f\rho}^{(0)}} + \frac{1}{g_{f\rho}^{(\pi)} v_{f\rho}^{(\pi)}} \right), \quad (\text{D.32})$$

respectively. Again, the above is not a complete parameterization of all density-density interactions allowed in the harmonic fixed-point theory, but for general positive g_b and v_b it certainly lies *within* the most general theory, and thus serves as a useful starting point for assessing the potential stability of this highly unconventional $c = 5$ mode Luttinger liquid.

D.2 Stability Analysis in the Presence of all Allowed Short-Range Interactions

In addition to the parton density-density interactions which are strictly marginal and only contribute to the bosonized action at quadratic order (e.g., intraband forward scattering resulting in the general g_b and v_b above), there are several additional four-fermion interactions allowed by the symmetries of the system—lattice symmetries, time-reversal invariance, and SU(2) spin-rotation invariance—which produce cosines of the bosonized fields and thus interact beyond quadratic order. In this section, we show that all such nonharmonic interactions are at least potentially irrelevant (in the renormalization group sense) in generic parameter regimes, and so the above $c = 5$ mode d -wave metal theory represents a stable phase as a matter of principle.

In the chargon sector, as in the $c = 3$ mode state of Chapter 4 and Ref. [82], we have only the following four- d_1 term:

$$\mathcal{H}_{RL,w}^{d1} = w^{d1} \left[d_{1R}^{(0)\dagger} d_{1L}^{(0)\dagger} d_{1L}^{(\pi)} d_{1R}^{(\pi)} + \text{H.c.} \right] = 2w^{d1} \cos\left(2\sqrt{2}\varphi_{d1-}\right). \quad (\text{D.33})$$

This interaction has scaling dimension $\Delta[\mathcal{H}_{RL,w}^{d1}] = \Delta[\cos(2\sqrt{2}\varphi_{d1-})]$ which we analyze below with respect to the fixed-point theory \mathcal{L}^ρ described above [see Eq. (D.20)].

We can delineate all allowed four-fermion terms in the two-band spinon sector using “chiral currents” (see Refs. [108, 104, 151] and also Appendix B). That is, if we define

$$\mathbf{J}_{Pab} = \frac{1}{2} f_{Paa}^\dagger \boldsymbol{\sigma}_{\alpha\beta} f_{Pb\beta}, \quad J_{Pab} = f_{Paa}^\dagger f_{Pb\alpha}, \quad (\text{D.34})$$

where summation over the spin indices $\alpha, \beta = \uparrow, \downarrow$ is implied and the band indices $a, b = 1, 2$ correspond to transverse momenta $k_y = 0 \leftrightarrow 1, \pi \leftrightarrow 2$, then the (nonchiral) four- f interactions

are given by

$$\mathcal{H}_{RL}^{f\rho} = \sum_{a,b} \left(w_{ab}^{f\rho} J_{Rab} J_{Lab} + \lambda_{ab}^{f\rho} J_{Raa} J_{Lbb} \right), \quad (\text{D.35})$$

$$\mathcal{H}_{RL}^{f\sigma} = - \sum_{a,b} \left(w_{ab}^{f\sigma} \mathbf{J}_{Rab} \cdot \mathbf{J}_{Lab} + \lambda_{ab}^{f\sigma} \mathbf{J}_{Raa} \cdot \mathbf{J}_{Lbb} \right). \quad (\text{D.36})$$

We take $w_{11}^{f\rho/\sigma} = w_{22}^{f\rho/\sigma} = 0$ (redundancy with $\lambda_{11}^{f\rho/\sigma}$, $\lambda_{22}^{f\rho/\sigma}$), $w_{12}^{f\rho/\sigma} = w_{21}^{f\rho/\sigma}$ (from Hermiticity), and $\lambda_{12}^{f\rho/\sigma} = \lambda_{21}^{f\rho/\sigma}$ (from $R \leftrightarrow L$ symmetry), leaving eight independent couplings: $w_{12}^{f\rho/\sigma}$, $\lambda_{11}^{f\rho/\sigma}$, $\lambda_{22}^{f\rho/\sigma}$, $\lambda_{12}^{f\rho/\sigma}$.

The intraband forward scattering density-density interactions $\lambda_{11}^{f\rho}$ and $\lambda_{22}^{f\rho}$ are accounted for in the general velocities $v_{f\rho}^{(k_y)}$ and Luttinger parameters $g_{f\rho}^{(k_y)}$ above. For simplicity, we ignore the corresponding interband term $\lambda_{12}^{f\rho}$. (Similar considerations apply to the d_1 sector when spelling out all density-density interactions.)

Next, we consider the spin-charge coupling terms $w_{12}^{f\rho/\sigma}$, which when summed and bosonized result in the following expression (see Refs. [58, 151]):

$$\begin{aligned} \mathcal{H}_{RL,w}^{f\sigma} &= \left(w_{12}^{f\rho} J_{R12} J_{L12} - w_{12}^{f\sigma} \mathbf{J}_{R12} \cdot \mathbf{J}_{L12} \right) + \text{H.c.} \\ &= \cos(2\varphi_{f\rho-}) \left\{ 4w_{12}^{f\rho} \left[\cos(2\varphi_{f\sigma-}) - \hat{\Gamma} \cos(2\theta_{f\sigma-}) \right] \right. \\ &\quad \left. - w_{12}^{f\sigma} \left[\cos(2\varphi_{f\sigma-}) + \hat{\Gamma} \cos(2\theta_{f\sigma-}) + 2\hat{\Gamma} \cos(2\theta_{f\sigma+}) \right] \right\}, \end{aligned} \quad (\text{D.37})$$

where $\hat{\Gamma}$ is a product of Klein factors not important to the present discussion. In the fixed-point theory, this interaction has scaling dimension $\Delta[\mathcal{H}_{RL,w}^{f\sigma}] = \Delta[\cos(2\varphi_{f\rho-})] + 1$, where the 1 comes from the spin sector \mathcal{L}^σ and its trivial Luttinger parameters [see Eq. (D.19)]. Below, as with $\Delta[\mathcal{H}_{RL,w}^{d1}]$, we compute $\Delta[\mathcal{H}_{RL,w}^{f\sigma}]$ with respect to the fixed-point theory \mathcal{L}^ρ .

Finally, bosonizing the backscattering terms $\lambda_{11}^{f\sigma}$, $\lambda_{22}^{f\sigma}$, and $\lambda_{12}^{f\sigma}$,

$$\mathcal{H}_{RL,\lambda}^{f\sigma} = - \sum_a \lambda_{aa}^{f\sigma} \mathbf{J}_{Raa} \cdot \mathbf{J}_{Laa} - \lambda_{12}^{f\sigma} (\mathbf{J}_{R11} \cdot \mathbf{J}_{L22} + \mathbf{J}_{L11} \cdot \mathbf{J}_{R22}) = V_z + V_\perp, \quad (\text{D.38})$$

results in expressions for V_z and V_\perp given in Eqs. (B.82)-(B.85). Due to SU(2) symmetry, all these interactions have scaling dimension equal to two in the fixed-point theory [see Eq. (D.19)] and are thus marginal. If the term $\mathcal{H}_{RL,w}^{f\sigma}$ above is strictly irrelevant, then the terms in $\mathcal{H}_{RL,\lambda}^{f\sigma}$ are marginally irrelevant if $\lambda_{11}^{f\sigma}$, $\lambda_{22}^{f\sigma}$, and $\lambda_{12}^{f\sigma}$ are initially positive [58]. The system could in principle be tuned such that the latter condition is met, and we show below that the former condition arises naturally in the full gauge theory.

There are no other generally allowed four-fermion interactions which could destabilize the $c = 5$ mode state described above and depicted in Fig. D.1. In particular, there are no allowed nonharmonic terms which mix the d_1 , d_2 , and/or f sectors. As such, the above interactions do not contain the fields θ_a or θ_A pinned by gauge fluctuations; this is promising for the potential stability of the phase. Furthermore, the interactions $\mathcal{H}_{RL,w}^{d1}$ and $\mathcal{H}_{RL,w}^{f\sigma}$ contain only φ_b fields; we thus expect that the process of pinning θ_a and θ_A will only render $\mathcal{H}_{RL,w}^{d1}$ and $\mathcal{H}_{RL,w}^{f\sigma}$ less relevant with respect to the mean field (fully fluctuating θ_a and θ_A combinations). In what follows, we will explicitly show that this is indeed the case starting from a completely noninteracting mean-field state.

To this end, we set all original Luttinger parameters to their trivial values, $g_b = 1$, effectively turning off all forward scattering interactions. With respect to this mean field, $\mathcal{H}_{RL,w}^{d1}$ and $\mathcal{H}_{RL,w}^{f\sigma}$, being four-fermion interactions are of course marginal: $\Delta[\mathcal{H}_{RL,w}^{d1}] = \Delta[\mathcal{H}_{RL,w}^{f\sigma}] = 2$. We now turn on gauge fluctuations by pinning θ_a and θ_A and compute the scaling dimensions $\Delta[\mathcal{H}_{RL,w}^{d1}]$ and $\Delta[\mathcal{H}_{RL,w}^{f\sigma}]$ by computing $\Delta[\cos(2\sqrt{2}\varphi_{d1-})]$ and $\Delta[\cos(2\varphi_{f\rho-})] + 1$, respectively,

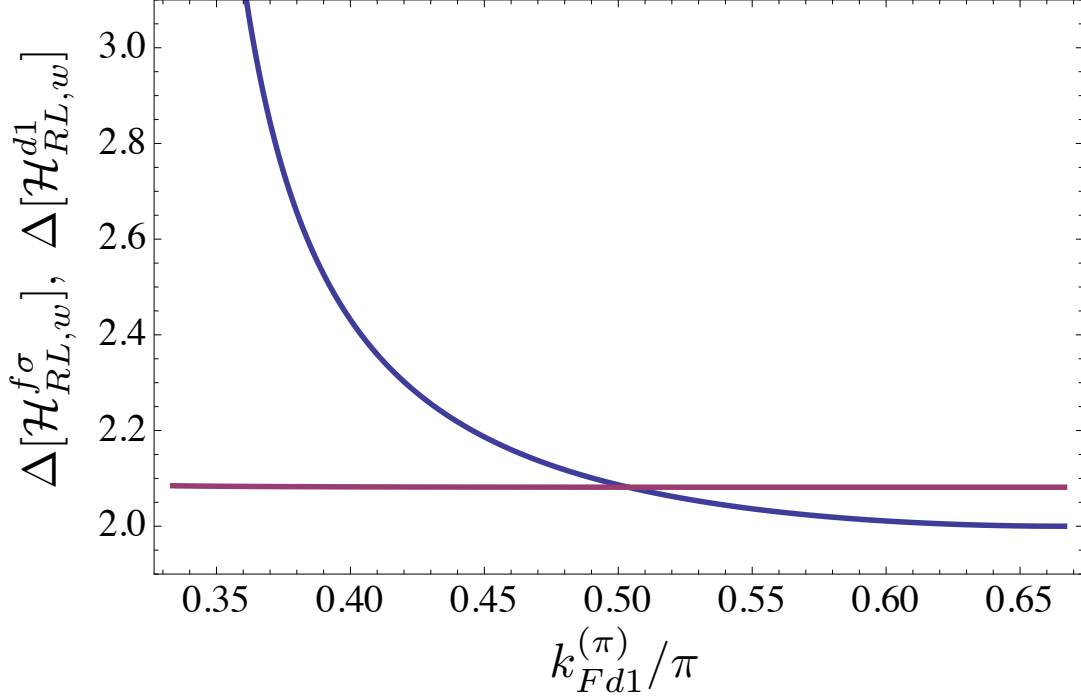


Figure D.2: Scaling dimensions of the interactions $\mathcal{H}_{RL,w}^{d1}$ [Eq. (D.33)] and $\mathcal{H}_{RL,w}^{f\sigma}$ [Eq. (D.37)] versus $k_{Fd1}^{(\pi)}$. Here, we assume free-fermion cosine dispersions at density $\rho = 2/3$ as in Fig. D.1. The nearly flat red curve is $\Delta[\mathcal{H}_{RL,w}^{f\sigma}]$, while the blue curve is $\Delta[\mathcal{H}_{RL,w}^{d1}]$. We see that both scaling dimensions are greater than two and so the interactions are irrelevant, except at $k_{Fd1}^{(\pi)} \rightarrow \pi\rho = 2\pi/3$ where $\mathcal{H}_{RL,w}^{d1}$ is marginal.

in the fixed-point theory \mathcal{L}^ρ . The calculations are performed numerically, as we have to diagonalize the three-mode system Eq. (D.20) with coefficients given by Eqs. (D.21)-(D.32). The calculations are straightforward following the standard procedure (see, e.g., Ref. [151]). We find that for $g_b = 1$ and general positive velocities v_b , $\Delta[\mathcal{H}_{RL,w}^{d1}], \Delta[\mathcal{H}_{RL,w}^{f\sigma}] \geq 2$, so that $\mathcal{H}_{RL,w}^{d1}$ and $\mathcal{H}_{RL,w}^{f\sigma}$ are generally irrelevant and are at worst marginal. Therefore, as expected, gauge fluctuations only make these interactions, which contain only φ_b fields, less relevant.

To constrain the parameter space and get a feel for trends, we now focus on electron density $\rho = 2/3 > 1/2$ as shown in Fig. D.1 and assume that all dispersions are simple cosines with equal bandwidths. Then, with all $g_b = 1$ the velocities v_b are simply the slopes of these cosine

curves at the Fermi points. With this parameterization, in Fig. D.2 we plot $\Delta[\mathcal{H}_{RL,w}^{d1}]$ and $\Delta[\mathcal{H}_{RL,w}^{f\sigma}]$ versus all allowed values of $k_{Fd1}^{(\pi)}$: $k_{Fd1}^{(\pi)} = 2\pi\rho - \pi = \pi/3$ corresponds to equivalent d_1 and d_2 configurations, while $k_{Fd1}^{(\pi)} = \pi\rho = 2\pi/3$ corresponds to equivalent bonding and antibonding d_1 bands. We fix the spinon velocities $v_{f\rho}^{(0)}$ and $v_{f\rho}^{(\pi)}$ such that they correspond to filling two spinful bands at this density with isotropic hopping patterns. We see from Fig. D.2 that $\mathcal{H}_{RL,w}^{d1}$ is marginal in the limit $k_{Fd1}^{(\pi)} \rightarrow k_{Fd1}^{(0)} = \pi\rho$ but is strictly irrelevant for all other values of $k_{Fd1}^{(\pi)}$. Also, $\Delta[\mathcal{H}_{RL,w}^{f\sigma}]$ is a very weak function of $k_{Fd1}^{(\pi)}$, which is natural since in the above fixed-point theory the “ $f\rho-$ ” and “ $d1-$ ” sectors are not directly coupled but only talk to each other through the “ ρ tot” sector [see Eqs. (D.20)-(D.32)]. On the other hand (data not shown), $\Delta[\mathcal{H}_{RL,w}^{f\sigma}]$ depends on $k_{Ff}^{(\pi)}$ in a very similar fashion to how $\Delta[\mathcal{H}_{RL,w}^{d1}]$ depends on $k_{Fd1}^{(\pi)}$ in Fig. D.2 and is at worst marginal in the limit $k_{Ff}^{(\pi)} \rightarrow k_{Ff}^{(0)} = \pi\rho/2$. Also, $\Delta[\mathcal{H}_{RL,w}^{d1}]$ is, as expected, only a very weak function of the spinon configuration as parameterized by $k_{Ff}^{(\pi)}$.

D.3 Conclusion

Ultimately, this analysis shows that the $c = 5$ mode two-leg d -wave metal state described above is in principle a stable quantum phase, i.e., the action of introducing gauge fluctuations by itself does not naturally render the state unstable. However, initial DMRG attempts have been unsuccessful in stabilizing this state against the opening of a spin gap in the microscopic t - J - K ring model considered in Chapter 4 and Ref. [82]. It seems unlikely that we can understand this instability from the perspective of the simple scaling dimension analysis presented in this appendix which basically ignores the spin sector interactions of Eq. (D.38) entirely. A more complete RG analysis is thus desirable, perhaps along the lines of the approach of

Ref. [151]. This would still almost undoubtedly be a rather crude analysis, however, since the t - J - K model is inherently at strong coupling from the start. We leave such endeavors for future work.

Bibliography

- [1] N. W. Ashcroft and N. D. Mermin, *Solid State Physics* (Thomson, United States, 1976).
- [2] L. D. Landau, “The theory of a Fermi liquid,” Sov. Phys. JETP **3**, 920 (1957).
- [3] G. Baym and C. Pethick, *Landau Fermi-Liquid Theory: Concepts and Applications* (Wiley-VCH, Germany, 1991).
- [4] T. Giamarchi, *Quantum Physics in One Dimension* (Oxford University Press, New York, 2003).
- [5] G. R. Stewart, “Non-Fermi-liquid behavior in d - and f -electron metals,” Rev. Mod. Phys. **73**, 797 (Oct 2001).
- [6] F. S. Philipp Gegenwart, Qimiao Si, “Quantum criticality in heavy-fermion metals,” Nature Phys. **4**, 186 (2008).
- [7] J. M. Luttinger, “Fermi Surface and Some Simple Equilibrium Properties of a System of Interacting Fermions,” Phys. Rev. **119**, 1153 (Aug 1960).
- [8] N. F. Mott and R. Peierls, “Discussion of the paper by de Boer and Verwey,” Proceedings of the Physical Society **49**(4S), 72 (1937).

- [9] J. H. de Boer and E. J. W. Verwey, “Semi-conductors with partially and with completely filled 3 d -lattice bands,” Proceedings of the Physical Society **49**(4S), 59 (1937).
- [10] N. F. Mott, *Metal-Insulator Transitions* (Taylor & Francis Inc., USA, 1990).
- [11] M. Imada, A. Fujimori, and Y. Tokura, “Metal-insulator transitions,” Rev. Mod. Phys. **70**(4), 1039 (Oct 1998).
- [12] A. H. MacDonald, S. M. Girvin, and D. Yoshioka, “ $\frac{t}{U}$ expansion for the Hubbard model,” Phys. Rev. B **37**(16), 9753 (Jun 1988).
- [13] K. Terakura, T. Oguchi, A. R. Williams, and J. Kübler, “Band theory of insulating transition-metal monoxides: Band-structure calculations,” Phys. Rev. B **30**, 4734 (Oct 1984).
- [14] R. B. Laughlin, “Hartree-Fock computation of the high- T_c cuprate phase diagram,” Phys. Rev. B **89**, 035134 (Jan 2014).
- [15] M. B. Hastings, “Lieb-Schultz-Mattis in higher dimensions,” Phys. Rev. B **69**, 104431 (Mar 2004).
- [16] E. Lieb, T. Schultz, and D. Mattis, “Two soluble models of an antiferromagnetic chain,” Annals of Physics **16**(3), 407 (1961).
- [17] L. Balents, “Spin liquids in frustrated magnets,” Nature **464**, 199 (2010).
- [18] P. Anderson, “Resonating valence bonds: A new kind of insulator?” Materials Research Bulletin **8**(2), 153 (1973).

- [19] X.-G. Wen, “Quantum orders and symmetric spin liquids,” Phys. Rev. B **65**(16), 165113 (Apr 2002).
- [20] X. Wen, *Quantum Field Theory of Many-Body Systems: From the Origin of Sound to an Origin of Light and Electrons*, Oxford Graduate Texts (OUP Oxford, 2004).
- [21] H.-C. Jiang, Z. Wang, and L. Balents, “Identifying topological order by entanglement entropy,” Nature Physics **8**, 902 (Dec. 2012).
- [22] Y. Zhang, T. Grover, and A. Vishwanath, “Entanglement Entropy of Critical Spin Liquids,” Phys. Rev. Lett. **107**(6), 067202 (Aug 2011).
- [23] P. W. Anderson, “The Resonating Valence Bond State in La₂CuO₄ and Superconductivity,” Science **235**(4793), 1196 (1987).
- [24] Y. Shimizu, K. Miyagawa, K. Kanoda, M. Maesato, and G. Saito, “Spin Liquid State in an Organic Mott Insulator with a Triangular Lattice,” Phys. Rev. Lett. **91**(10), 107001 (Sep 2003).
- [25] Y. Kurosaki, Y. Shimizu, K. Miyagawa, K. Kanoda, and G. Saito, “Mott Transition from a Spin Liquid to a Fermi Liquid in the Spin-Frustrated Organic Conductor $\kappa - (ET)_2Cu_2(CN)_3$,” Phys. Rev. Lett. **95**(17), 177001 (Oct 2005).
- [26] T. Itou, A. Oyamada, S. Maegawa, M. Tamura, and R. Kato, “¹³C NMR study of the spin-liquid state in the triangular quantum antiferromagnet EtMe₃Sb[Pd(dmit)₂]₂,” Journal of Physics: Conference Series **145**, 012039 (2009).

- [27] T. Itou, A. Oyamada, S. Maegawa, M. Tamura, and R. Kato, “Quantum spin liquid in the spin- 1/2 triangular antiferromagnet $EtMe_3Sb[Pd(dmit)_2]_2$,” Phys. Rev. B **77**(10), 104413 (Mar 2008).
- [28] Y. Shimizu, H. Akimoto, H. Tsujii, A. Tajima, and R. Kato, “Reentrant Mott transition from a Fermi liquid to a spin-gapped insulator in an organic spin-1/2 triangular-lattice antiferromagnet,” Journal of Physics: Condensed Matter **19**, 145240 (2007).
- [29] J. S. Helton, K. Matan, M. P. Shores, E. A. Nytko, B. M. Bartlett, Y. Yoshida, Y. Takano, A. Suslov, Y. Qiu, J.-H. Chung, D. G. Nocera, and Y. S. Lee, “Spin Dynamics of the Spin-1/2 Kagome Lattice Antiferromagnet $ZnCu_3(OH)_6Cl_2$,” Phys. Rev. Lett. **98**, 107204 (Mar 2007).
- [30] J. S. Helton, K. Matan, M. P. Shores, E. A. Nytko, B. M. Bartlett, Y. Qiu, D. G. Nocera, and Y. S. Lee, “Dynamic Scaling in the Susceptibility of the Spin-1/2 Kagome Lattice Antiferromagnet Herbertsmithite,” Phys. Rev. Lett. **104**, 147201 (Apr 2010).
- [31] T.-H. Han, J. S. Helton, S. Chu, D. G. Nocera, J. A. Rodriguez-Rivera, C. Broholm, and Y. S. Lee, “Fractionalized excitations in the spin-liquid state of a kagome-lattice antiferromagnet,” Nature **492**, 406 (Dec. 2012).
- [32] Y. Okamoto, M. Nohara, H. Aruga-Katori, and H. Takagi, “Spin-Liquid State in the S=1/2 Hyperkagome Antiferromagnet $Na_4Ir_3O_8$,” Phys. Rev. Lett. **99**, 137207 (Sep 2007).
- [33] C. Nayak, S. H. Simon, A. Stern, M. Freedman, and S. Das Sarma, “Non-Abelian anyons and topological quantum computation,” Rev. Mod. Phys. **80**, 1083 (Sep 2008).

- [34] P. A. Lee, N. Nagaosa, and X.-G. Wen, “Doping a Mott insulator: Physics of high-temperature superconductivity,” Rev. Mod. Phys. **78**(1), 17 (2006).
- [35] J. Bardeen, L. N. Cooper, and J. R. Schrieffer, “Microscopic Theory of Superconductivity,” Phys. Rev. **106**, 162 (Apr 1957).
- [36] J. Bardeen, L. N. Cooper, and J. R. Schrieffer, “Theory of Superconductivity,” Phys. Rev. **108**, 1175 (Dec 1957).
- [37] J. Schrieffer, *Theory of Superconductivity*, Advanced Book Program Series (Advanced Book Program, Perseus Books, 1999).
- [38] M. Tinkham, *Introduction to Superconductivity: Second Edition*, Dover Books on Physics (Dover Publications, Mineola, New York, 2004).
- [39] B. J. Powell and R. H. McKenzie, “Quantum frustration in organic Mott insulators: from spin liquids to unconventional superconductors,” Reports on Progress in Physics **74**(5), 056501 (May 2011).
- [40] K. Kanoda and R. Kato, “Mott Physics in Organic Conductors with Triangular Lattices,” Annual Review of Condensed Matter Physics **2**(1), 167 (2011).
- [41] D. A. Huse and V. Elser, “Simple Variational Wave Functions for Two-Dimensional Heisenberg Spin-½ Antiferromagnets,” Phys. Rev. Lett. **60**(24), 2531 (Jun 1988).
- [42] L. Capriotti, A. E. Trumper, and S. Sorella, “Long-Range Néel Order in the Triangular Heisenberg Model,” Phys. Rev. Lett. **82**, 3899 (May 1999).

- [43] S. R. White and A. L. Chernyshev, “Neél Order in Square and Triangular Lattice Heisenberg Models,” Phys. Rev. Lett. **99**, 127004 (Sep 2007).
- [44] S. Yamashita, Y. Nakazawa, M. Oguni, Y. Oshima, H. Nojiri, Y. Shimizu, K. Miyagawa, and K. Kanoda, “Thermodynamic properties of a spin-1/2 spin-liquid state in a κ -type organic salt,” Nature Phys. **4**, 459 (2008).
- [45] S. Yamashita, T. Yamamoto, Y. Nakazawa, M. Tamura, and R. Kato, “Gapless spin liquid of an organic triangular compound evidenced by thermodynamic measurements,” Nature Commun. **2**, 275 (2011).
- [46] D. Watanabe, M. Yamashita, S. Tonegawa, Y. Oshima, H. M. Yamamoto, R. Kato, I. Sheikin, K. Behnia, T. Terashima, S. Uji, T. Shibauchi, and Y. Matsuda, “Novel Pauli-paramagnetic quantum phase in a Mott insulator,” Nature Communications **3** (Sep. 2012).
- [47] M. Yamashita, N. Nakata, Y. Senshu, M. Nagata, H. M. Yamamoto, R. Kato, T. Shibauchi, and Y. Matsuda, “Highly Mobile Gapless Excitations in a Two-Dimensional Candidate Quantum Spin Liquid,” Science **328**(5983), 1246 (2010).
- [48] M. Yamashita, N. Nakata, Y. Kasahara, T. Sasaki, N. Yoneyama, N. Kobayashi, S. Fujimoto, T. Shibauchi, and Y. Matsuda, “Thermal-transport measurements in a quantum spin-liquid state of the frustrated triangular magnet κ -(BEDT-TTF)₂Cu₂(CN)₃,” Nature Phys. **5**, 44 (2009).
- [49] O. I. Motrunich, “Variational study of triangular lattice spin-1/2 model with ring ex-

changes and spin liquid state in $\kappa - (ET)2Cu2(CN)3$,” Phys. Rev. B **72**(4), 045105 (Jul 2005).

- [50] S.-S. Lee and P. A. Lee, “U(1) Gauge Theory of the Hubbard Model: Spin Liquid States and Possible Application to $\kappa - (BEDT-TTF)2Cu2(CN)3$,” Phys. Rev. Lett. **95**(3), 036403 (Jul 2005).

- [51] N. Nagaosa and P. A. Lee, “Normal-state properties of the uniform resonating-valence-bond state,” Phys. Rev. Lett. **64**, 2450 (May 1990).

- [52] P. A. Lee and N. Nagaosa, “Gauge theory of the normal state of high- T_c superconductors,” Phys. Rev. B **46**(9), 5621 (Sep 1992).

- [53] B. I. Halperin, P. A. Lee, and N. Read, “Theory of the half-filled Landau level,” Phys. Rev. B **47**, 7312 (Mar 1993).

- [54] J. Polchinski, “Low-energy dynamics of the spinon-gauge system,” Nucl. Phys. B **422**(3), 617 (1994).

- [55] B. L. Altshuler, L. B. Ioffe, and A. J. Millis, “Low-energy properties of fermions with singular interactions,” Phys. Rev. B **50**(19), 14048 (Nov 1994).

- [56] C. Nayak and F. Wilczek, “Non-Fermi liquid fixed point in 2 + 1 dimensions,” Nuclear Physics B **417**(3), 359 (1994).

- [57] C. Nayak and F. Wilczek, “Renormalization group approach to low temperature properties of a non-Fermi liquid metal,” Nuclear Physics B **430**(3), 534 (1994).

- [58] D. N. Sheng, O. I. Motrunich, and M. P. A. Fisher, “Spin Bose-metal phase in a spin-(1/2) model with ring exchange on a two-leg triangular strip,” Phys. Rev. B **79**(20), 205112 (2009).
- [59] M. S. Block, D. N. Sheng, O. I. Motrunich, and M. P. A. Fisher, “Spin Bose-Metal and Valence Bond Solid Phases in a Spin-1/2 Model with Ring Exchanges on a Four-Leg Triangular Ladder,” Phys. Rev. Lett. **106**(15), 157202 (Apr 2011).
- [60] S. Florens and A. Georges, “Slave-rotor mean-field theories of strongly correlated systems and the Mott transition in finite dimensions,” Phys. Rev. B **70**, 035114 (Jul 2004).
- [61] T. Senthil, “Theory of a continuous Mott transition in two dimensions,” Phys. Rev. B **78**(4), 045109 (2008).
- [62] M. P. A. Fisher, P. B. Weichman, G. Grinstein, and D. S. Fisher, “Boson localization and the superfluid-insulator transition,” Phys. Rev. B **40**(1), 546 (1989).
- [63] K. Sun, H. Yao, E. Fradkin, and S. A. Kivelson, “Topological Insulators and Nematic Phases from Spontaneous Symmetry Breaking in 2D Fermi Systems with a Quadratic Band Crossing,” Phys. Rev. Lett. **103**, 046811 (Jul 2009).
- [64] T. Grover, N. Trivedi, T. Senthil, and P. A. Lee, “Weak Mott insulators on the triangular lattice: Possibility of a gapless nematic quantum spin liquid,” Phys. Rev. B **81**(24), 245121 (Jun 2010).
- [65] L. F. Tocchio, A. Parola, C. Gros, and F. Becca, “Spin-liquid and magnetic phases in

the anisotropic triangular lattice: The case of κ -(ET)₂X,” Phys. Rev. B **80**, 064419 (Aug 2009).

- [66] L. F. Tocchio, H. Feldner, F. Becca, R. Valentí, and C. Gros, “Spin-liquid versus spiral-order phases in the anisotropic triangular lattice,” Phys. Rev. B **87**, 035143 (Jan 2013).
- [67] Y. Qi, C. Xu, and S. Sachdev, “Dynamics and Transport of the Z_2 Spin Liquid: Application to κ -(ET)₂Cu₂(CN)₃,” Phys. Rev. Lett. **102**, 176401 (Apr 2009).
- [68] R. R. Biswas, L. Fu, C. R. Laumann, and S. Sachdev, “SU(2)-invariant spin liquids on the triangular lattice with spinful Majorana excitations,” Phys. Rev. B **83**, 245131 (Jun 2011).
- [69] M. Barkeshli, H. Yao, and S. A. Kivelson, “Gapless spin liquids: Stability and possible experimental relevance,” Phys. Rev. B **87**, 140402 (Apr 2013).
- [70] J. G. Bednorz and K. A. Müller, “Possible high T_c superconductivity in the Ba-La-Cu-O system,” Zeitschrift für Physik B Condensed Matter **64**, 189 (1986), 10.1007/BF01303701.
- [71] R. J. Cava, R. B. van Dover, B. Batlogg, and E. A. Rietman, “Bulk superconductivity at 36 K in La_{1.8}Sr_{0.2}CuO₄,” Phys. Rev. Lett. **58**, 408 (Jan 1987).
- [72] M. K. Wu, J. R. Ashburn, C. J. Torng, P. H. Hor, R. L. Meng, L. Gao, Z. J. Huang, Y. Q. Wang, and C. W. Chu, “Superconductivity at 93 K in a new mixed-phase Y-Ba-Cu-O compound system at ambient pressure,” Phys. Rev. Lett. **58**(9), 908 (Mar 1987).

- [73] A. Schilling, M. Cantoni, J. D. Guo, and H. R. Ott, “Superconductivity above 130 K in the Hg-Ba-Ca-Cu-O system,” *Nature* **363**, 56 (1993).
- [74] L. Gao, Z. Huang, R. Meng, J. Lin, F. Chen, L. Beauvais, Y. Sun, Y. Xue, and C. Chu, “Study of superconductivity in the Hg-Ba-Ca-Cu-O system,” *Physica C: Superconductivity* **213**(3-4), 261 (1993).
- [75] J. Paglione and R. L. Greene, “High-temperature superconductivity in iron-based materials,” *Nature Physics* **6**, 645 (Aug. 2010).
- [76] L. E. Hayward, D. G. Hawthorn, R. G. Melko, and S. Sachdev, “Angular Fluctuations of a Multicomponent Order Describe the Pseudogap of $\text{YBa}_2\text{Cu}_3\text{O}_{6+x}$,” *Science* **343**(6177), 1336 (2014).
- [77] P. Corboz, T. M. Rice, and M. Troyer, “Competing states in the t-J model: uniform d-wave state versus stripe state,” arXiv:1402.2859 [cond-mat.str-el] (Feb. 2014).
- [78] R. A. Cooper, Y. Wang, B. Vignolle, O. J. Lipscombe, S. M. Hayden, Y. Tanabe, T. Adachi, Y. Koike, M. Nohara, H. Takagi, C. Proust, and N. E. Hussey, “Anomalous Criticality in the Electrical Resistivity of $\text{La}_{2-x}\text{Sr}_x\text{CuO}_4$,” *Science* **323**(5914), 603 (2009).
- [79] A. Damascelli, Z. Hussain, and Z.-X. Shen, “Angle-resolved photoemission studies of the cuprate superconductors,” *Rev. Mod. Phys.* **75**, 473 (Apr 2003).
- [80] G. S. Boebinger, “An Abnormal Normal State,” *Science* **323**(5914), 590 (2009).

- [81] R. Shankar, “Renormalization-group approach to interacting fermions,” Rev. Mod. Phys. **66**(1), 129 (Jan 1994).
- [82] H.-C. Jiang, M. S. Block, R. V. Mishmash, J. R. Garrison, D. N. Sheng, O. I. Motrunich, and M. P. A. Fisher, “Non-Fermi-liquid d -wave metal phase of strongly interacting electrons,” Nature **493**, 39 (2013).
- [83] K. G. Wilson, “Confinement of quarks,” Phys. Rev. D **10**, 2445 (Oct 1974).
- [84] D. N. Sheng, O. I. Motrunich, S. Trebst, E. Gull, and M. P. A. Fisher, “Strong-coupling phases of frustrated bosons on a two-leg ladder with ring exchange,” Phys. Rev. B **78**(5), 054520 (2008).
- [85] M. S. Block, R. V. Mishmash, R. K. Kaul, D. N. Sheng, O. I. Motrunich, and M. P. A. Fisher, “Exotic Gapless Mott Insulators of Bosons on Multileg Ladders,” Phys. Rev. Lett. **106**(4), 046402 (Jan 2011).
- [86] R. V. Mishmash, M. S. Block, R. K. Kaul, D. N. Sheng, O. I. Motrunich, and M. P. A. Fisher, “Bose metals and insulators on multileg ladders with ring exchange,” Phys. Rev. B **84**, 245127 (Dec 2011).
- [87] S.-S. Lee, “Stability of the U(1) spin liquid with a spinon Fermi surface in 2+1 dimensions,” Phys. Rev. B **78**, 085129 (Aug 2008).
- [88] M. Hermele, T. Senthil, M. P. A. Fisher, P. A. Lee, N. Nagaosa, and X.-G. Wen, “Stability of $U(1)$ spin liquids in two dimensions,” Phys. Rev. B **70**(21), 214437 (Dec 2004).

- [89] A. Altland and B. Simons, *Condensed Matter Field Theory: Second Edition* (Cambridge University Press, 2010).
- [90] E. Fradkin and S. H. Shenker, “Phase diagrams of lattice gauge theories with Higgs fields,” Phys. Rev. D **19**, 3682 (Jun 1979).
- [91] D. F. Mross and T. Senthil, “Charge Friedel oscillations in a Mott insulator,” Phys. Rev. B **84**, 041102 (Jul 2011).
- [92] O. I. Motrunich and M. P. A. Fisher, “ d -wave correlated critical Bose liquids in two dimensions,” Phys. Rev. B **75**(23), 235116 (2007).
- [93] L. B. Ioffe and A. I. Larkin, “Gapless fermions and gauge fields in dielectrics,” Phys. Rev. B **39**(13), 8988 (May 1989).
- [94] M. Y. Reizer, “Relativistic effects in the electron density of states, specific heat, and the electron spectrum of normal metals,” Phys. Rev. B **40**, 11571 (Dec 1989).
- [95] P. A. Lee, “Gauge field, Aharonov-Bohm flux, and high- T_c superconductivity,” Phys. Rev. Lett. **63**, 680 (Aug 1989).
- [96] Y. B. Kim, A. Furusaki, X.-G. Wen, and P. A. Lee, “Gauge-invariant response functions of fermions coupled to a gauge field,” Phys. Rev. B **50**, 17917 (Dec 1994).
- [97] S.-S. Lee, “Low-energy effective theory of Fermi surface coupled with U(1) gauge field in $2 + 1$ dimensions,” Phys. Rev. B **80**, 165102 (Oct 2009).
- [98] M. A. Metlitski and S. Sachdev, “Quantum phase transitions of metals in two spatial dimensions. I. Ising-nematic order,” Phys. Rev. B **82**, 075127 (Aug 2010).

- [99] D. F. Mross, J. McGreevy, H. Liu, and T. Senthil, “Controlled expansion for certain non-Fermi-liquid metals,” Phys. Rev. B **82**, 045121 (Jul 2010).
- [100] M. P. A. Fisher, O. I. Motrunich, and D. N. Sheng, “Spin, Bose, and Non-Fermi Liquid Metals in Two Dimensions: Accessing via Multi-Leg Ladders,” arXiv:0812.2955 [cond-mat.str-el] (2008).
- [101] F. D. M. Haldane, “Luttinger liquid theory of one-dimensional quantum fluids: I. Properties of the Luttinger model and their extension to the general 1D interacting spinless Fermi gas,” J. Phys. C: Solid State Phys. **14**, 2585 (1981).
- [102] F. D. M. Haldane, “Effective Harmonic-Fluid Approach to Low-Energy Properties of One-Dimensional Quantum Fluids,” Phys. Rev. Lett. **47**(25), 1840 (Dec 1981).
- [103] C. L. Kane and M. P. A. Fisher, “Transmission through barriers and resonant tunneling in an interacting one-dimensional electron gas,” Phys. Rev. B **46**, 15233 (Dec 1992).
- [104] H.-H. Lin, L. Balents, and M. P. A. Fisher, “Exact SO(8) symmetry in the weakly-interacting two-leg ladder,” Phys. Rev. B **58**, 1794 (Jul 1998).
- [105] M. P. A. Fisher, “Mott insulators, Spin liquids and Quantum Disordered Superconductivity,” in *Topological aspects of low dimensional systems*, edited by A. Comtet, T. Jolicoeur, S. Ouvry, and F. David (Springer, Berlin, 1999), vol. 69 of *Les Houches Lecture Series*, pp. 575–641.
- [106] J. M. Luttinger, “An Exactly Soluble Model of a Many-Fermion System,” Journal of Mathematical Physics **4**(9), 1154 (1963).

- [107] F. D. M. Haldane, “General Relation of Correlation Exponents and Spectral Properties of One-Dimensional Fermi Systems: Application to the Anisotropic S=12 Heisenberg Chain,” Phys. Rev. Lett. **45**, 1358 (Oct 1980).
- [108] L. Balents and M. P. A. Fisher, “Weak-coupling phase diagram of the two-chain Hubbard model,” Phys. Rev. B **53**(18), 12133 (May 1996).
- [109] S. R. White, “Density matrix formulation for quantum renormalization groups,” Phys. Rev. Lett. **69**(19), 2863 (Nov 1992).
- [110] S. R. White, “Density-matrix algorithms for quantum renormalization groups,” Phys. Rev. B **48**(14), 10345 (Oct 1993).
- [111] U. Schollwock, “The density-matrix renormalization group,” Rev. Mod. Phys. **77**(1), 259 (2005).
- [112] U. Schollwöck, “The density-matrix renormalization group in the age of matrix product states,” Annals of Physics **326**(1), 96 (2011).
- [113] M. Troyer and U.-J. Wiese, “Computational Complexity and Fundamental Limitations to Fermionic Quantum Monte Carlo Simulations,” Phys. Rev. Lett. **94**(17), 170201 (May 2005).
- [114] E. Stoudenmire and S. R. White, “Studying Two-Dimensional Systems with the Density Matrix Renormalization Group,” Annual Review of Condensed Matter Physics **3**(1), 111 (2012).

- [115] S. Yan, D. A. Huse, and S. R. White, “Spin-Liquid Ground State of the $S = 1/2$ Kagome Heisenberg Antiferromagnet,” *Science* **332**(6034), 1173 (2011).
- [116] S. Depenbrock, I. P. McCulloch, and U. Schollwöck, “Nature of the Spin-Liquid Ground State of the $S=1/2$ Heisenberg Model on the Kagome Lattice,” *Phys. Rev. Lett.* **109**, 067201 (Aug 2012).
- [117] H.-C. Jiang, H. Yao, and L. Balents, “Spin liquid ground state of the spin-1/2 square J1-J2 Heisenberg model,” *Phys. Rev. B* **86**, 024424 (Jul 2012).
- [118] S.-S. Gong, W. Zhu, D. N. Sheng, O. I. Motrunich, and M. P. A. Fisher, “Plaquette ordered phase and quantum spin liquid in the spin-1/2 J1-J2 square Heisenberg model,” arXiv:1311.5962 [cond-mat.str-el] (Nov. 2013).
- [119] G. Golub and C. Van Loan, *Matrix Computations*, Johns Hopkins Studies in the Mathematical Sciences (Johns Hopkins University Press, 1996).
- [120] G. Vidal, “Efficient Classical Simulation of Slightly Entangled Quantum Computations,” *Phys. Rev. Lett.* **91**(14), 147902 (2003).
- [121] G. Vidal, “Efficient Simulation of One-Dimensional Quantum Many-Body Systems,” *Phys. Rev. Lett.* **93**(4), 040502 (2004).
- [122] F. Verstraete, D. Porras, and J. I. Cirac, “Density Matrix Renormalization Group and Periodic Boundary Conditions: A Quantum Information Perspective,” *Phys. Rev. Lett.* **93**(22), 227205 (Nov 2004).

- [123] M. Fannes, B. Nachtergaelle, and R. F. Werner, “Finitely correlated states on quantum spin chains,” *Commun. Math. Phys.* **144**, 443 (1992).
- [124] S. Östlund and S. Rommer, “Thermodynamic Limit of Density Matrix Renormalization,” *Phys. Rev. Lett.* **75**(19), 3537 (Nov 1995).
- [125] S. Rommer and S. Östlund, “Class of ansatz wave functions for one-dimensional spin systems and their relation to the density matrix renormalization group,” *Phys. Rev. B* **55**(4), 2164 (Jan 1997).
- [126] A. J. Daley, C. Kollath, U. Schollwöck, and G. Vidal, “Time-dependent density-matrix renormalization-group using adaptive effective Hilbert spaces,” *J. Stat. Mech.* p. P04005 (2004).
- [127] M. L. Wall, *Quantum Many-Body Physics of Ultracold Molecules in Optical Lattices: Models and Simulation Methods*, Ph.D. thesis, Colorado School of Mines (2012).
- [128] P. Calabrese and J. Cardy, “Entanglement entropy and quantum field theory,” *J. Stat. Mech.* **2004**(06), P06002 (2004).
- [129] D. Gioev and I. Klich, “Entanglement Entropy of Fermions in Any Dimension and the Widom Conjecture,” *Phys. Rev. Lett.* **96**(10), 100503 (Mar 2006).
- [130] B. Swingle, “Entanglement Entropy and the Fermi Surface,” *Phys. Rev. Lett.* **105**(5), 050502 (Jul 2010).
- [131] F. Verstraete and J. I. Cirac, “Renormalization algorithms for Quantum-Many Body Systems in two and higher dimensions,” arXiv:cond-mat/0407066 [cond-mat.str-el] (2004).

- [132] R. Orus, “A Practical Introduction to Tensor Networks: Matrix Product States and Projected Entangled Pair States,” arXiv:1306.2164 [cond-mat.str-el] (Jun. 2013).
- [133] P. Corboz and G. Vidal, “Fermionic multiscale entanglement renormalization ansatz,” Phys. Rev. B **80**(16), 165129 (Oct 2009).
- [134] P. Corboz, G. Evenbly, F. Verstraete, and G. Vidal, “Simulation of interacting fermions with entanglement renormalization,” Phys. Rev. A **81**(1), 010303 (Jan 2010).
- [135] P. Corboz, R. Orús, B. Bauer, and G. Vidal, “Simulation of strongly correlated fermions in two spatial dimensions with fermionic projected entangled-pair states,” Phys. Rev. B **81**(16), 165104 (Apr 2010).
- [136] G. Evenbly and G. Vidal, “A class of highly entangled many-body states that can be efficiently simulated,” arXiv:1210.1895 [quant-ph] (Oct. 2012).
- [137] R. B. Laughlin, “Anomalous Quantum Hall Effect: An Incompressible Quantum Fluid with Fractionally Charged Excitations,” Phys. Rev. Lett. **50**, 1395 (May 1983).
- [138] C. Gros, “Superconductivity in correlated wave functions,” Phys. Rev. B **38**(1), 931 (Jul 1988).
- [139] C. Gros, “Physics of projected wavefunctions,” Annals of Physics **189**(1), 53 (1989).
- [140] D. Ceperley, G. V. Chester, and M. H. Kalos, “Monte Carlo simulation of a many-fermion study,” Phys. Rev. B **16**(7), 3081 (Oct 1977).
- [141] T. Tay and O. I. Motrunich, “Failure of Gutzwiller-type wave function to capture gauge

- fluctuations: Case study in the exciton Bose liquid context," Phys. Rev. B **83**(23), 235122 (Jun 2011).
- [142] R. V. Mishmash, I. Gonzalez, R. G. Melko, O. I. Motrunich, and M. P. A. Fisher, "A continuous Mott transition between a metal and a quantum spin liquid," arXiv:1403.4258 [cond-mat.str-el] (Mar. 2014).
- [143] R. V. Mishmash, J. R. Garrison, S. Bieri, and C. Xu, "Theory of a Competitive Spin Liquid State for Weak Mott Insulators on the Triangular Lattice," Phys. Rev. Lett. **111**, 157203 (Oct 2013).
- [144] A. Zylbersztein and N. F. Mott, "Metal-insulator transition in vanadium dioxide," Phys. Rev. B **11**, 4383 (Jun 1975).
- [145] P. Limelette, A. Georges, D. Jerome, P. Wzietek, P. Metcalf, and J. M. Honig, "Universality and Critical Behavior at the Mott Transition," Science **302**(5642), 89 (2003).
- [146] P. Limelette, P. Wzietek, S. Florens, A. Georges, T. A. Costi, C. Pasquier, D. Jérôme, C. Mézière, and P. Batail, "Mott Transition and Transport Crossovers in the Organic Compound κ -(BEDT-TTF)₂Cu[N(CN)₂]Cl," Phys. Rev. Lett. **91**, 016401 (Jul 2003).
- [147] F. Kagawa, T. Itou, K. Miyagawa, and K. Kanoda, "Transport criticality of the first-order Mott transition in the quasi-two-dimensional organic conductor κ -(BEDT-TTF)₂Cu[N(CN)₂]Cl," Phys. Rev. B **69**, 064511 (Feb 2004).
- [148] F. Kagawa, K. Miyagawa, and K. Kanoda, "Unconventional critical behaviour in a quasi-two-dimensional organic conductor," Nature **436**, 534 (2005).

- [149] D. F. Mross and T. Senthil, “Decohering the Fermi liquid: A dual approach to the Mott transition,” Phys. Rev. B **84**, 165126 (Oct 2011).
- [150] K. Kanoda, “talk at ‘KITP Conference on Exotic Phases of Frustrated Magnets’,” (October 2012, http://online.kitp.ucsb.edu/online/fragnets_c12/ kanoda/).
- [151] H.-H. Lai and O. I. Motrunich, “Two-band electronic metal and neighboring spin Bose-metal on a zigzag strip with longer-ranged repulsion,” Phys. Rev. B **81**(4), 045105 (Jan 2010).
- [152] T. Yoshioka, A. Koga, and N. Kawakami, “Quantum Phase Transitions in the Hubbard Model on a Triangular Lattice,” Phys. Rev. Lett. **103**, 036401 (Jul 2009).
- [153] H.-Y. Yang, A. M. Läuchli, F. Mila, and K. P. Schmidt, “Effective Spin Model for the Spin-Liquid Phase of the Hubbard Model on the Triangular Lattice,” Phys. Rev. Lett. **105**(26), 267204 (Dec 2010).
- [154] J. Kokalj and R. H. McKenzie, “Thermodynamics of a Bad Metal-Mott Insulator Transition in the Presence of Frustration,” Phys. Rev. Lett. **110**, 206402 (May 2013).
- [155] Z. Y. Meng, T. C. Lang, S. Wessel, F. F. Assaad, and A. Muramatsu, “Quantum spin liquid emerging in two-dimensional correlated Dirac fermions,” Nature **464**, 847 (2010).
- [156] K. Nakamura, Y. Yoshimoto, T. Kosugi, R. Arita, and M. Imada, “*Ab initio* Derivation of Low-Energy Model for κ -ET Type Organic Conductors,” Journal of the Physical Society of Japan **78**(8), 083710 (2009).

- [157] K. Louis, J. V. Alvarez, and C. Gros, “Fermi surface renormalization in Hubbard ladders,” Phys. Rev. B **64**(11), 113106 (Aug 2001).
- [158] G. I. Japaridze, R. M. Noack, D. Baeriswyl, and L. Tincani, “Phases and phase transitions in the half-filled $t - t'$ Hubbard chain,” Phys. Rev. B **76**(11), 115118 (Sep 2007).
- [159] D. J. Amit, Y. Y. Goldschmidt, and S. Grinstein, “Renormalisation group analysis of the phase transition in the 2D Coulomb gas, Sine-Gordon theory and XY-model,” Journal of Physics A: Mathematical and General **13**(2), 585 (1980).
- [160] H. Weber and P. Minnhagen, “Monte Carlo determination of the critical temperature for the two-dimensional XY model,” Phys. Rev. B **37**, 5986 (Apr 1988).
- [161] H.-H. Lai and O. I. Motrunich, “Effects of impurities in spin Bose-metal phase on a two-leg triangular strip,” Phys. Rev. B **79**(23), 235120 (2009).
- [162] N. Sedlmayr, P. Korell, and J. Sirker, “Two-band Luttinger liquid with spin-orbit coupling: Applications to monatomic chains on surfaces,” Phys. Rev. B **88**, 195113 (Nov 2013).
- [163] S. R. White and I. Affleck, “Dimerization and incommensurate spiral spin correlations in the zigzag spin chain: Analogies to the Kondo lattice,” Phys. Rev. B **54**, 9862 (Oct 1996).
- [164] L. F. Tocchio, F. Becca, and C. Gros, “Interaction-induced Fermi-surface renormalization in the $t_1 - t_2$ Hubbard model close to the Mott-Hubbard transition,” Phys. Rev. B **81**(20), 205109 (May 2010).

- [165] P. A. Lee, “An End to the Drought of Quantum Spin Liquids,” *Science* **321**(5894), 1306 (2008).
- [166] H. D. Zhou, E. S. Choi, G. Li, L. Balicas, C. R. Wiebe, Y. Qiu, J. R. D. Copley, and J. S. Gardner, “Spin Liquid State in the $S = 1/2$ Triangular Lattice $\text{Ba}_3\text{CuSb}_2\text{O}_9$,” *Phys. Rev. Lett.* **106**, 147204 (Apr 2011).
- [167] J. G. Cheng, G. Li, L. Balicas, J. S. Zhou, J. B. Goodenough, C. Xu, and H. D. Zhou, “High-Pressure Sequence of $\text{Ba}_3\text{NiSb}_2\text{O}_9$ Structural Phases: New $S = 1$ Quantum Spin Liquids Based on Ni^{2+} ,” *Phys. Rev. Lett.* **107**, 197204 (Nov 2011).
- [168] A. P. Ramirez, “Quantum spin liquids: A flood or a trickle,” *Nature Phys.* **4**, 442 (2008).
- [169] Y. Shimizu, K. Miyagawa, K. Kanoda, M. Maesato, and G. Saito, “Emergence of inhomogeneous moments from spin liquid in the triangular-lattice Mott insulator κ - $(\text{ET})_2\text{Cu}_2(\text{CN})_3$,” *Phys. Rev. B* **73**, 140407 (Apr 2006).
- [170] C. Xu, F. Wang, Y. Qi, L. Balents, and M. P. A. Fisher, “Spin Liquid Phases for Spin-1 Systems on the Triangular Lattice,” *Phys. Rev. Lett.* **108**, 087204 (Feb 2012).
- [171] S. Bieri, M. Serbyn, T. Senthil, and P. A. Lee, “Paired chiral spin liquid with a Fermi surface in $S = 1$ model on the triangular lattice,” *Phys. Rev. B* **86**, 224409 (Dec 2012).
- [172] E.-G. Moon and C. Xu, in progress.
- [173] W. LiMing, G. Misguich, P. Sindzingre, and C. Lhuillier, “From Néel long-range order to spin liquids in the multiple-spin exchange model,” *Phys. Rev. B* **62**, 6372 (Sep 2000).

- [174] V. Kalmeyer and R. B. Laughlin, “Equivalence of the resonating-valence-bond and fractional quantum Hall states,” Phys. Rev. Lett. **59**, 2095 (Nov 1987).
- [175] X. G. Wen, F. Wilczek, and A. Zee, “Chiral spin states and superconductivity,” Phys. Rev. B **39**, 11413 (Jun 1989).
- [176] T. Jolicoeur, E. Dagotto, E. Gagliano, and S. Bacci, “Ground-state properties of the $S = 1/2$ Heisenberg antiferromagnet on a triangular lattice,” Phys. Rev. B **42**, 4800 (Sep 1990).
- [177] P. Lecheminant, B. Bernu, C. Lhuillier, and L. Pierre, “ J_1 - J_2 quantum Heisenberg antiferromagnet on the triangular lattice: A group-symmetry analysis of order by disorder,” Phys. Rev. B **52**, 6647 (Sep 1995).
- [178] A. J. Schofield, “Non-Fermi liquids,” Contemporary Physics **40**(2), 95 (1999).
- [179] P. W. Anderson and Z. Zou, ““Normal” Tunneling and “Normal” Transport: Diagnostics for the Resonating-Valence-Bond State,” Phys. Rev. Lett. **60**, 132 (Jan 1988).
- [180] C. M. Varma, P. B. Littlewood, S. Schmitt-Rink, E. Abrahams, and A. E. Ruckenstein, “Phenomenology of the normal state of Cu-O high-temperature superconductors,” Phys. Rev. Lett. **63**, 1996 (Oct 1989).
- [181] T. Senthil, “Critical Fermi surfaces and non-Fermi liquid metals,” Phys. Rev. B **78**(3), 035103 (Jul 2008).
- [182] T. Faulkner, N. Iqbal, H. Liu, J. McGreevy, and D. Vegh, “Strange Metal Transport Realized by Gauge/Gravity Duality,” Science **329**(5995), 1043 (2010).

- [183] S. Sachdev, “Holographic Metals and the Fractionalized Fermi Liquid,” *Phys. Rev. Lett.* **105**, 151602 (Oct 2010).
- [184] G. Baskaran, Z. Zou, and P. W. Anderson, “The resonating valence bond state and high- T_c superconductivity – A mean field theory,” *Solid State Commun.* **63**(11), 973 (1987).
- [185] X.-G. Wen and P. A. Lee, “Theory of Underdoped Cuprates,” *Phys. Rev. Lett.* **76**, 503 (Jan 1996).
- [186] P. W. Anderson, G. Baskaran, Z. Zou, and T. Hsu, “Resonating valence-bond theory of phase transitions and superconductivity in La_2CuO_4 -based compounds,” *Phys. Rev. Lett.* **58**, 2790 (Jun 1987).
- [187] M. V. Feigelman, V. B. Geshkenbein, L. B. Ioffe, and A. I. Larkin, “Two-dimensional Bose liquid with strong gauge-field interaction,” *Phys. Rev. B* **48**(22), 16641 (Dec 1993).
- [188] R. Shankar, “Bosonization: how to make it work for you in condensed matter,” *Acta Phys. Pol. B* **26**, 1835 (1995).
- [189] J. O. Fjærstad and J. B. Marston, “Staggered orbital currents in the half-filled two-leg ladder,” *Phys. Rev. B* **65**, 125106 (Mar 2002).
- [190] C. S. Hellberg and E. J. Mele, “Phase diagram of the one-dimensional t-J model from variational theory,” *Phys. Rev. Lett.* **67**(15), 2080 (Oct 1991).
- [191] D. M. Ceperley, “Fermion Nodes,” *J. Stat. Phys.* **63**, 1237 (1991).
- [192] B. Normand and A. M. Oleś, “Circulating-current states and ring-exchange interactions in cuprates,” *Phys. Rev. B* **70**, 134407 (Oct 2004).

- [193] M. Imada and T. Miyake, “Electronic Structure Calculation by First Principles for Strongly Correlated Electron Systems,” Journal of the Physical Society of Japan **79**(11), 112001 (2010).
- [194] P. Calabrese, M. Campostrini, F. Essler, and B. Nienhuis, “Parity Effects in the Scaling of Block Entanglement in Gapless Spin Chains,” Phys. Rev. Lett. **104**(9), 095701 (Mar 2010).
- [195] M. B. Hastings, I. González, A. B. Kallin, and R. G. Melko, “Measuring Renyi Entanglement Entropy in Quantum Monte Carlo Simulations,” Phys. Rev. Lett. **104**(15), 157201 (Apr 2010).
- [196] R. Nandkishore, M. A. Metlitski, and T. Senthil, “Orthogonal metals: The simplest non-Fermi liquids,” Phys. Rev. B **86**, 045128 (Jul 2012).
- [197] G. Vidal, “Entanglement Renormalization,” Phys. Rev. Lett. **99**(22), 220405 (2007).
- [198] G. Vidal, “Class of Quantum Many-Body States That Can Be Efficiently Simulated,” Phys. Rev. Lett. **101**(11), 110501 (2008).
- [199] G. Moore and N. Read, “Nonabelions in the fractional quantum hall effect,” Nuclear Physics B **360**(23), 362 (1991).
- [200] I. Bloch, J. Dalibard, and W. Zwerger, “Many-body physics with ultracold gases,” Rev. Mod. Phys. **80**(3), 885 (2008).
- [201] G. Evenbly and G. Vidal, “A real space decoupling transformation for quantum many-body systems,” arXiv:1205.0639 [quant-ph] (May 2012).

- [202] B. Swingle, “Conformal field theory approach to Fermi liquids and other highly entangled states,” Phys. Rev. B **86**, 035116 (Jul 2012).
- [203] W. Ding, A. Seidel, and K. Yang, “Entanglement Entropy of Fermi Liquids via Multidimensional Bosonization,” Phys. Rev. X **2**, 011012 (Mar 2012).
- [204] B. Swingle, “Entanglement Sum Rules,” Phys. Rev. Lett. **111**, 100405 (Sep 2013).
- [205] J. Shao, E.-A. Kim, F. D. M. Haldane, and E. H. Rezayi, “Entanglement entropy of the $\nu = 1/2$ composite fermion non-Fermi liquid state,” arXiv:1403.0577 [cond-mat.str-el] (Mar. 2014).
- [206] A. M. Essin and M. Hermele, “Classifying fractionalization: Symmetry classification of gapped Z2 spin liquids in two dimensions,” Phys. Rev. B **87**, 104406 (Mar 2013).
- [207] G. Misguich, C. Lhuillier, B. Bernu, and C. Waldtmann, “Spin-liquid phase of the multiple-spin exchange Hamiltonian on the triangular lattice,” Phys. Rev. B **60**, 1064 (Jul 1999).
- [208] O. I. Motrunich, private communications.
- [209] S.-S. Lee, P. A. Lee, and T. Senthil, “Amperean Pairing Instability in the U(1) Spin Liquid State with Fermi Surface and Application to κ -(BEDT-TTF)₂Cu₂(CN)₃,” Phys. Rev. Lett. **98**, 067006 (Feb 2007).
- [210] R. V. Mishmash, I. González, R. G. Melko, O. I. Motrunich, and M. P. A. Fisher, in preparation.

- [211] A. E. Feiguin and M. P. A. Fisher, “Exotic Paired States with Anisotropic Spin-Dependent Fermi Surfaces,” Phys. Rev. Lett. **103**(2), 025303 (2009).
- [212] A. E. Feiguin and M. P. A. Fisher, “Exotic paired phases in ladders with spin-dependent hopping,” Phys. Rev. B **83**(11), 115104 (Mar 2011).
- [213] Bouchaud, J.P., Georges, A., and Lhuillier, C., “Pair wave functions for strongly correlated fermions and their determinantal representation,” J. Phys. France **49**(4), 553 (1988).